U. S. DEPARTMENT OF THE INTERIOR

U.S. GEOLOGICAL SURVEY

# Temporal, spatial and petrologic variations of lava flows from the Mount Bachelor volcanic chain, central Oregon High Cascades

Cynthia A. Gardner [1]

Open-File Report 94-261



1. David A. Johnston Cascades Volcano Observatory
5400 MacArthur Blvd.
Vancouver, Washington 98661

# Table of Contents

## ABSTRACT

The 25-km-long, N-S-trending, 18-8 ka Mount Bachelor volcanic chain (MBVC) consists of cinder cones, lava flows, and shield volcanoes, which record a history of petrologically diverse mafic volcanism in the central Oregon High Cascades. Between 30 and 50 $km^3$ of basalt and basaltic andesite (49-57 percent $SiO_2$) were produced during four eruptive episodes. Most lava flows along the chain are plagioclase- and olivine-phyric and contain plagioclase, olivine, magnetite, and, in some samples, clinopyroxene in the groundmass. Lava flows from the summit cone of Mount Bachelor are distinctive because they have the highest silica contents (55.6 to 56.9 percent $SiO_2$), contain phenocrysts of clinopyroxene in addition to plagioclase and rare olivine, and contain pigeonite in the groundmass.

Three magma types (MT) were distinguished on the basis of major-, minor- and rare-earth-element data. Two of the magma types (MT1 and MT2) contain both basalt and basaltic andesite; the third magma type (MT3) contains only basaltic andesite. Basalt of the volumetrically dominant MT1 are less evolved (Mg#=66-62; FeO*=8.0-7.3 percent; $TiO_2$=1.5-1 percent; Cr 295 ppm) than MT2 basalt (Mg#=59-54; FeO*=10.7-10 percent; $TiO_2$=1.95-1.75 percent; Cr 215 ppm) and have lower REE values. MT3 basaltic-andesite lava flows, however, have the lowest REE values.

Petrologic modeling suggests that some basaltic andesite was derived from basalt by crystal fractionation in a closed system, but that differentiation was generally more complex involving open-system processes of crystal fractionation, recharge, and extrusion. Magma mixing between magma types or assimilation of more silicic material improves most models. No basaltic parent was identified for the REE-depleted MT3 basaltic andesite; thus, these lavas may represent 'near-primary' basaltic andesite (Hughes, 1983).

Eruptive activity along the MBVC occurred as four discrete episodes, which are defined on the basis of paleomagnetic data. During two of the eruptive episodes, more than one magma type was emplaced. Geochemical data coupled with spatial and temporal data indicate that the MBVC was underlain by more than one magma chamber or more likely a series of dikes tapping discrete magma sources. Vents of the volumetrically dominant MT1 lava flows are located along the central axis of the chain, whereas vents for the volumetrically much smaller MT2 and MT3 lava flows are found along the periphery or off the main axis of the chain.


## INTRODUCTION

The central Oregon High Cascades are unique with respect to the rest of the range because of the predominance of mafic over silicic volcanism. During the past 2 million years, mafic rocks have comprised about 85 volume percent of the rocks erupted in the central Oregon High Cascades, and about 60 volume percent of the total extrusive rocks for the entire High Cascades (White and McBirney, 1978). Until recently, however (Taylor, 1978; Hughes and Taylor, 1986), attention has tended to focus on the silicic composite volcanoes that dominate the landscape and not on the basalt and basaltic andesite cones and lava flows that occupy the regions between them.

The Mount Bachelor volcanic chain (MBVC), a 25-km-long, N-S-trending chain of cinder cones, lava flows, and shield volcanoes located about 50 km west of Bend, Oregon, typifies one style of mafic volcanism found throughout the central Oregon High Cascades: effusive eruptions of lava from aligned vents over a short time period (fig. 1). Approximately 40 $km^3$ of basalt and basaltic andesite (49 to 57 percent $SiO_2$) were erupted over the 8,000 to 10,000 yr history of the chain (Scott and Gardner, 1985; 1992).

This report describes the eruptive history and geochemical variations of lava flows of the MBVC. Geologic mapping by Scott and Gardner (1992) provided the basic stratigraphic framework in which to refine the temporal evolution of the MBVC and in which to evaluate its geochemical diversity. Results from this study provide a detailed temporal and petrochemical history of a single mafic system and supplement the growing geochemical data base of mafic rocks from the central Oregon High Cascades (see Hughs, 1983; Hughs and Taylor, 1986; Conrey and Sherrod, 1988; Conrey, 1991).

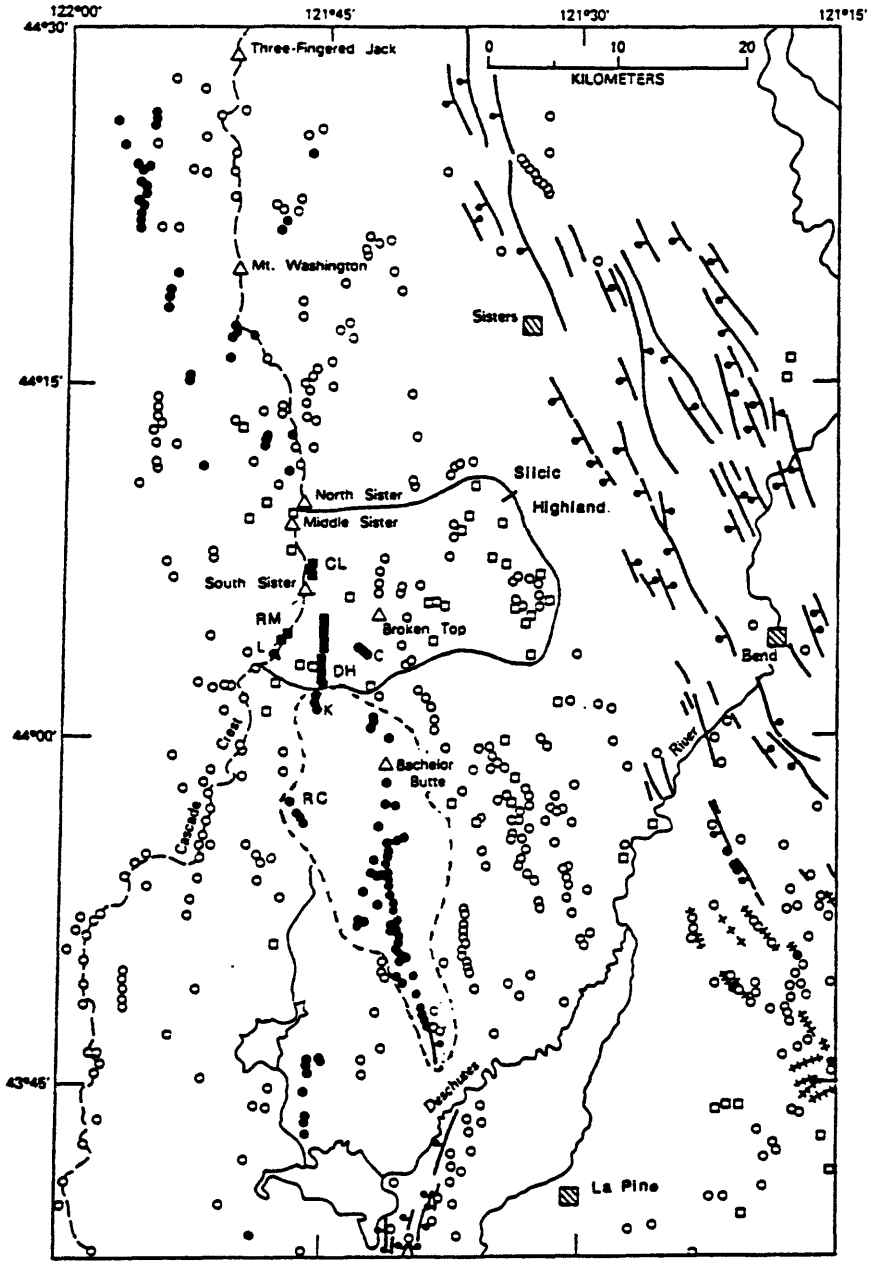


*Figure 1. Compilation of Quaternary vents and faults in the Mount Bachelor-Three Sisters area (modified from Scott, 1987). Triangles are stratovolcanoes; circles are mafic vents (basalt and basaltic andesite); K–Katsuk Butte; R–Red Crater chain of cones; L–Le Conte Crater; C–Cayuse Crater; squares are silicic vents (primarily dacite and rhyodacite), RM - Rock Mesa, CL - Carver Lake, DH - Devil's Hill chain of domes. Filled circles and squares represent vents of latest Quaternary age (<15 ka), open circles and squares are older than latest Quaternary age (>15 ka). Heavy solid lines are faults, the bar and ball symbol are on the downthrown side. Crossed lines are fissures. The dashed area represents the general outline of the Mount Bachelor volcanic chain. The solid line is the approximate outline of the silicic highland (from Hill, 1985).*

## Geologic Setting of the Mount Bachelor Volcanic Chain

The landscape around the MBVC is primarily volcanic in origin with subsequent modification mostly by glacial processes. During Pleistocene time, basalt and basaltic-andesite shield volcanoes built a broad mafic platform (Williams, 1944; McBirney and others, 1974; Taylor, 1978). Concurrent with these early mafic eruptions, silicic products were intermittently erupted along the east side of the mafic platform, creating a highland that was locally inundated by younger basalt and basaltic andesite (Taylor, 1978; Hill, 1985; fig. 1). The glaciated Three Sisters stratovolcanoes overlie the mafic platform and silicic highlands (Taylor, 1987) and were constructed after deposition of the Bend Pumice-Tumalo Tuff, from which K-Ar ages ranging from 0.4-0.29 Ma (Sarna-Wojcicki and others, 1989) have been obtained. During the latest Pleistocene, glacier ice from the Three

Sisters region flowed east and south over the silicic highlands and Bachelor area. The maximum extent of latest Pleistocene glaciation occurred between 22-18 ka (Porter and others, 1983).

The age of the MBVC is bracketed between latest Pleistocene glacial deposits and deposits of Mazama ash (6,850 yr B. P.; Bacon, 1983). During the last Pleistocene glaciation, glacial ice from the Three Sisters-Broken Top area flowed southward into the pre-Mount Bachelor lowlands, depositing moraines and outwash. The earliest lava flows of MBVC are from the Sheridan segment and overlie unweathered till of these end moraines that crop out to the east of Bench Mark Butte (fig. 2). Outwash and loess locally bury these lava flows, which suggests that although ice had retreated from its maximum by the time the lava flows were emplaced, ice probably still remained in the drainage basin (Scott and Gardner, 1989). This hypothesis is supported by field evidence from Katsuk Butte. Lava flows from Katsuk Butte (mk; fig. 2) conformably overlie hyaloclastite deposits suggesting that initially the vent lay below ice or lake height. As eruptive material was deposited around the vent, the vent area was built above ice or water level and lava flows were produced. Ice still may have been present nearby as the west side of Katsuk Butte forms a steep sided plateau suggestive of lava flows abutting against a barrier such as glacial ice. However, no till or striations occur on top of Katsuk Butte which would have been below ice height during the late Pleistocene glacial maximum, indicating that Katsuk Butte postdates that maximum. These lines of evidence suggest a maximum age for the MBVC to be about 18 ka. Growth of the Mount Bachelor shield and cone is estimated to have occurred between 18 and 11 ka. Glacial striations on a cinder cone approximately 1 km northward from the base of Mount Bachelor (7000-ft contour line) indicate that the southward flow of glacial ice was not obstructed by a constructional high in the location of Mount Bachelor during the latest Pleistocene maximum. However morainal deposits that extend beyond the neoglacial limit indicate that the summit cone of Mount Bachelor predates a regional readvance or glacial standstill called the Canyon Creek stade (Scott, 1977) which occurred between 12.5 and 11 ka (Porter and others, 1983). These morainal deposits (fig. 3) have equilibrium-line altitudes similar to moraines on Broken Top that predate the Cayuse Crater scoria, which makes the moraines older than 9500 yr BP (Scott, 1989). Mazama ash--from the cataclysmic eruption of Mount Mazama, dated at 6,850 yr B.P. (Bacon, 1983)--overlies lava flows of the MBVC and provides the limiting younger age for the chain.

North and northwest of the MBVC, post-glacial, pre-Mazama basalt lavas were erupted from the Cayuse Crater (minimum radiocarbon age of 9,520 ± 100 B.P., Scott, 1987) and from Le Conte Crater (fig. 1). The youngest eruptions in the Mount Bachelor area occurred on the south and northeast sides of South Sister volcano. Rhyolite lava flows, domes, and related tephra deposits form the 2000-yr-old Carver Lake and Devil's Hill chain of domes, and the 2300-yr-old Rock Mesa flows (fig. 1; Williams, 1944; Taylor, 1978; Clark, 1983; Scott, 1987; Taylor, 1987).

A geologic map of the MBVC simplified from Scott and Gardner (1992) is shown in figure 2: table 1 gives descriptions of map units . The MBVC is divided into eight major units (mb1-mb6, mk, and mr) primarily on the basis of vent locations; subdivisions within map units are based on local stratigraphic relations and petrologic variations (Scott and Gardner, 1992). Nearly all units consist of lava flows 1 to 5 meters thick that are generally rubbly topped and range from highly vesicular to dense. Tephra deposits are rare and are commonly confined to near-vent areas.

The earliest eruptions of the MBVC were centered in the Sheridan Mountain area (fig. 2; table 1). Three basaltic andesite units were mapped. Unit mb1a consists of two lithologic types (1) plagioclase-phyric lava flows containing large (up to 4 mm in length), blocky euhedral plagioclase phenocrysts and (2) plagioclase- and olivine-phyric lava flows containing abundant fine grained plagioclase. Unit mb1b consists of porphyritic olivine and plagioclase lava flows, and unit mb1c consists of aphanitic lava flows, some with rare euhedral plagioclase phenocrysts to 8 mm, that erupted from cinder cones on the west flank of the Sheridan shield.

The center of eruptive activity migrated south to the Siah segment after eruptions along the Sheridan segment ceased. The Siah segment is composed of numerous cinder cones

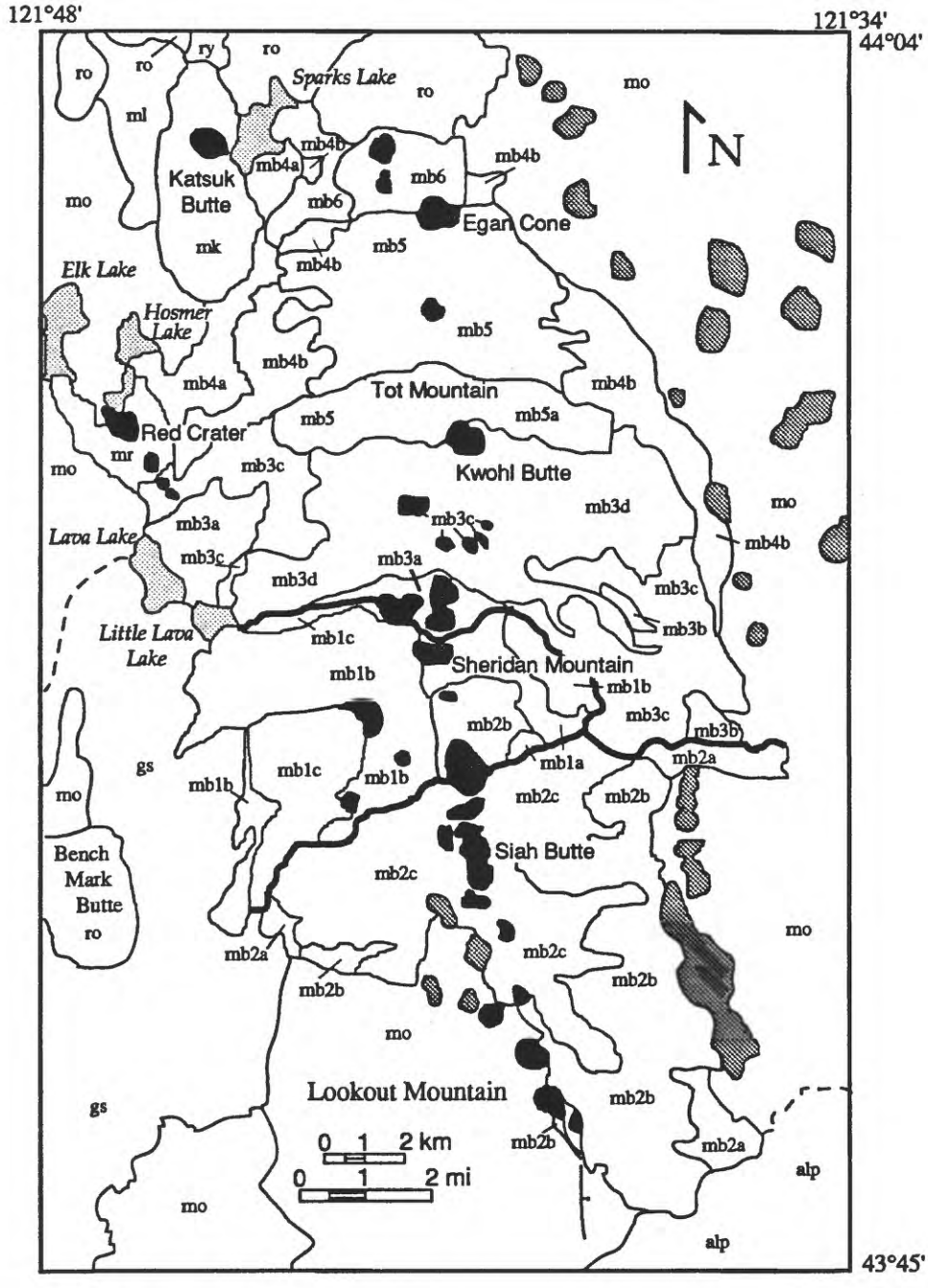


*Figure 2. Simplified geologic map of the Mount Bachelor volcanic chain (modified from Scott and Gardner, 1992). Bar and ball denote fault at the southern end of the chain - ball is on downthrown side. Dark stipple pattern denotes vents of the MBVC, medium stipple pattern denotes older vents not part of the MBVC. Heavy lines separate the Bachelor-Kwohl, Sheridan, and Siah segments. See table 1 for description of map units.*

*Table 1. Description of map units for simplified geologic map of the Mount Bachelor volcanic chain and surrounding area*

| Map Unit | Sub Unit | Lithologic Descriptions |
|---|---|---|
| | *Lava flows from the Mount Bachelor volcanic chain from oldest to youngest* | |
| **mb1** | | low-silica (52-55 percent $SiO_2$) basaltic-andesite lava flows and scoria from the Sheridan segment |
| | mb1a | medium dark gray, abundant large euhedral plagioclase pheoncrysts (up to 4 mm) with very minor olivine; medium gray, very abundant fine laths of plagioclase with minor olivine |
| | mb1b | medium gray, porphyritic and glomerophyric (olivine>plagioclase) |
| | mb1c | medium gray to medium dark gray, aphyric with very rare plagioclase phenocrysts to 8 mm |
| **mb2** | | basalt (<52 percent $SiO_2$) lava flows and scoria from the Siah segment |
| | mb2a | medium gray, porphyritic, olivine with minor plagioclase; equivalent in age to mb1c |
| | mb2b | medium gray, porphyrictic, olivine with minor plagioclase |
| | mb2c | medium gray, porphyritic and glomerophyric, olivine>plagioclase |
| **mb3** | | basalt and low-silica basaltic andesite lava flows and scoria from the Kwohl Butte shield |
| | mb3a | medium gray to light gray, porphyritic olivine basalt with abundant laths of very fine plagioclase; lava flows dam Lava and Little Lava Lakes |
| | mb3b | medium dark gray, porphyritic basaltic andesite lava flows with large euhedral plagioclase crystals to 4 mm and minor olivine |
| | mb3c | medium dark gray basalt with olivine or with olivine and plagioclase |
| | mb3d | medium gray baslatic andesite, porphyritic and glomerophyric, olvine and plagioclase in roughly equal proportions |
| **mb4** | | basalts and low-silica basaltic-andesite lava flows and scoria that form the Mount Bachelor shield |
| | mb4a | medium gray basalt, porphyritic with olivine or olivine and fine-grained plagioclase |
| | mb4b | medium gray basalt and basaltic andesite, porphyritic and glomerophyric with fine-grained plagioclase and olivine (plagioclase>olivine) |
| **mb5** | | high-silica basaltic-andesite lava flows and scoria from the Mount Bachelor summit cone and Tot Mountain |
| | mb5 | medium gray to light gray basaltic andesite from the summit of Mount Bachelor, highly porphyritic and glomerophyric with plagioclase, augite, and olivine; plagioclase dominant with subordinate amounts of augite and rare olivine |
| | mb5a | medium gray basaltic andesite from Tot Mountain, in appearance similar to the Mount Bachelor summit lithology but lacking augite |

Table 1. continued

| Map Unit | Sub Unit | Lithologic Descriptions |
|---|---|---|
| **mb6** | | medium gray basalt and low-silica basaltic andesite lava flows and scoria from Egan Cone, basalt lava flows contain scattered olivine with a few large euhedral plagioclase phenocrysts to 6 mm; basaltic andesite lava flows are plagioclase and olivine phyric |
| **mk** | | medium dark gray olivine basalt lava flows with minor plagioclase thay froms Katsuk Butte |
| **mr** | | medium dark gray olivine basalt lava flows and scoria with from the Red Crater chain of cinder cones |
| | *Other volcanic units* | |
| **ml** | | medium dark gray olivine basalt lava flows and scoria from Le Conte Crater |
| **ry** | | light gray rhyolite lava flows and tephra deposits from the Devils Hill chain of domes |
| **mo** | | mafic and andesitic volcanic rocks older then pre-latest Pleistocene glaciation (>18,000 yrs) |
| **ro** | | older rhyolitic and dacitic lava flows of Pleistocene age |
| | *Non-volcanic units* | |
| **gs** | | glacial deposits, upper Pleistocene (last major glaciation) |
| **alp** | | middle to lower Pleistocene alluvial and lacustrine deposits of the La Pine basin |

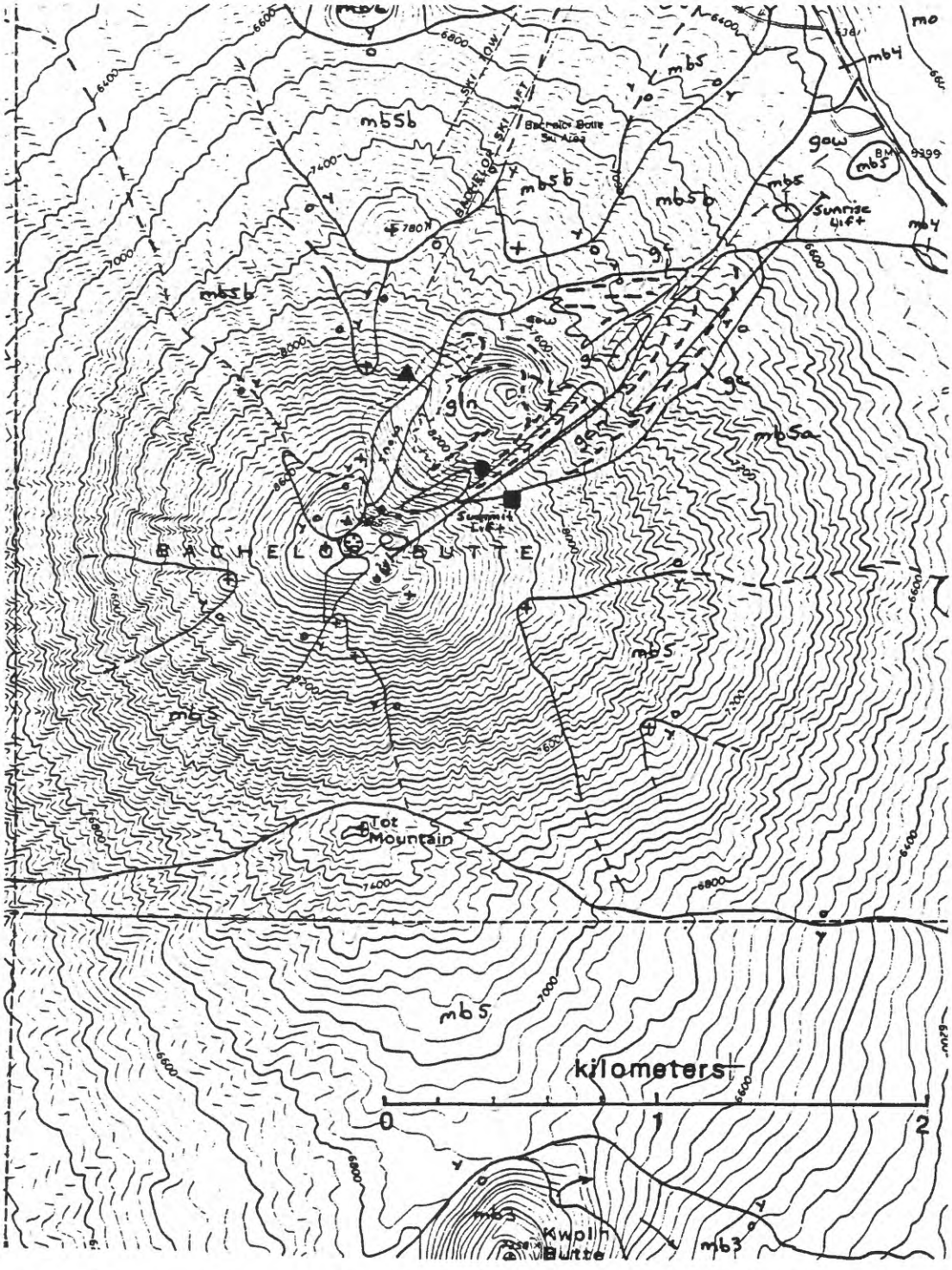


*Figure 3. Geologic map of the uper flanks of Mount Bachelor. (modified from Scott, 1989) Map units are the same as those given in table 1 except that the glacial deposits and lava flows on Mount Bachelor are subdivided into lava flows that predate the moraines of Canyon Creek age (mb5a) and those that post-date those moraines (mb5b). Glacial deposits are divided into gow - glacial outwash; gen - early neoglacial drift; gln - late neoglacial drift; gc - drift of Canyon Creek age . Symbols show locations of paleomagnetic sites: triangle - G85-14; circle - G86-4; square G85-15 (see section on paleomagnetic results).*

and their basalt lava flows. Two basalt units were mapped; an olivine-phyric basalt (mb2a and b) which is overlain by olivine- and plagioclase-phyric basalt (mb2c). Field relations show that at least some of the younger plagioclase-bearing basalt emanated from vents of olivine-phyric basalt cinder cones.

After eruptions along the Siah segment had largely ceased, activity shifted to the north where basalt and basaltic andesite were erupted along the Bachelor-Kwohl segment (figs. 2; mb3, mb4, and mb5). Basalt lava flows from the Kwohl shield (mb3) overlie lava flows from both the Sheridan and Siah segments (mb1 and mb2). In turn, basalt and low-silica basaltic-andesite (52-54 percent $SiO_2$) lava flows from the Mount Bachelor shield (mb4) overlie basalt from the Red Crater chain of cinder cones (mr), Katsuk Butte (mk), and the Kwohl shield (mb3). The Mount Bachelor shield is capped by a high-silica basaltic-andesite (mb5; 54-57 percent $SiO_2$). Tot Mountain (mb5a), a vent on the south flank of Mount Bachelor, post-dates the main constructional phase of the summit cone, but it is not known if it is younger than all of the Mount Bachelor summit cone vents. Activity along the MBVC ended with basaltic eruptions from the Egan cone (mb6). Tephra from the climatic eruption of Mount Mazama overlies Egan cone and thus all of the MBVC units (Scott and Gardner, 1992). The contact between the overlying Mazama ash and Egan scoria is sharp, and there is no evidence of weathering or reworking of material at the contact. This suggests that the Egan eruptions probably occurred shortly before the cataclysmic eruption of Mount Mazama and indicates a minimum age for the MBVC of about 8 ka.

A fault at the southern end of the MBVC (fig. 2) slightly offsets the Pleistocene lava flows of Lookout Mountain; however, none of the lavas from the MBVC are disturbed. The age of the fault is unknown, except that it pre-dates MBVC activity. There is no evidence of folding or faulting along the chain, athough there has been minor tiliting of flow surfaces related to flowage and cooling.

Only one radiocarbon age directly relates to the eruptive activity along the MBVC. Organic-rich sediment from the base of a 3.5-m-long sediment core from a shallow valley dammed by lava flows of the Sheridan segment (unit mb1b; fig. 2) yielded a radiocarbon age of 12,200 ± 150 yr B. P. (Scott and Gardner, 1989; 1992), which falls within the time frame deduced from glacial and volcanic stratigraphy. The radiocarbon age is considered a minimum age because: 1) organic material did not begin accumulating until after the lava flow was emplaced; 2) it would take some time for the amount of organic material needed for a sample to accumulate; and 3) the sample may be contaminated by roots of younger organic material.

## PALEOMAGNETIC DATA

### Introduction

Lava flows of the MBVC are either too young or too K-poor for determination of numerical ages by means of radiometric (K-Ar, Ar-Ar, or U-Th) dating techniques. This, coupled with the lack of flow-related organic material for carbon-14 analysis, prompted a paleomagnetic secular-variation (PSV) study to correlate spatially separated lava flows. Paleomagnetic directions can be used for correlation because volcanic rocks record the direction of the ambient geomagnetic field as they cool, and because the ambient field direction changes rapidly enough to see differences on the order of centuries (Champion, 1980; Hoblitt and others, 1985; Kuntz and others, 1986). Lava flows that have dissimilar paleomagnetic directions are of different ages. Lava flows that have similar paleomagnetic directions may be of similar age or of different ages because the orientation of the secular field has been in the same direction at different times in the past (Champion, 1980; Tarling, 1983). Thus, knowledge of basic stratigraphic relationships is needed to interpret the PSV data.

### Field and Laboratory Techniques

Lava flows at approximately 50 sites (fig. 4) were drilled in the MBVC area, and at each site several blocks separated by joints were sampled. All samples were drilled in the field by means of a portable drill, and oriented with both magnetic and sun compasses. Between 6 and 16 samples were collected at each site. Samples from roadcuts gave the best results;

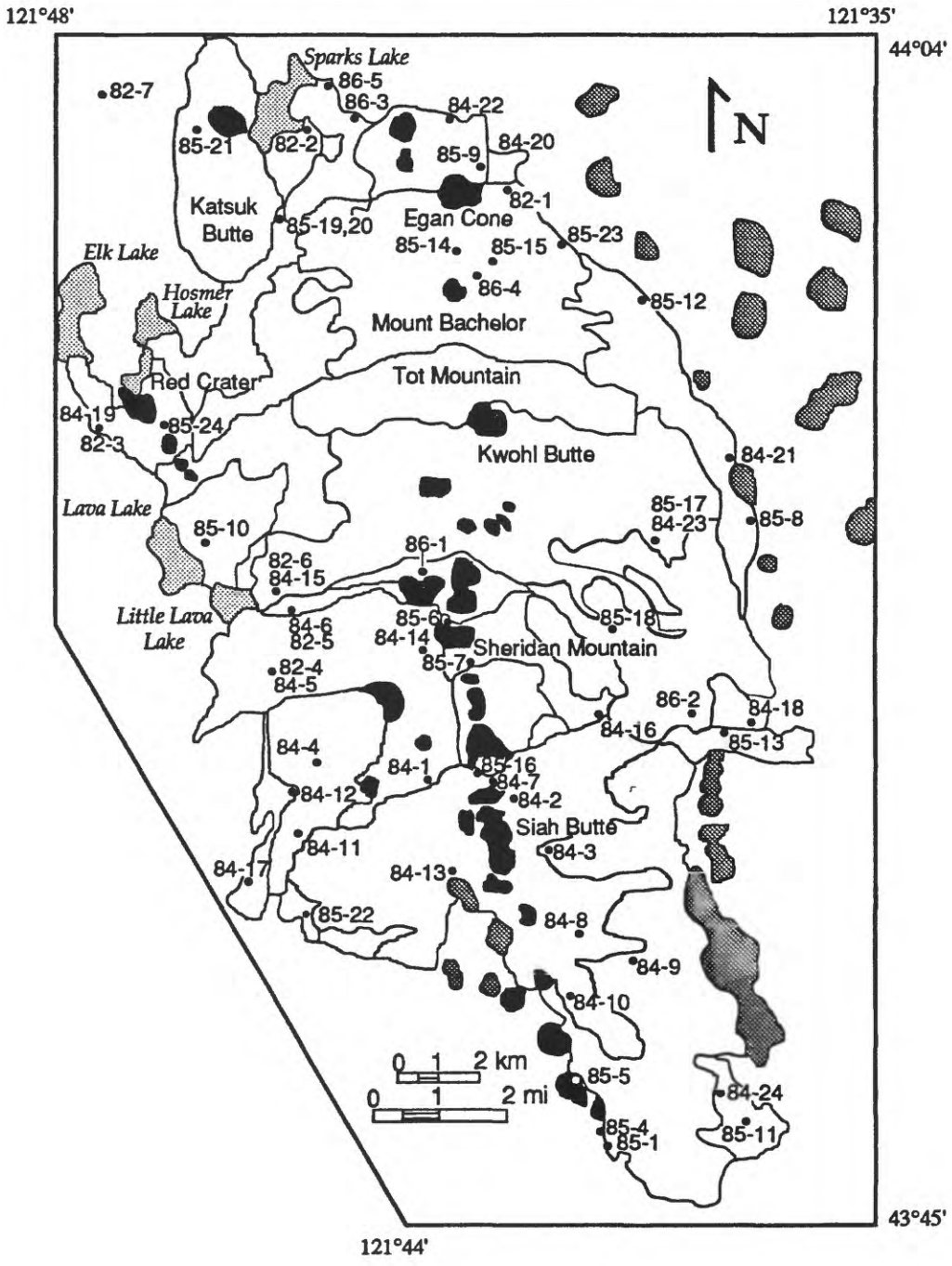


*Figure 4. Map of paleomagnetic site locations. In some cases more than one site was drilled from the same general area (for example, 82-6 and 84-15). Unit outlines from figure 2.*

samples from lava levees, roofs and walls of collapsed lava tubes, pit craters, flow tops, and lava flows exposed in the west wall of the Mount Bachelor cirque were tried with variable results. Conventional, well-established methods were used to collect paleomagnetic samples and to process them in the laboratory; excellent summaries of these techniques can be found, for example, in Champion (1980) and Tarling (1983).

Field-oriented samples between 4 and 6 cm in length and 2.4 cm in diameter were cut to 2.3-cm specimen lengths for laboratory analysis. Remanent magnetization for each specimen was measured by means of a spinner magnetometer, and the results were corrected for the attitude of the sample in the field to determine the paleodeclination (D) and paleoinclination (I; in this report all inclinations are down, i.e. are of normal polarity). After initial measurement of natural remanent magnetization (NRM), all samples were demagnetized in an alternating field-demagnetizer progressively at 5, 10, 20, 30, 40, and 50 milliteslas (mT) or until 50 percent of the remanence was removed—to test the stability of the remanent magnetism—and remeasured. As is often the case in young volcanic rocks, the samples showed little to no signs of a viscous or chemical overprint.

The time represented by two different paleomagnetic directions is a function of the rate and direction of change of the geomagnetic field, neither of which is constant. An average rate of change of about 4° per century (determined for the last 2000 years in central California, Mankinen and others, 1986) should differentiate between rocks whose cooling times are separated by 50 to 100 years. However, the path of the geomagnetic field vector is not unidirectional and the rate of change of the field is not constant over time. Because of these uncertainties I have not determined absolute ages for the MBVC lava flows or the time period separating various eruptions.

## Results

A compilation of the paleomagnetic data is given in table 2. Sites G84-11, G85-22, G85-24, G86-1, G85-19, and 82-1 (table 2), are excluded from the following discussions either because the dispersions about their respective site means are too large (high $\alpha 95$, $k<100$) to allow for meaningful interpretation or because the direction (G85-19) appeared anomalous for the area. Samples of the first five excluded sites were taken from flow margins that were thought in the field to be only marginally reliable because of suspicions of post-cooling rotation. Samples of the last excluded site were from a roadcut, but the dispersion of specimen directions suggests that it had either been hit by lightning (a cable from a ski lift terminus is grounded in the outcrop) or disturbed by blasting.

Mean site directions and corresponding cones of 95 percent confidence (fig. 5a) indicate two major groupings of directions: a shallow, slightly eastward trending group (D = 350° to 15°; I= 45° to 55°), and a steep, more westerly trending group (D = 330° to 5°; I = 62° to 72°). When mean site directions are keyed to vent locations, both major groups can be subdivided into subgroups (fig. 5b). Paleomagnetic directions of the major shallow group cluster about D=0° and I=50° down and about D=5° to 10° and I=45° and correspond to lava flows from vents mainly along the axis and west flank of the Sheridan segment respectively. Directions of the steeper group cluster about D=0° and I=70° and about D=340° and I=65° and correspond to lava flows from the Siah segment and Bachelor-Kwohl segment vents respectively. Paleomagnetic directions for basaltic lava flows from Egan cone (the youngest lava flows of the MBVC) are about D=358° I=66°. I have assigned each group to an eruptive episode on the basis of similarity of paleomagnetic direction and vent locations for the lava flows. The Sheridan Mountain flows are assigned to episode I (a and b to distinguish between the two shallow clusters), the Siah flows to episode II (D=0° and I=70°), the Bachelor-Kwohl segment lava flows (D=340° and I=65°) to episode III, and the basalt Egan cone lava flows to episode IV.

Lava flows with paleomagnetic directions clustered around D=0°, I=54° (episode Ia) include the porphyritic, low-silica basaltic-andesite lava flows erupted from vents along the main axis of the Sheridan shield (mb1a and mb1b), and the basaltic lava flows of Red Crater (mr) and Katsuk Butte (mk; fig. 4). The similarity in paleomagnetic directions (table 2; fig. 5b) from these centers suggests that their eruptions were broadly coeval, which is consistent with stratigraphic relations. Early lavas from the Sheridan segment directly

*Table 2. Summary of paleomagnetic data.*

| Map unit | outcrop | Site | Expt | Dec | Inc | N/N1 | a95 | k | Arith av J |
|---|---|---|---|---|---|---|---|---|---|
| mb1a | rd cut | G84-16 | 5 mT | 1 | 51 | 11/11 | 1.9 | 561 | 0.801 |
| mb1a | pit | G84-14 | 20 mT | 6 | 56 | 14/8 | 2.5 | 512 | 0.291 |
| mb1b | flow front | G84-12 | 20 mT | 355 | 52 | 14/14 | 2.5 | 261 | 0.470 |
| mb1b | rd cut | G84-17 | 20 mT | 358 | 53 | 16/16 | 2.1 | 337 | 1.124 |
| mb1b | rd cut | G84-1 | 10 mT | 357 | 55 | 14/14 | 1.4 | 852 | 0.760 |
| mb1b | rd cut | 82-4 | 5 mT | 355 | 54 | 5/5 | 2.4 | 980 | 0.568 |
| mb1b | rd cut | G84-5 | 20 mT | 359 | 52 | 7/6 | 3.6 | 343 | 0.357 |
| | | avg | | 359 | 53 | 7/7 | 2.3 | 727 | 0.624 |
| mr | rd cut | 82-3 | 10 mT | 0 | 56 | 9/8 | 2.1 | 692 | 0.250 |
| mr | rd cut | G84-19 | 10 mT | 358 | 55 | 8/8 | 1.6 | 1225 | 0.231 |
| mr | tube | G85-24 | 10 mT | 336 | 47 | 10/9 | 3.7 | 192 | 0.982 |
| mr | flow mar | G85-21 | 10 mT | 5 | 57 | 12/9 | 2.1 | 621 | 0.822 |
| | | avg | | 1 | 56 | 4/3 | 3.1 | 1556 | 0.434 |
| mb1c | rd cut | G84-6 | 5 mT | 5 | 46 | 6/5 | 2.2 | 1190 | 0.559 |
| mb1c | flow mar | G84-11 | 30 mT | 8 | 72 | 12/10 | 12.8 | 15 | 0.129 |
| mb1c | flow top | G85-6 | 10 mT | 9 | 51 | 10/7 | 2.7 | 518 | 1.628 |
| mb1c | rd cut | G84-4 | 5 mT | 11 | 49 | 14/12 | 2.5 | 394 | 0.506 |
| mb1c | rd cut | 82-5 | 20 mT | 6 | 44 | 5/4 | 2.5 | 1390 | 0.345 |
| mb1c | pit | G85-7 | 30 mT | 8 | 46 | 11/10 | 2.0 | 611 | 0.270 |
| mb2a | flow mar | G85-13 | 5 mT | 8 | 51 | 8/3 | 5.2 | 558 | 0.635 |
| mb2a | tube | G84-24 | 20 mT | 11 | 48 | 14/14 | 1.7 | 543 | 0.496 |
| mb2a | flow mar | G85-22 | NRM | 10 | 56 | 12/12 | 5.2 | 70 | 1.363 |
| | | avg | | 8 | 48 | 9/7 | 2.3 | 718 | 0.634 |
| mb2b | levee | G85-5 | 10 mT | 358 | 71 | 7/6 | 3.0 | 498 | 0.379 |
| mb2b | agglu | G85-4 | 10 mT | 330 | 73 | 9/9 | 3.1 | 279 | 0.773 |
| mb2b | rd cut | G85-1 | 10 mT | 355 | 73 | 11/11 | 1.4 | 1016 | 0.294 |
| mb2b | tumuli | G84-10 | 10 mT | 7 | 71 | 15/15 | 2.4 | 272 | 0.884 |
| mb2b | flow top | G84-7 | 10 mT | 10 | 69 | 16/14 | 1.3 | 935 | 0.527 |
| mb2b | flow mar | G84-3 | 5 mT | 357 | 67 | 9/6 | 3.9 | 300 | 0.578 |
| mb2b | rd cut | G84-9ab | 5 mT | 1 | 70 | 15/13 | 1.8 | 528 | 0.463 |
| mb2b | rd cut | G85-16 | 10 mT | 348 | 70 | 14/13 | 1.8 | 526 | 0.883 |
| mb2c | rd cut | G84-2 | 20 mT | 357 | 70 | 12/12 | 1.3 | 1116 | 0.267 |
| mb2c | rd cut | G84-8b | 10 mT | 351 | 73 | 10/9 | 2.3 | 513 | 0.481 |
| mb2c | rd cut | G84-13 | 10 mT | 359 | 72 | 14/14 | 1.7 | 554 | 0.644 |
| mb2c | rd cut | G84-8a | 5 mT | 353 | 70 | 4/4 | 1.7 | 2919 | 0.903 |
| | | avg | | 358 | 71 | 12/11 | 1.6 | 846 | 0.573 |
| mb4a? | flow mar | 82-2 | 20 mT | 6 | 63 | 5/5 | 0.9 | 6594 | 0.595 |
| mb3b | tumuli | G85-10 | NRM | 13 | 59 | 12/12 | 2.6 | 274 | 0.778 |
| mb3b | flow mar | G84-18 | 10 mT | 338 | 63 | 10/8 | 3.8 | 210 | 1.027 |
| mb3c | flow mar | G86-2 | NRM | 338 | 63 | 7/7 | 4.1 | 221 | 0.603 |
| mb3c | flow mar | G86-1 | NRM | 351 | 57 | 7/5 | 10.8 | 51 | 1.522 |
| mb3c | flow mar | G85-18 | NRM | 341 | 65 | 9/6 | 4.9 | 190 | 2.018 |
| mb3d | flow mar | G85-17 | 30 mT | 345 | 66 | 12/12 | 4.3 | 103 | 1.018 |
| mb3d | rd cut | 82-6 | 50 mT | 342 | 68 | 7/7 | 2.6 | 527 | 0.481 |
| mb3d | flow mar | G84-23 | NRM | 355 | 63 | 11/7 | 4.2 | 206 | 1.504 |
| mb3d | rd cut | G84-15 | 20 mT | 336 | 67 | 15/14 | 1.3 | 968 | 0.386 |
| mb4a | levee | G85-20 | 20 mT | 352 | 69 | 8/8 | 2.2 | 634 | 0.381 |
| mb4a | tumuli | G85-19 | 20 mT | 326 | 57 | 7/7 | 2.8 | 456 | 0.295 |
| mb4b | rd cut | G84-21 | 20 mT | 346 | 66 | 15/15 | 1.5 | 624 | 0.475 |
| mb4b | rd cut | G85-8 | 20 mT | 347 | 65 | 9/9 | 2.2 | 529 | 0.766 |
| mb4b | flow mar | G85-12 | 40 mT | 339 | 65 | 13/13 | 2.0 | 410 | 0.733 |
| mb4b | rd cut | G84-20 | 5 mT | 342 | 60 | 13/13 | 1.7 | 567 | 0.611 |
| mb5 | rd cut | 82-1 | 20 mT | 293 | 30 | 6/6 | 31.2 | 6 | 0.991 |
| mb5 | levee | G86-4 | 40 mT | 336 | 61 | 8/7 | 2.5 | 569 | 1.345 |
| mb5 | flow top | G86-15 | 5 mT | 357 | 65 | 8/6 | 3.6 | 357 | 0.460 |
| mb5 | flow mar | G86-14 | NRM | 331 | 67 | 6/5 | 4.4 | 301 | 0.195 |
| mb5 | tumuli | G85-23 | 30 mT | 334 | 65 | 13/10 | 4.6 | 110 | 0.484 |
| mb6 | rd cut | G86-5 | 10 mT | 329 | 70 | 9/9 | 2.0 | 663 | 1.469 |
| mb6 | rd cut | G86-3 | NRM | 335 | 69 | 10/8 | 4.0 | 188 | 2.124 |
| | | avg | | 341 | 65 | 22/18 | 1.8 | 389 | 0.949 |
| mb6 | rd cut | G84-22 | 5 mT | 2 | 65 | 13/11 | 1.9 | 575 | 1.071 |
| mb6 | gutter | G85-9 | 20 mT | 356 | 71 | 11/11 | 2.4 | 361 | 0.810 |
| lc | rd cut | 82-7 | 5 mT | 338 | 69 | 5/4 | 5.3 | 304 | 0.626 |

*Explanation: Map unit, geologic map units shown in figure 2 and described in table 1; Expt., demagnetization level resulting in the least dispersion; Dec, declination in degrees N; inclination in degrees, positive downwards; N/N1 - total number of samples for site/number of samples used for statistical analysis; a95, semiangle of cone of of 95% confidence in degrees; k precision parameter (Fisher 1953); Arith av j, arithmetic average intensity in Am-1.*

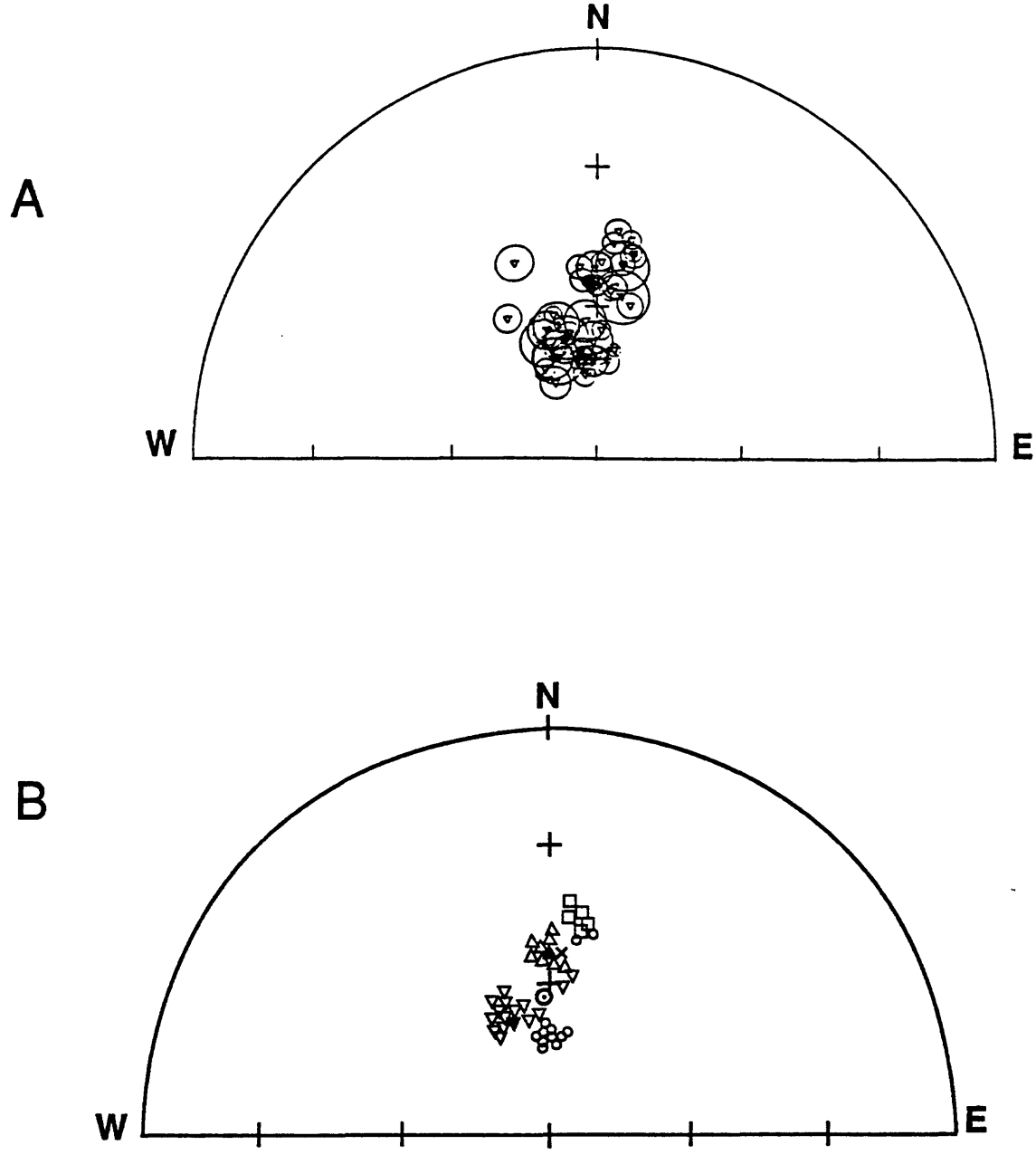


*Figure 5. Lower hemisphere equal-area stereonet of mean site paleomagnetic directions. Tick inerval in 30 degrees. A. Mean site paleomagnetic directions and corresponding cones of 95 percent confidence for all MBVC sites except 82-1 (cone of confidence too large). B. Mean site directions correlated to vent locations: open triangles up - vents along the central axis of Sheridan Mountain; open squares - vents of the aphanitic lava flows on the west flank of Sheridan Mountain; open circles - Siah-segment vents; open triangles down - Bachelor-Kwohl segment vents; circle with dot - Egan cone basalt; filled triangle up - Red Crater; x - Katsuk Butte; filled traingle down - Le Conte Crater.*

overlie morainal deposits, tephra of Red Crater lies on unweathered till, and lavas from Katsuk Butte are interpreted as having erupted near the end of the glacial maximum (Scott and Gardner, 1989; 1992).

Aphanitic low-silica basaltic-andesite lava flows that erupted from vents on the west flank of the Sheridan shield (mb1c) and an olivine basalt lava flow exposed in a pit crater just south of Sheridan Mountain (site G85-7; mb1c) overlie rocks of map units mb1a and mb1b (fig. 2) and are assigned to episode Ib. Paleomagnetic directions from these flows (D=8°, I=47°) are shallower and more easterly than directions determined for episode Ia (fig. 5b). In addition, two lava flows (fig. 2, mb2a) on the eastern margin of the Siah segment (sites, G84-24,G85-22, and G85-13, fig. 4) have directions similar to these younger lava flows of the Sheridan segment and thus are also assigned to eruptive episode Ib. Stratigraphically, these two Siah lava flows are among the oldest of the Siah chain, although chemically they are indistinguishable from later Siah lava flows. I have chosen to include all the eruptive activity that occurred along the Sheridan segment under episode I, because of the general coincidence of vent locations and paleomagnetic directions. However, to highlight the change in paleomagnetic direction that also corresponds to a change in vent location and petrography of eruptive products during episode I, the subscripts, a and b, are added. The slight change in paleomagnetic direction from episode Ia to episode Ib may correspond to a minor hiatus in eruptive activity.

Basalt lava flows from numerous cinder cones coalesced along the Siah segment during episode II. Two temporally related rock types are exposed: an olivine phyric basalt (mb2b) that is everywhere overlain by an olivine- and plagioclase-phyric basalt (mb2c). Paleomagnetic directions for these two rock types, however, are indistinguishable (D=0°, I=71°). Similarity in paleomagnetic directions of all lava flows sampled in the Siah area (fig. 5b), excluding those of episode Ib, indicates that eruptive activity along the Siah chain was brief, probably lasting no more than a century or two. The considerable difference in paleomagnetic directions between episodes Ib and II suggests that a hiatus in eruptive activity occurred along the MBVC between these two episodes which probably lasted on the order of several hundred to a few thousands of years.

Eruptive activity shifted northward to the Bachelor-Kwohl segment during episode III. Lava flows from Mount Bachelor and Kwohl Butte vents overlie lava flows from the Sheridan and Siah segments as well as from the Red Crater chain of cones and Katsuk Butte. Although paleomagnetic directions from the Bachelor-Kwohl segment are moderately well grouped (fig. 5b) and the mean of the site mean distinct from those of other eruptive episodes (table 2), it is difficult to match paleomagnetic directions with known stratigraphic position. The resolution of the paleomagnetic data is poor largely because of the lack of suitable drill sites. Few roads intersect lava flows in this area and it is difficult to find unrotated blocks on the youthful, rubbly topped lava flows.

No roadcuts intersect the oldest lavas of the Bachelor segment (mb3a-c; figs. 2 and4). Paleomagnetic directions from four sites within these earliest flows (sites G84-18, G85-18, G85-20, and G86-2) range from D=352°, I=69° (a95-2.2), for an olivine basalt tumulus on the west side of Mount Bachelor (G85-20), to D=338°, I=63° (a95-3.8), for a basaltic andesite lava flow front, southeast of Sheridan Mountain (G84-18; table 2). The similarity between the direction from the olivine tumulus and the average direction for episode II suggests, but in no way verifies, that early activity along the Bachelor segment may have begun soon after, or during, eruptive activity along the Siah segment.

Low-silica basaltic-andesite lava flows from Kwohl Butte (mb3d) and from the upper flanks of Mount Bachelor shield (mb4b) are younger than the basalt lava flows that built much of the Mount Bachelor and Kwohl shields and older than the high-silica basaltic-andesite flows of the Mount Bachelor summit cone and Tot Mountain (mb5). Four roadcut and two flow-margin sites were drilled (G84-21; G85-8; G84-20; G84-15; G85-12; and G84-23) and give a mean direction of D=346°, I=63°. The data from these sites indicate that after episode II there was an overall shift in the geomagnetic field vector towards a more westerly direction (Fig 5b; table 2).

Four high-silica basaltic-andesite lava flows from the summit cone of Mount Bachelor

(G85-14, G86-4, G85-15, and G85-23; fig. 4) have similar directions. These paleomagnetic directions are slightly westward of the directions from the low-silica basaltic-andesites lava flows. The stratigraphic relation between sites G85-14, G86-4, and G85-15 and the moraines correlative with the Canyon Creek advance is speculative; however, site G85-14 appears to be younger and sites G86-4 and G85-15 appear to be older than the moraines (see fig. 3). Paleomagnetic directions for the three sites, however, are indistinguishable. Thus, if the field correlations are correct, the implication of the paleomagnetic data is that the surface of a volcanic edifice may cool sufficiently and that a glacier can grow, erode, and retreat on the order of centuries before substantial change in the direction of the geomagnetic field has occurred. Alternatively, the geomagnetic field may have rather fortuitously returned to the pre-glacial direction after deposition of the moarainal deposits.

Although the paleomagnetic results from the Bachelor-Kwohl segment are too poor to resolve the progression of the magnetic field vector from the oldest to youngest lava flows, the following points are made. 1) Paleomagnetic directions from Bachelor-Kwohl segment lava flows are moderately well grouped indicating that no major hiatus occurred during the emplacement of these flows At the same time, there appears to be a general westward shift in the direction of the magnetic field vector during episode III, indicating that eruptions occurred over a long enough time span, perhaps on the order of centuries to a thousand years (?), for the direction of the geomagnetic field vector to change. 2) The mean of the site means of episode III lava flows is distinctly different from either that of episodes I, II, or IV. 3) Combined paleomagnetic and field data suggest that most, if not all, of the activity along the Bachelor segment occurred after magmatism had ceased along the Sheridan and Siah segments.

Numerous olivine-phyric basalt cinder cones and associated small lava flows of uncertain age are present on the north and south flanks of the Sheridan shield (fig. 2). The basalt cinder cones and associated lava flows overlie lava flows of episode I and are chemically similar to basalt erupted throughout the MBVC. Only one lava flow on the south flank was sampled (G85-16, fig. 4; table 2) and it yielded a paleomagnetic direction similar to that of episode II. Based on this one direction, I have tentatively assigned the cinder cones on the south flank of the Sheridan shield to episode II. Only one lava flow on the north flank was sampled (G86-1, table 2) and it yielded a spurious direction; thus it cannot be assigned to an eruptive episode on the basis of paleomagnetic direction. However, based on geographic location and its high intensity of remanent magnetization (the Bachelor-Kwohl lava flows on average have a higher intensity than lava flows from the other segments; table 2), I have assigned the north flank cinder cones to episode III. The placement of these cinder cones within eruptive episodes is admittedly tenuous; however, difficulties in finding suitable drilling sites coupled with the similarity of basalt chemistry throughout the MBVC makes it difficult to determine the relative ages of these deposits.

Three site directions (G85-10, 82-2, and G84-22) do not correspond to the eruptive episodes discussed above. All three sites have similar directions (table 2) but stratigraphic relations dictate that they are not the same age. Lava flows of sites 82-2 and G85-10 are amongst the earliest lava flows from the Bachelor-Kwohl segment, whereas basaltic lava flows from the Egan cone (sites G84-22 and G85-9; table 2) overlie flows from the summit cone of Mount Bachelor. Neither site direction for the two older flows is thought to be reliable; 82-2 samples all came from the same block, and G85-10 samples are from a tumulus. Because of the uncertainty as to whether these are reliable sites, I have not assigned either site to an eruptive episode, but recognize that the directions may be valid. If the directions are valid it would suggest that some of the earliest Bachelor shield lava flows were emplaced at a time distinctly different than the bulk of the edifice.

Paleomagnetic directions for the basalt lava flows of Egan cone are different than directions for the Bachelor-Kwohl segment. However, earlier basaltic-andesite lava flows that also appeared to emanate from the Egan have directions similar to those of episode III (mb6, table 2). If the basalt directions are reliable, it suggests that there was a hiatus in activity both between eruptive activity of the

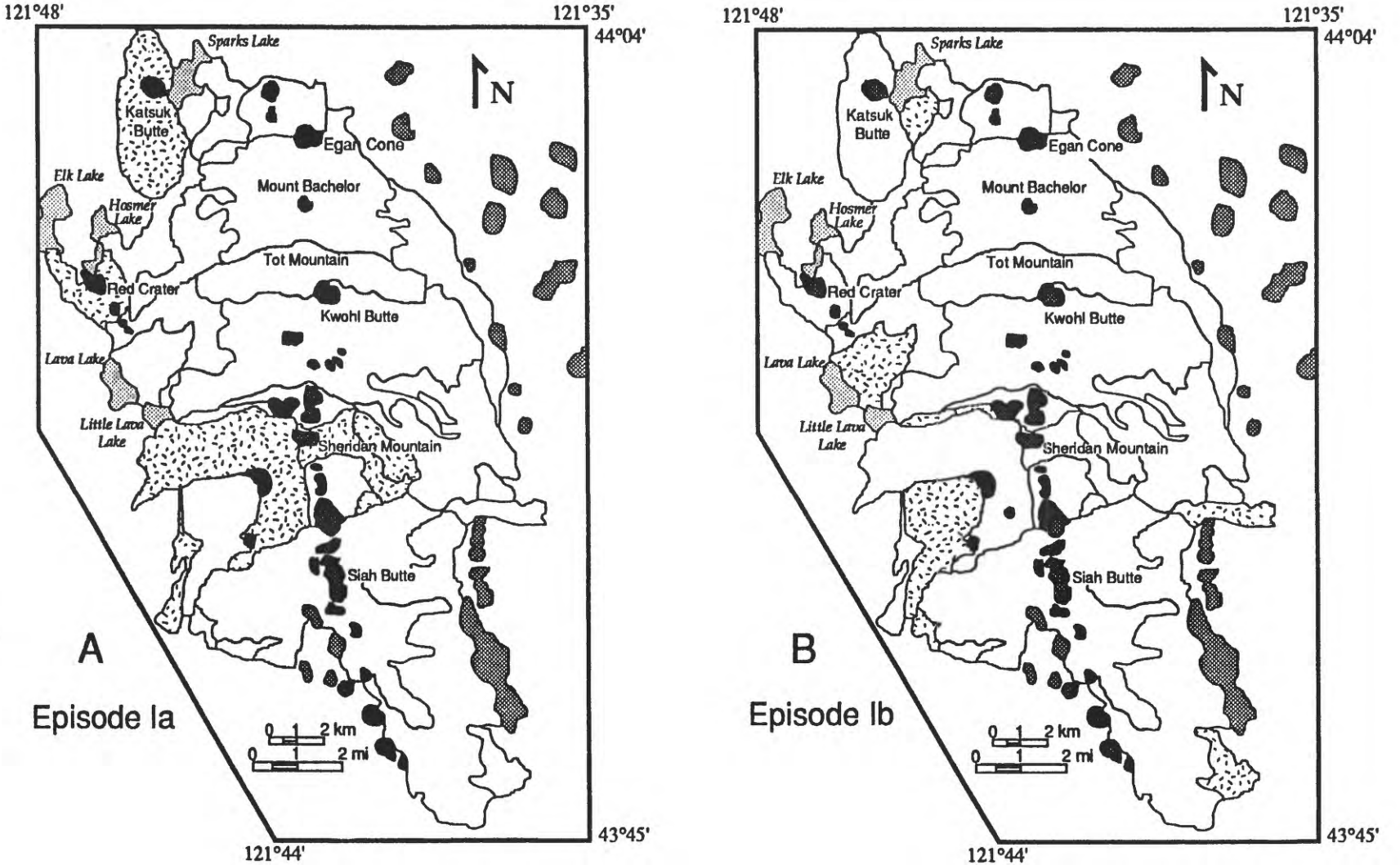


*Figure 6. Maps showing the spatial and temporal evolution of the MBVC based on field and paleomagnetic studies. Patterns indicate areas of eruptive activity during each eruptive episode: A - eruptive episode Ia; B - eruptive episode Ib; C - eruptive episode II; D - eruptive episode III; E - eruptive episode IV. Dark stipple pattern outlines vents of the MBVC, medium stipple pattern are older vents. Unit oulines from figure 2.*

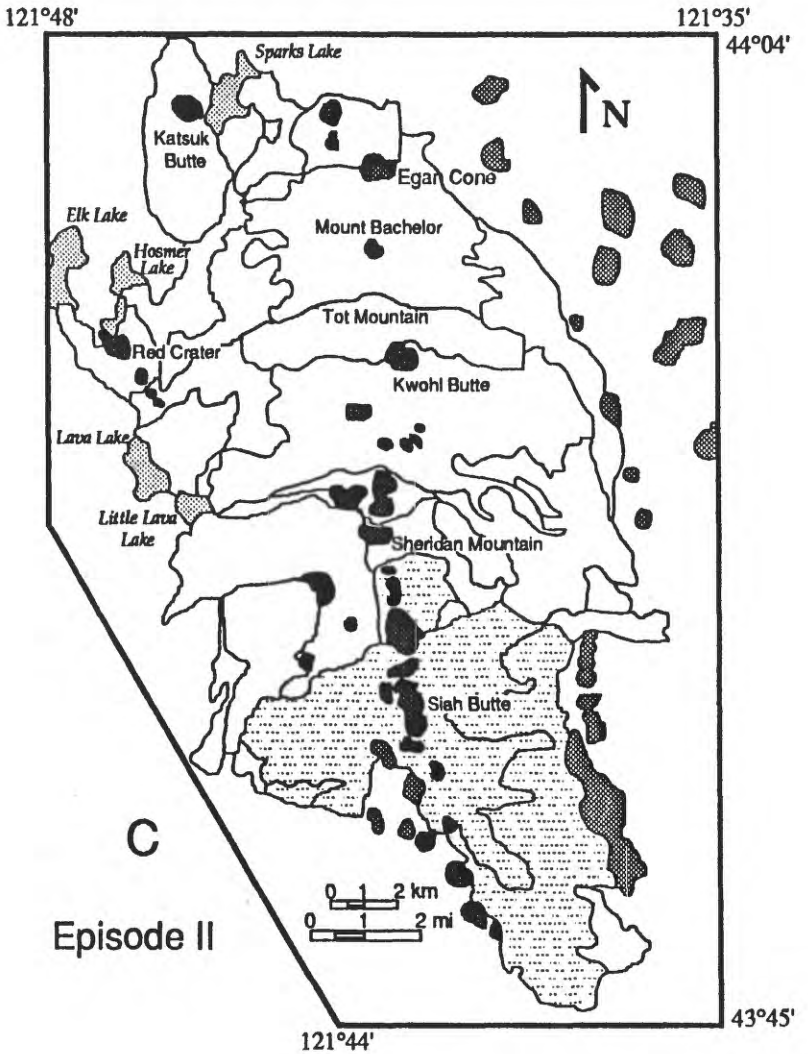


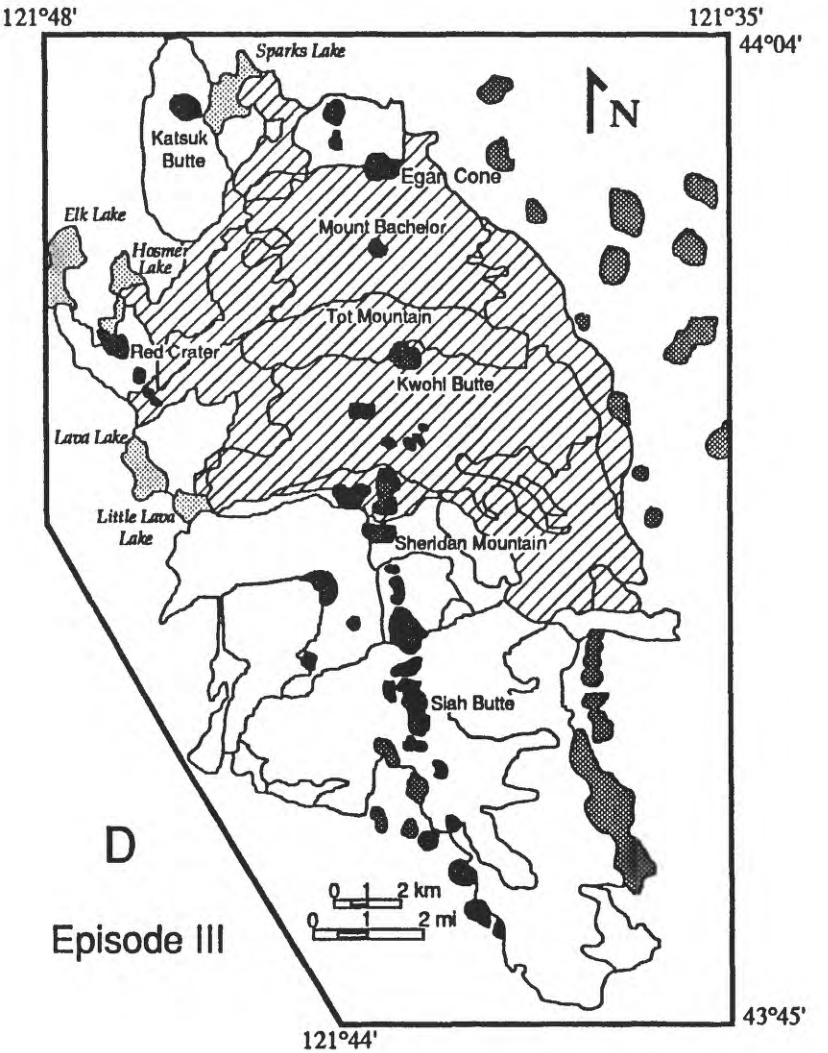


*Figure 6 continued*

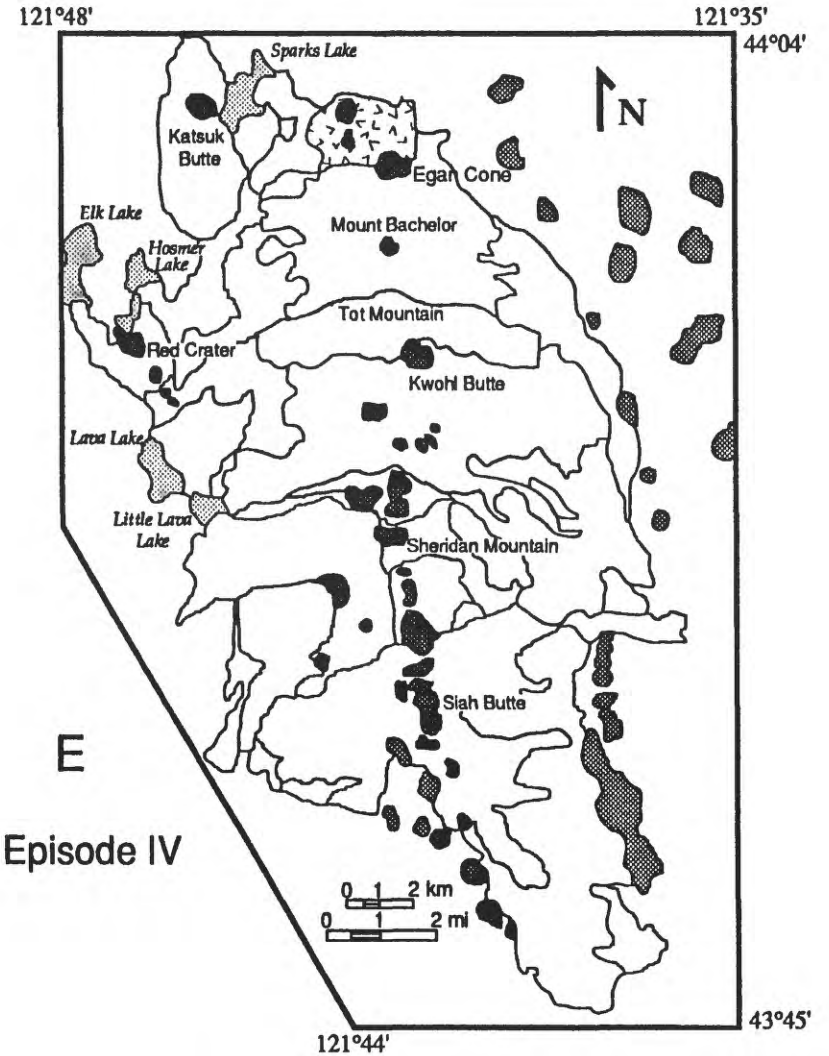


*Figure 6. continued.*

Bachelor-Kwohl segment and the youngest Egan activity, and between the older and younger Egan lava flows. Because of the relationship between the basalt lava flows from Egan cone with Mazama ash and because the basalt sites appear unrotated, I have considered the direction reliable and assigned the basalt Egan lava flows to episode IV.

Map units were assigned to eruptive episodes on the basis of the paleomagnetic data to create new maps that show the distribution of eruptive products of each episode (fig. 6). Early eruptions (episode Ia and Ib) were widespread along the entire chain, whereas subsequent eruptions were more localized.

**Eruption Rates**

The volume of material extruded during each eruptive episode was calculated based on assumptions regarding the pre-eruptive topography (Scott, unpub. data) of the MBVC. About 10, 3, 25, and 0.5 $km^3$ of material were erupted during episodes I, II, III, and IV, respectively, for a total of 38.5 $km^3$. Thus, approximately two-thirds of the volume of the chain was extruded during episode III. Assuming a maximum life-time for the chain of 10,000 years as suggested by field evidence, eruption rates for the MBVC are 3.9 $km^3$/1000

*Table 3. Comparison of eruption rates.*

| Volcano or Volcanic region | Output rate ($km^3$/1000 yr) | Output rate ($m^3$/sec) | References |
|---|---|---|---|
| Mount Bachelor | | | |
| Avg based on 10,000 yr | 3.9 | 0.12 | this study |
| episode I | 10.0 | 0.32 | " |
| episode III | 25.0 | 0.79 | " |
| Great Rift, Idaho | | | |
| Avg (15-2ka) | 2.4 | 0.08 | Kuntz and others (1986) |
| Arenal (1973-1980) | 9.5 | 0.30 | Wadge (1982) |
| Santiaguito (1922-1977) | 15.8 | 0.5 | " |
| Kilauea (1823-1975) | 22.0 | 0.7 | " |
| Mauna Loa (1823-1975) | 22.0 | 0.7 | " |
| Etna (1759-1974) | 9.5 | 0.3 | " |
| Fuego (1932-1980) | 15.8 | 0.5 | " |
| Oshima (500-1951) | 1.6 | 0.05 | " |
| Iceland (last 10,000 yrs) | 500.0 | 15.8 | " |
| Columbia Plateau | 1000.0 | 31.7 | " |

yr or 0.12 $m^3$/sec (table 3). Based on the paleomagnetic data, eruption rates during eruptive episodes 1 and III were probably much greater than the mean rate (see table 3 for speculative rates) because similarity in paleomagnetic direction for lava flows within each eruptive episode suggests these episodes were of relatively brief duration lasting on the order of 1000 years or less.

Eruption rates calculated for the MBVC (table 3) are much lower than eruption rates for flood basalt and the large-volume shield volcanoes, such as in Iceland, are moderately lower than eruption rates for historic eruptions at composite and Hawaiian shield volcanoes, and similar to long-term rates for the Great Rift area in Idaho. If the suggestion that the duration of episodes I and III was about 1000 yeas is correct within a factor of 2, the data suggest that small to moderate-sized Cascades shield volcanoes can erupt at rates similar to composite volcanoes. This points out the difficulty in comparing eruption rates for historic and pre-historic eruptions. In the latter case, the duration of individual eruptive episodes is generally poorly known, the total volume of eruptive products is often not well known, and average rates may include long repose intervals. All these reasons combine to render most pre-historic eruptive rates lower than they probably were.

## PETROGRAPHIC AND GEOCHEMICAL VARIATION

### Petrographic Description

Thin sections of samples from each map unit (table 1; fig. 2) were examined by petrographic microscope and for most map units at least one was point counted to determine relative percentages of mineral phases (table 4). In general, the lavas are sparsely porphyritic; phenocrysts (≥ 0.5 mm) comprise at most 15 percent and more commonly less than 10 percent of the total area (vesicle free; table 4). Basalt and low-silica basaltic andesite contain phenocrystic olivine and plagioclase with groundmass plagioclase, olivine, opaques, and in some thin sections, clinopyroxene. Lava flows from the summit cone of Mount Bachelor (mb5) contain phenocrystic clinopyroxene in addition to plagioclase and olivine, and two clinopyroxene phases, augite and pigeonite, are recognized in the groundmass in addition to plagioclase, opaques, and rare olivine . In most thin sections, phenocrysts and microphenocrysts are subhedral to euhedral.

Textures, which range from intersertal (most common) to intergranular, trachytic to non-aligned, seriate to glomeroporphyritic to subophitic, range as much within lava flows from the same rock unit as within lava flows from different rock units. Vesicularity also varies considerably within lava flows from the same and from different rock units, from being almost absent (<2 percent ) to one-fourth of a thin section; however, in general, lava flows from the summit cone of Mount Bachelor, Egan cone, and Red Crater are more vesicular than the other lava flows (table 4). Voids range from spherical to highly irregular in shape. In a few thin sections from low-silica basaltic-andesite lava flows, patchy areas of less porphyritic material are present: the mineralogy of these areas is similar to the more porphyritic areas.

Olivine is an early-forming phase in all samples, except for samples 8407214 and 8407244 (map units mb1a and mb3b, fig. 2), which contain the large plagioclase phenocrysts. In these two samples, olivine precipitated mostly after plagioclase, although some groundmass olivine occurs as inclusions along the margins of some of the larger plagioclase phenocrysts. In general, however, olivine phenocrysts and microphenocrysts are euhedral to subhedral, lack reaction rims, and occur singularly, in cumulocrysts with plagioclase, or in glomerocrysts. Rare olivine grains are embayed or skeletal; however, these shapes generally occur in thin sections which also contain euhedral to subhedral olivine phenocrysts. In basalt and low-silica basaltic andesite, dark brown, euhedral spinel inclusions are common in the olivine phenocrysts. In these rocks, olivine also occurs as a common late-forming groundmass phase. In the high-silica basaltic-andesite lava flows of the summit cone of Mount Bachelor, olivine is a subordinate phenocryst phase and is rare in the groundmass. In these lava flows, spinel inclusions in olivine grains are rare, and some olivine phenocrysts and microphenocrysts have reaction rims.

Calcium-rich plagioclase is the only phenocryst phase other than olivine in basalt

*Table 4. Summary of point count data*

| Sample No. [wt % SiO2] | MU | Phenocrysts phases | % (area) | max (mm) | GM phases | Vesicles % /shape | Groundmass Textural Description |
|---|---|---|---|---|---|---|---|
| 840721-4 [52.3] | mb1a | pl<br>ol | 2.8/0<br>0.2 | 0.9<br>1.8 | gl>>pl>>m>>op | 2.0/irr | v-fine grained; intersertal to intergranular; some cumulos |
| 840721-5 [54.0] | mb1b | pl<br>ol | 9/(<1)<br>0.1 | 1.4<br>0.6 | pl>>gl,m,>>op | 1.2/sph | crse-grained; intergranular; pl gloms; some sieve-texutred pl microphenos |
| 840706-4 [53.1] | mb1c | pl<br>ol | 0.4/(0.5)<br>0.5 | 0.6<br>0.5 | gl>pl>m>>op | 4.4/sph | crse-grained; trachytic; embayed ol; seriate |
| 840705-3 [50.6] | mb2a | pl<br>ol | 2.1(<.1)<br>3.7 | 0.9<br>1.8 | gl>>pl>>m>>op | 2.0/irr | v-fine grained; intersertal to intergranular; some cumulos |
| 840803-2 [50.8] | mb2b | pl<br>ol | 0.1/(0)<br>3.1 | 0.9<br>1.2 | pl>gl,m>>op | 2.4/irr | fine-grained; trachytic; intersertal to intergranular; some ols embayed |
| 840719-2 [50.3] | mb2b | pl<br>ol | 1.5/(<.1)<br>4.6 | 1.0<br>1.7 | gl>>pl>>m>>op | 6.5/sph | v. fine-grained; cumulocrysts common; seriate |
| 840703-2 [50.7] | mb2c | pl<br>ol | 5.3/(0.3)<br>6.3 | 1.1<br>0.7 | pl>>m>gl>>op, cpx | 6.8/sph | med-grained; almost cryptocrystalline; intergranular; cumulocrysts common |
| 840805-2 [51.7] | mb3a | pl<br>ol | 1.3(0.4)<br>1.7 | 1.5<br>2.0 | pl>>gl>>m>>op | 17.8/irr | crse-grained; intersertal |
| 840724-4 | mb3b | pl<br>ol | 4.5/(0)<br>0.1 | 2.6<br>0.9 | pl>>gl>>m>>op | 10.9/irr | crse-grained; intersertal to intergranular; plag gloms; some cumulos |
| 840806-5 [50.3] | mb3c | ol | 3 | 1.1 | gl,pl,m>op | 4.6/sph | v-fine grained; felty; intersertal to intergranular; some small ol gloms |
| 840722-4 [50.4] | mb3c | ol | 2.2 | 1.1 | gl,pl>>m>op | 6.3/sph | med-grained; intersertal to intergranular |
| 85-19 | mb3c | pl<br>ol | 0.1/(0)<br>3.5 | 0.6<br>1.0 | pl>>gl>>m>>cpx, op | 14.7/irr | med-grained; almost cryptocrystalline; trachytic; intergranular; some ol gloms |
| 840727-1 [50.6] | mb3c | pl<br>ol | 1.2/(1)<br>0.7 | 1.1<br>0.7 | gl>>pl>>>m>cpx,op | 15.4/irr | crse-grained; intersertal to intergranular; some cumlos |

| Sample No. [wt % SiO2] | MU | Phenocrysts phases | Phenocrysts area % | Phenocrysts max (mm) | GM phases | Vesicles void/shape | Groundmass Textural Description |
|---|---|---|---|---|---|---|---|
| 840722-5 [52.9] | mb3d | pl<br>ol | 1.9/(0.2)<br>3.9 | 0.5<br>1.3 | pl>gl>>m>op,cpx | 1.7/irr | crse-grained; intersertal to intergranular; some cumulos; pl gloms |
| 850719-6 [52.9] | mb3d | pl<br>ol | 4.2/(0.1)<br>4.2 | 1.1 | pl>gl>>m>op | 11.4/irr | crse-grained; trachytic; seriate; some cumulos; plag gloms |
| 840729-4 [53.0] | mb4b | pl<br>ol | 3.7/(0.2)<br>4 | 0.8<br>1.4 | gl,pl,m>op | 5.1/sph | fine-grained; intergranular to intersertal; cumulos common |
| 840725-4 [55.8] | mb5 | pl<br>ol | 3.0/(<1)<br>2 | 1.4<br>1.0 | gl,pl>>m>op>pig | 12.0/sph | crse-grained; intersertal; pl gloms and cumulocrysts common |
| 840914-7 [56.4] | mb5 | pl<br>cpx | 3.0/(<1)<br><1.0 | 2.3<br>0.7 | gl,pl,>>m>op,cpx>pig | 23.0/irr | crse-grained; intersertal; pl gloms common |
| 840913-10 [56.7] | mb5 | pl<br>ol<br>cpx | 6/(<1)<br><1<br>1 | 1.9<br>1.2<br>0.7 | gl,pl>>m>op | 16/irr | crse-grained; intersertal; pl gloms and pl and cpx cumulos common |
| 840913-4 [56.8] | mb5 | pl<br>ol<br>cpx | 6/(2)<br><1<br>1 | 1.1<br>0.6<br>1.1 | gl,pl>>m>op,cpx>pig | 24/irr | crse-grained; intergranular; pl gloms and cumulos with cpx common |
| 850721-6 [51.3] | mb6 | pl<br>ol | 0.9/(0.3)<br>0.9 | 0.8<br>0.6 | gl>>pl>>m>>op | 17/sph to irr | crse-grained; trachytic; intersertal; some cumulos |
| 850710-4 [51.1] | mb6 | pl<br>ol | 0.2/(1)<br>0.4 | 0.6<br>0.5 | gl,pl>>m>op | 21/irr | crse-grained; trachytic; intergranular to intersertal; some cumulos |
| 84-19 [49.8] | mr | pl | 1.4/(0) | 0.5 | pl>>m>>gl>op,cpx | 24.5/sph to irr | fine-grained; intergranular; suboph; almost cryptocrystalline |

*Table 4. Summary of point count data (cont.) MU=map unit; pl=plagioclase; ol=olivine; m=mafics; op=opaques; cpx=clinopyroxene; pig=pigeonite; gloms=glomerocrysts; cumulos=cumulocrysts; sph=spherical; irr=irregular; > and , symbols give relative amounts of groundmass phases in relationship to preceeding phases such that gl,pl>>m>op reads that glass and plagioclase are about equal, pl is at least 2 times that of mafics (ol and pyx undifferentiated), and that mafics are more abundant than opaques but not by as much as by by two times; crse = coarse.*

and low-silica basaltic andesite. Although most plagioclase phenocrysts and microphenocrysts are euhedral to subhedral, two distinct textures were noted: 1) homogeneous plagioclase phenocrysts and; 2) sieve-textured plagioclase phenocrysts that show signs of resorption or skeletal growth. The most common sieve-textured plagioclase phenocrysts have sieved cores with homogeneous mantles and rims: less commonly, the cores and rims are homogeneous and the mantles are sieved. Homogeneous and sieve-textured plagioclase grains are similar in size and usually are normally zoned, although a few phenocrysts have minor oscillatory zonation near their rims. In all thin sections, plagioclase is the dominant groundmass mineral and is generally more sodic than the phenocrysts.

Clinopyroxene occurs as only a groundmass phase in basalt, in low-silica basaltic andesite, and in lava flows from Tot Mountain: it occurs as both phenocryst and groundmass phases in the summit lava flows of Mount Bachelor. The presence of groundmass clinopyroxene in basalt and low-silica basaltic andesite lava flows probably results from differences in cooling histories rather than differences in chemistry, as in chemically similar lava flows from the same map unit clinopyroxene may or may not be present. In general, samples with a fine-grained holocrystalline groundmass contain clinopyroxene, whereas those samples with a coarse-grained hypocrystalline groundmass do not. Groundmass clinopyroxene commonly occurs in clusters with plagioclase microlites. In the lava flows of the summit cone of Mount Bachelor subhedral to euhedral clinopyroxene is common both as a phenocryst and groundmass phases. In these lava flows, phenocrystic clinopyroxene occurs subophitically in cumulocrysts with plagioclase or with plagioclase and olivine, and as a solitary mineral.

Opaques, clinopyroxene, and spinel are common accessory phases present in the MBVC lava flows. Opaques are a common groundmass phase in all samples; however, it is often difficult to distinguish them from the dark brown to black glass. Where distinguishable, they are usually cubic and fill the areas between phenocrysts and other groundmass phases; thus they appear to be the last phase to have precipitated. A few opaques were examined by reflected light and were identified as magnetite on the basis of color and shape. Groundmass clinopyroxene occurs as augite in the basalt and low-silica basaltic-andesite lava flows and as pigeonite and augite in samples from the Mount Bachelor summit. In the summit lava flows pigeonite appears to supplant olivine as a groundmass phase. Dark reddish-brown to brownish-black spinel is a ubiquitous inclusion in olivine phenocrysts of basalt and low-silica basaltic andesite, but is rare in the high-silica basaltic-andesite lava flows from Tot Mountain and the summit cone of Mount Bachelor.

### Microprobe Analysis

Twelve thin sections were polished and analyzed to determine compositions of phenocryst and groundmass phases. A MAC 400 electron microprobe with a Kevex 7500 energy dispersive x-ray microanalyzer, with an accelerating voltage of 15.0 KeV, an aperture of 500 nanoamperes, and natural mineral standards, housed at the University of Colorado-Boulder, Geology Department, was used. Average compositions of phenocryst and groundmass phases are given in table 5: all analyses are given in Appendix A. Reported oxide values commonly summed to less than 100 percent most likely because minor oxide components such as MnO in pyroxene were not analyzed.

Olivine phenocrysts are generally non-zoned or exhibit slight normal zonation. Phenocryst core compositions range from forsterite ($Fo_{85}$) to $Fo_{67}$; microphenocryst and groundmass cores range from $Fo_{79}$ to $Fo_{57}$ (table 5). Olivine phenocrysts in the high-silica basaltic-andesite lava flows from the summit of Mount Bachelor (sample 8409134) had the lowest Fo value (table 5). There is a general trend towards lower Fo values with increasing $SiO_2$ although the trend is not uniform (fig. 7a).

Plagioclase phenocrysts are generally normally zoned, although both reversed and oscillatory zonation occurs. In the basaltic andesite samples, anorthite (An) content in phenocrysts appears to increase with increasing $SiO_2$ (fig. 7b). Groundmass compositions also appear to increase slightly with increasing $SiO_2$ until the summit lavas are reached. In

*Table 5. Summary of microprobe results. MU=map unit; for all phases avg relates to core average; range is total range for all grains in a given thin section from core to rim; normal zonation is indicated when range goes from larger to smaller numbers, reversed when the opposite is true; for spinels, avg refers to stociometrically determined averages for the ratio Al/Al+Cr for grains within a thin section.*

| Sample No [whole rock SiO2] | MU | Phenocrysts ol avg Fo | plag avg An (range) | cpx avg (range) | Microphenocrysts and Groundmass ol Fo avg (range) | plag An avg (range) | cpx avg (range) | pig avg (range) | spinel avg |
|---|---|---|---|---|---|---|---|---|---|
| G84-19 [49.5] | mr | 79 (81-70) | | | 59 (60-58) | 63 (69-60) | En42 (43-40) Wo39 (40-37) | | 59 |
| 840722-4 [50.4] | mb3c | 85 (86-80) | 78 (79-76) | | 78 (79-76) | | | | 75 |
| 840727-1 [50.6] | mb3c | 81 (81-80) | s89 (92-81) | | 75 (78-73) | 69 (73-65) | | | 65 |
| 840703-2 [50.7] | mb2c | 83 (85-81) | 79 (82-74) | | 65 (69-60) | 68 (75-65) | En 36 (41-30) Wo 44 (46-41) | | |
| 840805-2 [51.7] | mb3a | 77 (82-71) | 73 (83-65) | | 68 (76-61) | 66 (80-52) | | | 66 |
| 840721-4 [52.3] | mb1a | 81 (82-79) | 75 (85-66) s67 (67-85) | | 73 (74-72) | 67 -67 | | | |

*Table 5. continued*

| Sample No [wt % SiO2] | MU | Phenocrysts ol avg Fo (range) | plag avg An (range) | cpx avg (range) | Microphenocrysts and Groundmass ol Fo avg (range) | plag An avg (range) | cpx avg (range) | pig avg (range) | spinel avg |
|---|---|---|---|---|---|---|---|---|---|
| G84-18 [52.7] | mb3b | 70 (74-67) | 67 (75-56) | | 67 (74-57) | 71 (77-64) | | | |
| 840722-5 [52.9] | mb3d | 80 (82-75) | 72 (72-76) s82 (82-78) | | 74 (79-75) | 69 (80-61) | En46 (48-43) Wo 37 (38-35) | | |
| 850711-5 [54.2] | mb4b | 83 (83-82) | 79 (81-63) s87 (89-76) | | 77 (79-75) | 72 (87-65) | | | 63 |
| 840725-4 [55.8] | mb5 (Tot Mt) | 80 (82-74) | 89 (90-73) | | 72 (75-69) | 69 (77-64) 87 (90-82) | En 45 (46-44) Wo (43-38) | En 68 (70-66) Wo 5 (6-4) | 42 64 56 |
| 840913-9 [56.7] | mb5 | 67 (67-63) | 80 (80-74) | En 42 (42-42) Wo 43 (44-43) | 60 | 56 | | En 54 (55-53) Wo 10 (10-9) | |
| 840914-8 [56.3] | mb5 | 76 (77-68) | 85 (87-71) | En 51 (52-50) Wo 43 (44-42) | 67 (68-65) | 53 (55-47) | En 38 38 Wo 30 30 | En 63 (65-61) Wo 8 (10-8) | |

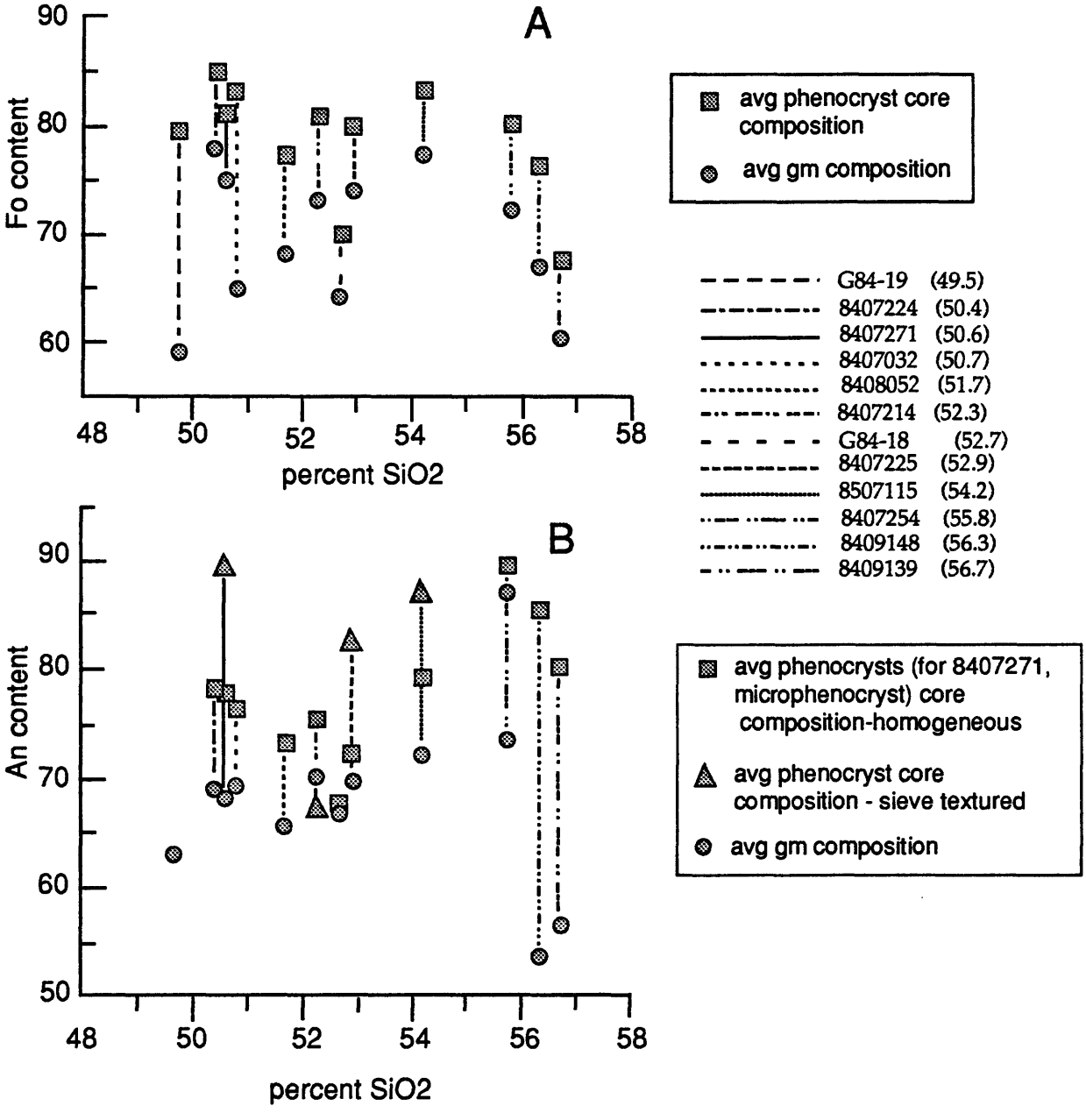


*Figure 7. Graphs showing average olivine and plagioclase phenocryst and groundmass core compositions as determined from microprobe analyses versus SiO2 of rocks. A. Olivine. B. Plagioclase.*

these lavas, groundmass compositions are well below both phenocryst rim compositions and groundmass compositions from other flows. The highest phenocrystic An content corresponds to two samples with widely different whole-rock silica values: sample 8407271 ($An_{92}$; 50.6 percent $SiO_2$) from the south flank of Kwohl Butteshield, and sample 8407254 ($An_{90}$, 55.8 percent $SiO_2$) from Tot Mountain. In the sample from Kwohl shield (8407271), microphenocryst and groundmass plagioclase core compositions are lower than phenocryst core composition. In the Tot Mountain sample (8407254), microphenocryst and groundmass plagioclase core compositions form two distinct populations: one $An_{90-82}$, which equals phenocryst core compositions, and one $An_{77-64}$, which is similar to or lower in An content than the rims of the phenocrysts (fig. 7b; Appendix A).

In three samples, 8407225, 8407115, and 8407214, both homogeneous and sieve-textured plagioclase phenocrysts were analyzed (fig. 7b; table 5). In samples 8407225 and 8407115, only the phenocryst cores were sieve-textured (homogenous mantles and rims) and they had a higher An content (12 and 9 mole percent, respectively) than cores of corresponding homogeneous plagioclase phenocrysts. In sample 8407214, the sieve-textured phenocryst had a lower core An content than homogeneous phenocrysts; this grain was sieve-textured throughout.

Microprobe analyses of the notably large euhdral plagioclase phenocrysts (samples 8407214 and G84-18) show that the phenocrysts have generally uniform compositions, differing by less than 5 mole percent from core to mantle (table 5). In a few cases, however, there is a moderate (5-14 mole percent An ) to dramatic (19-22 percent mole An) increase in An content at the rims, which commonly exhibit oscillatory zoning (Appendix A). Also some of the microphenocrysts have higher An core values than phenocryst core values; generally however, microphenocryst and groundmass compositions have An contents only slightly less ($\leq$ 5 mole percent) than the phenocrysts.

All groundmass clinopyroxene compositions plot in the augite field (fig. 8). Groundmass pigeonite was detected only in Mount Bachelor summit cone lava flows, although a single corroded pigeonite microphenocryst was probed in the Tot Mountain sample (8407254). Phenocrystic clinopyroxene compositions in the summit lavas vary from augite (sample 8409139), similar to groundmass augite, to endiopside (sample 8409148). Whether these two samples are representative of Mount Bachelor summit cone lava flows is unknown, as only one phenocryst was probed in each thin

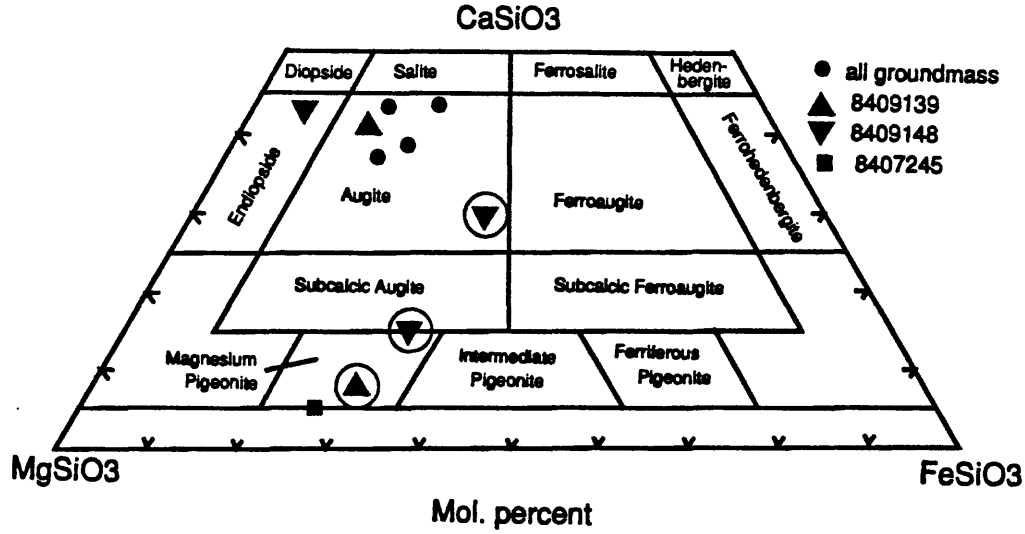


*Figure 8. Ternary diagram of average groundmass and phenocryst clinopyroxeme compositions: filled circle - groundmass compositions from basalt and low-silica basaltic-andesite samples; triangle up - phenocryst and groundmass (with circle) composition from sample 8409139 from the summit cone of Mount Bachelor; triangle down - phenocryst and groundmass (with circle) composition from sample 8409148 also from the summit cone of Mount Bachelror; and filled square - corroded microphenocryst from the Tot Mountain.*

section. Also, the lack of an augitic groundmass phase in sample 8409148 may be an artifact of inadequate sampling of the groundmass in this thin section, rather than the absence of the phase.

As previously noted, olivine phenocrysts in basalt and low-silica basaltic andesite contain numerous spinel inclusions; of these, nineteen spinels from six thin sections were probed (Appendix B). The spinel inclusions are classified as picotites, a variety of hercynite ($FeAl_2O_4$) in which there is moderate substitution of Mg for $Fe^{2+}$ and Cr for Al, but Al > Cr, and Fe:Mg is between 1 and 3 (Deer and others, 1983) based on calculated formulas. In most samples only two picotites (in two different olivine grains, respectively) were analyzed; their compositions within a given sample are similar (fig. 9). In contrast, eight picotites from eight olivine grains were probed in the Tot Mountain sample (8407254): they show a range of compositions (fig. 9). Seven of the eight picotites from Tot Mountain have compositions similar to those of picotites probed in the other five thin sections: one point, however, deviates significantly. It is difficult to determine from the present data if the deviant data point is due to analytical error or constitutes a significantly different population of picotite.

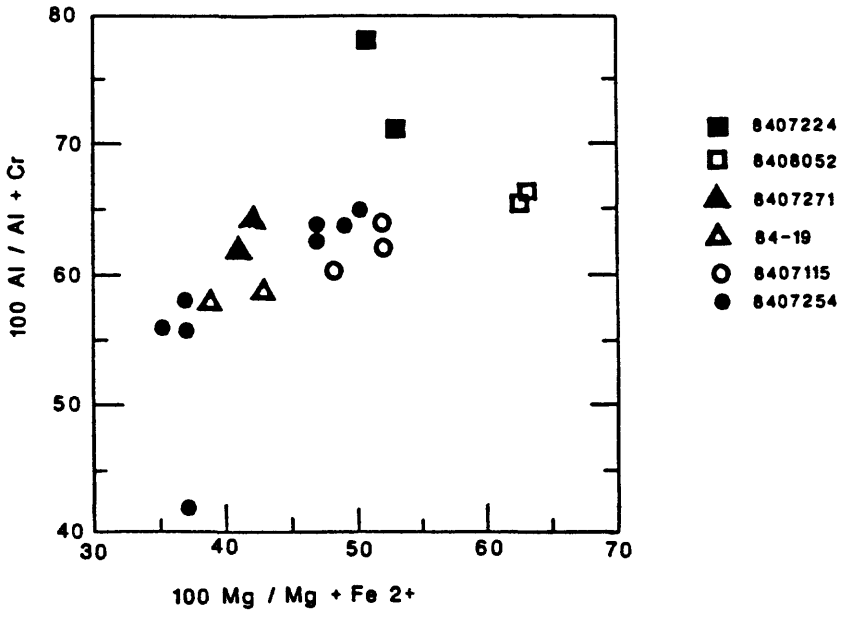


*Figure 9. Chromium spinel inclusion compositions as a function of whole-rock geochemistry. Symbols correspond to sample numbers.*

The scarcity of spinel inclusions in the high-silica basaltic andesite may be due to the precipitation of phenocrystic augite. Crystals will precipitate from a magma until its crystallization is terminated by a peritectic or reaction relation. Irvine (1967) noted that in the Muskox intrusion early formed spinel inclusions ceased to exist after precipitation of pyroxene, and he suggested that spinel crystallization was terminated because of a peritectic relation to clinopyroxene.

### Geochemical Analysis

Major-element data for 138 samples were obtained by wavelength-dispersive, X-ray-florescence spectroscopy (WDXRF). Trace-element data for 70 samples (Cr, Ni, Cu, Zn, Rb, Sr, Y, Zr, and Nb) were obtained by energy-dispersive, X-ray fluorescence spectroscopy (EDXRF). Nineteen samples were analyzed by instrumental neutron activation analysis (INAA) for rare earth element (REE) concentrations as well as Co, Sc, Ba, Cs, Rb, Sr, Hf, Ta, Sb, U, and Th. All analyses were done by the U. S. Geological Survey's Branch of Geochemistry in Denver, Colorado. A discussion of the laboratory's instrumentation, techniques, detection limits, and analytical errors is found in Baedecker (1987). Representative compositions for lava flows from each map unit are given in table 6; geochemical data for each sample are given in Appendix C and analytical limits of detection and accuracy for major- and trace-elements are

given in Appendix D. Compiled INAA data are reported in Appendix E.

## Major Element Analyses

Silica-variation diagrams (Harker diagrams) for the major oxides (figs. 10 and 11) are typical of suites from other orogenic areas (see Gill, 1981). With increasing silica, total iron (as $Fe_2O_3$), CaO, MgO, and $TiO_2$ decrease, and $K_2O$ and $Na_2O$ (not shown) increase. Manganese (MnO) concentrations range from 0.18 to 0.12 percent and in general decrease with increasing silica (fig. 11). Phosphorous ($P_2O_5$) concentrations range from 0.2 to 0.6 percent, are variable in range in the basalt and appear more uniform in the basaltic andesite. And in general, $Al_2O_3$ increases with increasing $SiO_2$, although maximum $Al_2O_3$ values occur at intermediate $SiO_2$ values.

Upon closer examination of the diagrams several nuances in the data can be seen. The data are keyed to the six major vent areas, Egan cone (mb6), Bachelor-Kwohl shield (mb5, mb4a and b, and mb3a,b,c, and d), Sheridan shield (mb1), Siah chain (mb2), Red Crater chain of cones (mr), and Katsuk Butte (mk), and to the outliers, Wuksi (mw), Cayuse Crater (mc) and Le Conte Crater (ml). Generally good correlation exists between vent area and chemistry. However, for the Sheridan lava flows (squares on the diagrams) there are two distinct geochemical groups at the same silica value. These two distinct groups are seen most readily on the plot of $Al_2O_3$ vs $SiO_2$ and are more subtly displayed on plots of CaO, $K_2O$, and $TiO_2$ vs $SiO_2$. The high alumina group corresponds to the large plagioclase bearing lavas (mb1a) that erupted early in the chain's history (episode 1a) and to aphanitic lavas (mb1c) that were erupted from vents on the west flank of the Sheridan shield during episode 1b. The lower alumina group corresponds to the moderately porphyritic lavas that make up the majority of the volume of the Sheridan shield lava flows (mb1a and mb1b) and appear to have vented along the central axis of the Sheridan shield. Samples corresponding to the large plagioclase lava flows on the east side of Mount Bachelor (mb3b) are distinct from the rest of the mb3ab group (filled triangles). Samples from Egan cone (open circles) cluster around 51 percent $SiO_2$ and around 53 percent $SiO_2$, showing that the Egan lava flows encompass both basalt and basaltic andesite compositions.

Samples from Red Crater, Egan cone, and the mb3b are generally higher in $Fe_2O_3$, $TiO_2$, and $P_2O_5$ and lower in MgO and CaO than other samples, although there is some overlap. These relationships are also expressed in the trace-element and rare earth-element data presented in the ensuing paragraphs. The combined geochemical data will serve as a basis for subdividing the lava flows into geochemical groups and magma types.

## Trace Elements

In general, the compatible trace elements decrease as $SiO_2$ increases, whereas incompatible element behaviors vary (figs. 11 and 12). Concentrations of the K-element group, Rb, Ba, and Cs, increase with increasing $SiO_2$, with subtle distinctions in absolute values between lava flows from different vent areas (fig. 11). The Ti group, Zr, Hf, and Ta, shows little variation with increasing $SiO_2$; the apparent decrease in concentration at the mid-silica level is generally associated with the Sheridan group of lava flows that have the high $Al_2O_3$ values (fig. 12). Both Th and U (fig. 12) increase with increasing $SiO_2$. Zinc and Y show a range in values but no apparent correlation with $SiO_2$ (fig. 12).

Variations in trace-element concentrations often distinguish the Red Crater, Egan, and mb3b samples from the rest of the chain. In general these samples have overall lower compatible trace-element and higher incompatible trace-element concentration than the other samples, although as on the major-element variation plots there is some overlap. The high-alumina Sheridan samples show up as unique concentrations on some plots (e. g. Zr and Ta) but do not conform to a set pattern (i.e. in some cases compatible elements are higher and in others lower than the other samples).

Strontium is a compatible element in the presence of plagioclase. When plagioclase is the only feldspar, Sr should show positive correlation with CaO and negative correlation with $K_2O$ and Rb (Cox and others, 1981). Although plagioclase is the only feldspar present in the MBVC lava flows, there is a general negative correlation between Sr and

*Table 6. Representative chemical analyses for each map unit. More than one analyses is given for units with more than one chemical type Trace-element group under Nb^ were analyzed by EDXRF; trace-element group under Ba# by INAA. Cayuse trace data * from Hill (1991) sample 3s073.*

| Sample No. | 8407223 | 84-16 | 8407011 | 8407024 | 8408024 | 8507062 | 8407033 | 8408061 | 8407244 | 8407272 | 8407251 | 8408172 | 8507221 |
|---|---|---|---|---|---|---|---|---|---|---|---|---|---|
| Map Unit | mb1a | mb1a | mb1b | mb1c | mb2a | mb2b | mb2c | mb3a | mb3b | mb3c | mb3d | mb4 | mb4a |
| SiO2 | 52.3 | 53.8 | 54.1 | 53.4 | 50.8 | 51.0 | 50.5 | 51.4 | 52.7 | 50.6 | 53.7 | 50.5 | 51.2 |
| Al2O3 | 18.3 | 17.4 | 17.3 | 18.1 | 17.1 | 17.0 | 17.3 | 17.0 | 17.4 | 17.3 | 17.7 | 16.9 | 17.2 |
| FeTO3 | 8.98 | 8.44 | 8.53 | 8.83 | 9.67 | 9.35 | 9.64 | 9.50 | 10.76 | 9.64 | 8.54 | 9.54 | 9.27 |
| MgO | 5.78 | 5.18 | 5.06 | 5.49 | 7.18 | 8.01 | 7.49 | 6.86 | 4.27 | 7.64 | 5.39 | 8.13 | 7.33 |
| CaO | 9.22 | 8.88 | 8.69 | 8.40 | 9.29 | 9.30 | 9.49 | 8.92 | 7.83 | 9.15 | 8.47 | 9.24 | 9.33 |
| Na2O | 3.33 | 3.58 | 3.59 | 3.56 | 3.35 | 3.12 | 3.17 | 3.39 | 3.81 | 3.27 | 3.53 | 3.23 | 3.28 |
| K2O | 0.61 | 0.91 | 1.01 | 0.70 | 0.65 | 0.61 | 0.60 | 0.77 | 0.90 | 0.58 | 1.01 | 0.63 | 0.67 |
| TiO2 | 1.12 | 1.18 | 1.22 | 1.14 | 1.41 | 1.00 | 1.37 | 1.60 | 1.72 | 1.33 | 1.20 | 1.29 | 1.28 |
| P2O5 | 0.20 | 0.35 | 0.39 | 0.27 | 0.32 | 0.27 | 0.30 | 0.40 | 0.43 | 0.28 | 0.34 | 0.29 | 0.28 |
| MnO | 0.13 | 0.13 | 0.14 | 0.13 | 0.15 | 0.15 | 0.15 | 0.15 | 0.16 | 0.15 | 0.13 | 0.17 | 0.15 |
| Nb^ | <10 | 15 | 18 | 11 | 15 | 13 | 11 | 15 | 16 | 14 | 18 | 13 | 10 |
| Pb | 15 | 17 | 29 | 19 | 18 | 16 | 13 | 14 | 15 | 15 | 28 | 10 | 13 |
| Sr | 602 | 490 | 545 | 656 | 479 | 475 | 457 | 519 | 549 | 507 | 566 | 412 | 446 |
| Zr | 98 | 150 | 176 | 119 | 165 | 141 | 140 | 192 | 169 | 137 | 163 | 132 | 141 |
| Y | 16 | 22 | 32 | 20 | 29 | 30 | 23 | 26 | 30 | 25 | 28 | 20 | 27 |
| Cu | 65 | 80 | 70 | 65 | 60 | 60 | 60 | 60 | 60 | 70 | | 65 | 75 |
| Ni | 75 | 50 | 35 | 80 | 110 | 150 | 115 | 90 | 30 | 140 | | 170 | 130 |
| Zn | 70 | 80 | 85 | 80 | 80 | 70 | 70 | 80 | 100 | 80 | | 80 | 80 |
| Cr | 80 | 110 | 100 | 110 | 220 | 320 | 215 | 200 | 30 | 250 | | 290 | 220 |
| Ba# | 362 | | 391 | | | | | 285 | 416 | | | 231 | |
| Co | 28.3 | | 26.9 | | | | | 34.8 | 31.3 | | | 38 | |
| Ni | 39 | | 48.6 | | | | | 117 | 48.8 | | | 161 | |
| Cr | 93.5 | | 95.2 | | | | | 166 | 23.6 | | | 259 | |
| Cs | 0.548 | | 0.553 | | | | | 0.314 | 0.311 | | | 0.256 | |
| Hf | 3.43 | | 3.61 | | | | | 4.07 | 3.94 | | | 2.96 | |
| Pb | 16.2 | | 20.1 | | | | | 10.1 | 11.5 | | | 9.41 | |
| Ta | 0.764 | | 0.766 | | | | | 0.817 | 0.807 | | | 0.542 | |
| Th | 1.62 | | 1.73 | | | | | 1.13 | 0.992 | | | 1.1 | |
| U | 0.625 | | 0.853 | | | | | 0.417 | 0.504 | | | 0.418 | |
| Zn | 91.3 | | 91.7 | | | | | 88.1 | 123 | | | 89.8 | |
| Zr | 157 | | 147 | | | | | 181 | 151 | | | 129 | |
| Sc | 26.1 | | 24.9 | | | | | 26.3 | 22.8 | | | 27.2 | |
| Latitude | 43 53 02 | 43 53 00 | 43 53 15 | 43 54 45 | 43 48 03 | 43 50 07 | 43 51 32 | 43 55 04 | 43 53 18 | 43 55 33 | 43 56 02 | 44 00 45 | 43 58 45 |
| Longitude | 121 39 16 | 121 38 42 | 121 14 02 | 121 42 15 | 121 36 26 | 121 36 43 | 121 40 10 | 121 45 47 | 121 36 28 | 121 40 35 | 121 41 44 | 121 42 10 | 121 45 27 |

*Table 6.*

| Sample No. | 8408076 | 8407254 | 8507114 | 84091310 | 8409147 | 8507111 | 84-22 | 8408062 | 8409123 | 8409121 | 840912 |
|---|---|---|---|---|---|---|---|---|---|---|---|
| Map Unit | mb4b | mb5 | mb5 | mb5a | mb5b | mb6 | mb6 | mr | mk | mc | ml |
| SiO2 | 54.1 | 55.8 | 56.5 | 56.7 | 56.4 | 53.6 | 51.2 | 49.5 | 51.0 | | |
| Al2O3 | 17.2 | 17.8 | 18.0 | 18.1 | 18.2 | 17.8 | 17.2 | 16.6 | 16.8 | 51.4 | 54.0 |
| FeTO3 | 8.40 | 7.80 | 7.64 | 7.82 | 7.63 | 8.58 | 11.26 | 11.91 | 9.71 | 16.6 | 16.4 |
| MgO | 6.16 | 4.47 | 3.64 | 3.16 | 3.54 | 5.78 | 5.37 | 6.71 | 7.56 | 9.31 | 8.87 |
| CaO | 8.20 | 8.09 | 7.87 | 7.44 | 7.82 | 8.40 | 8.32 | 8.63 | 9.23 | 8.37 | 6.54 |
| Na2O | 3.46 | 3.54 | 3.71 | 3.98 | 3.79 | 3.50 | 3.51 | 3.43 | 3.23 | 9.20 | 7.64 |
| K2O | 0.91 | 1.10 | 1.23 | 1.26 | 1.21 | 0.80 | 0.66 | 0.63 | 0.64 | 3.09 | 3.64 |
| TiO2 | 1.08 | 1.04 | 1.01 | 1.09 | 1.03 | 1.12 | 1.71 | 1.90 | 1.35 | 0.64 | 1.14 |
| P2O5 | 0.31 | 0.28 | 0.25 | 0.28 | 0.26 | 0.29 | 0.54 | 0.53 | 0.32 | 1.06 | 1.33 |
| MnO | 0.13 | 0.12 | 0.12 | 0.12 | 0.11 | 0.13 | 0.15 | 0.18 | 0.15 | 0.22 | 0.34 |
| | | | | | | | | | | 0.15 | 0.14 |
| Nb^ | 15 | 17 | 13 | 12 | 14 | <10 | 13 | 14 | 13 | | |
| Rb | 24 | 29 | 35 | 27 | 26 | 17 | <10 | 6 | 10 | 12 | 16 |
| Sr | 536 | 592 | 555 | 520 | 520 | 566 | 490 | 492 | 454 | 14 | 24 |
| Zr | 149 | 161 | 147 | 152 | 146 | 127 | 150 | 192 | 126 | 428 | 434 |
| Y | 25 | 23 | 24 | 20 | 24 | 20 | 30 | 33 | 20 | 100 | 160 |
| Cu | 65 | 60 | 70 | 50 | 60 | 70 | 40 | 65 | 55 | <20 | 25 |
| Ni | 85 | 50 | 28 | <20 | -20 | 115 | 50 | 110 | 100 | | |
| Zn | 80 | 80 | 80 | 80 | 80 | 80 | 90 | 100 | 70 | | |
| Cr | 165 | 85 | 35 | <20 | 25 | 130 | 50 | 180 | 295 | | |
| Ba# | | | | 461 | | | | 291 | 278 | | |
| Co | | | | 21.1 | | | | 39.7 | 36.4 | 173* | |
| Ni | | | | 20.7 | | | | 131 | 120 | 39.7 | |
| Cr | | | | 10.7 | | | | 172 | 253 | 148 | |
| Cs | | | | 0.954 | | | | 0.228 | 0.26 | 451 | |
| Hf | | | | 3.63 | | | | 4.17 | 2.89 | 0.6 | |
| Rb | | | | 28.1 | | | | 10.1 | 11.3 | 2.3 | |
| Ta | | | | 0.632 | | | | 0.792 | 0.544 | 11 | |
| Th | | | | 2.68 | | | | 0.625 | 0.887 | 0.48 | |
| U | | | | 0.781 | | | | 0.341 | 0.354 | 1.2 | |
| Zn | | | | 94.6 | | | | 122 | 93 | 0.5 | |
| Zr | | | | 157 | | | | 169 | 132 | 54 | |
| Sc | | | | 19.5 | | | | 26.1 | 26.5 | 105 | |
| Latitude | 43 58 18 | 43 57 00 | 43 59 19 | 43 58 40 | 43 59 09 | 44 00 25 | 44 00 50 | 43 55 58 | 44 00 55 | 44 03 30 | 44 01 30 |
| Longitude | 121 43 11 | 121 41 13 | 121 42 50 | 121 41 05 | 121 40 22 | 121 43 40 | 121 41 00 | 121 43 25 | 121 45 45 | 121 42 35 | 121 46 20 |

*Figure 10. Major- and trace-element variation diagrams*

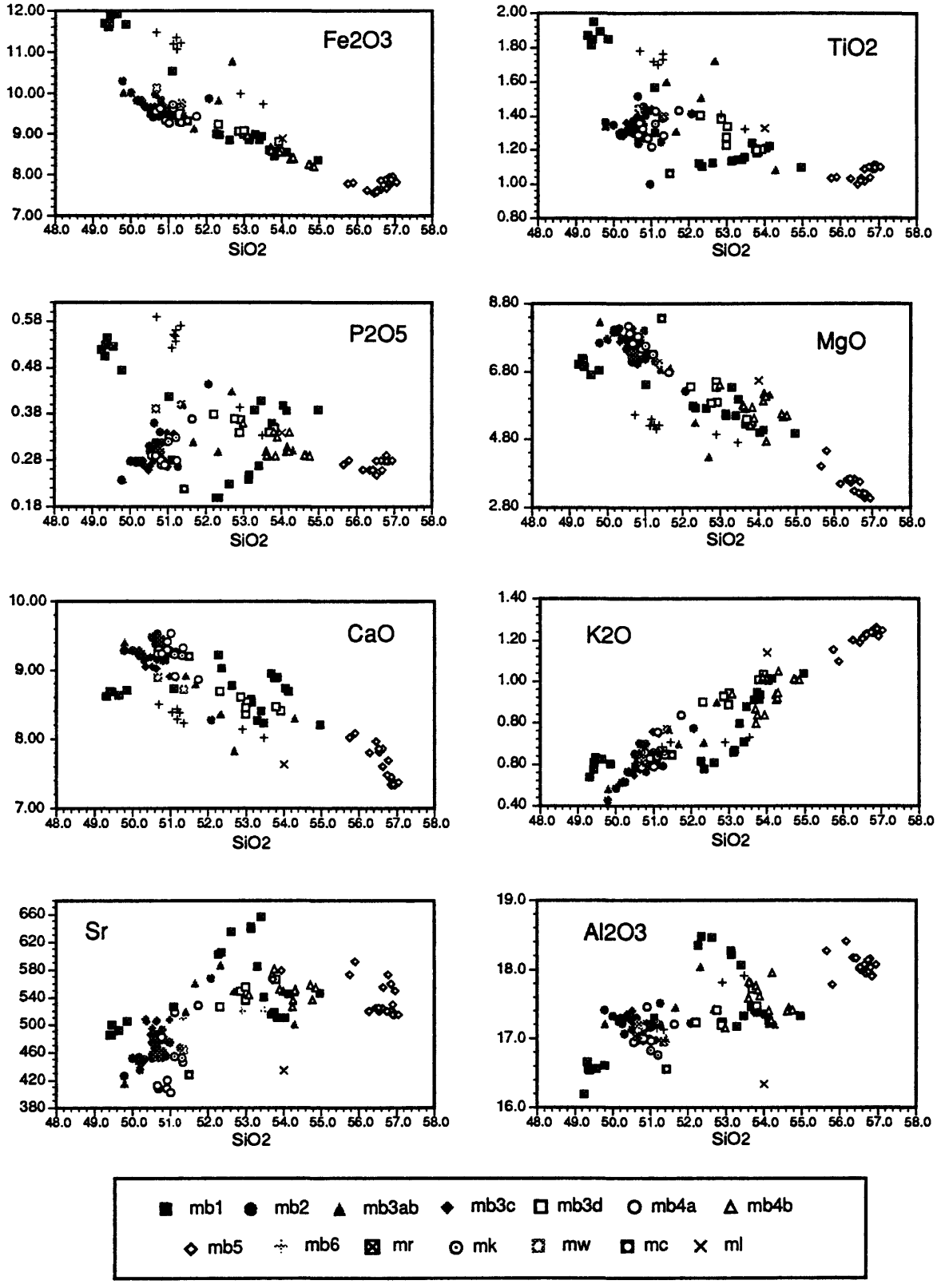

*Figure 11. Major and trace-element variation diagrams*

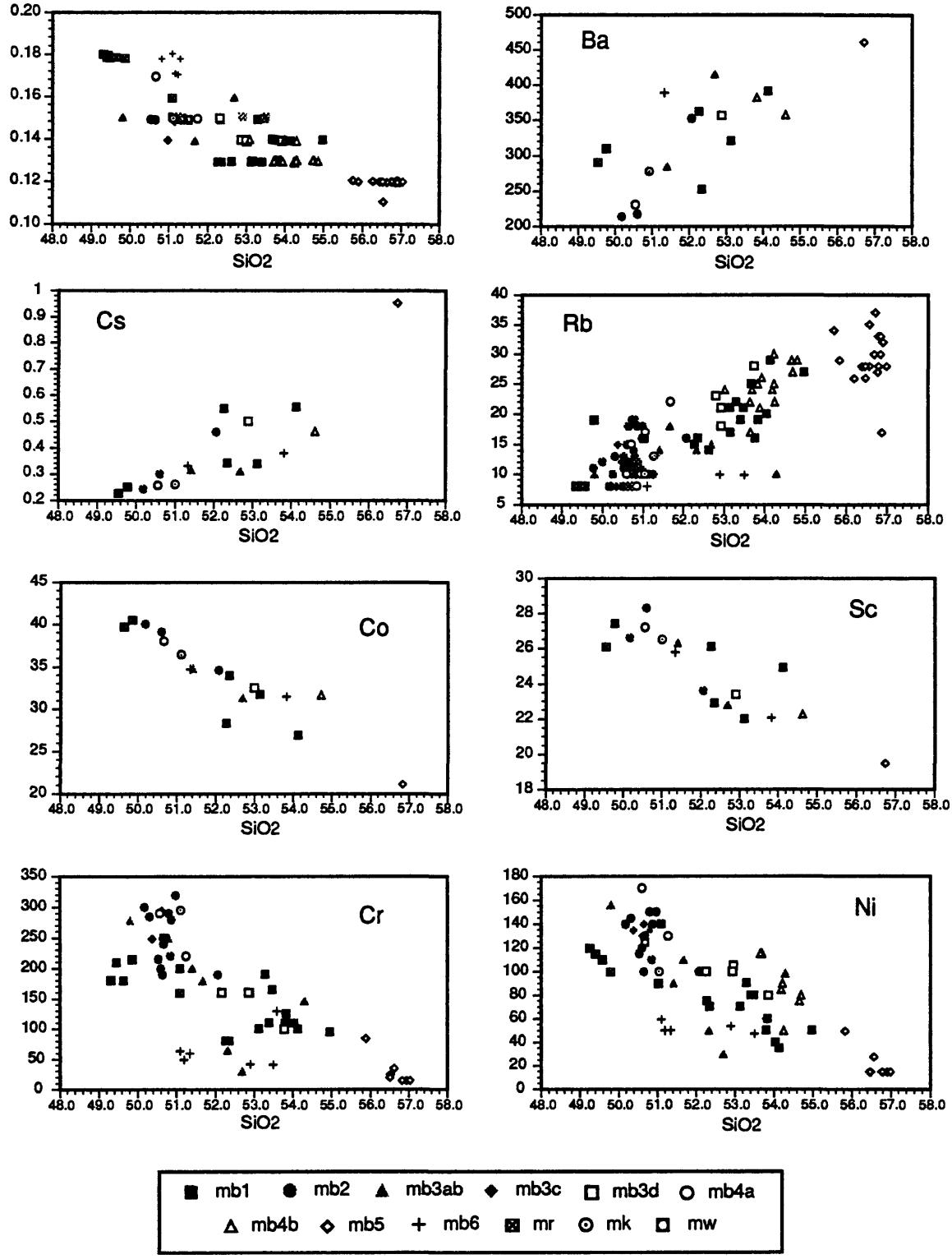

*Figure 12. Trace-element variation diagrams*

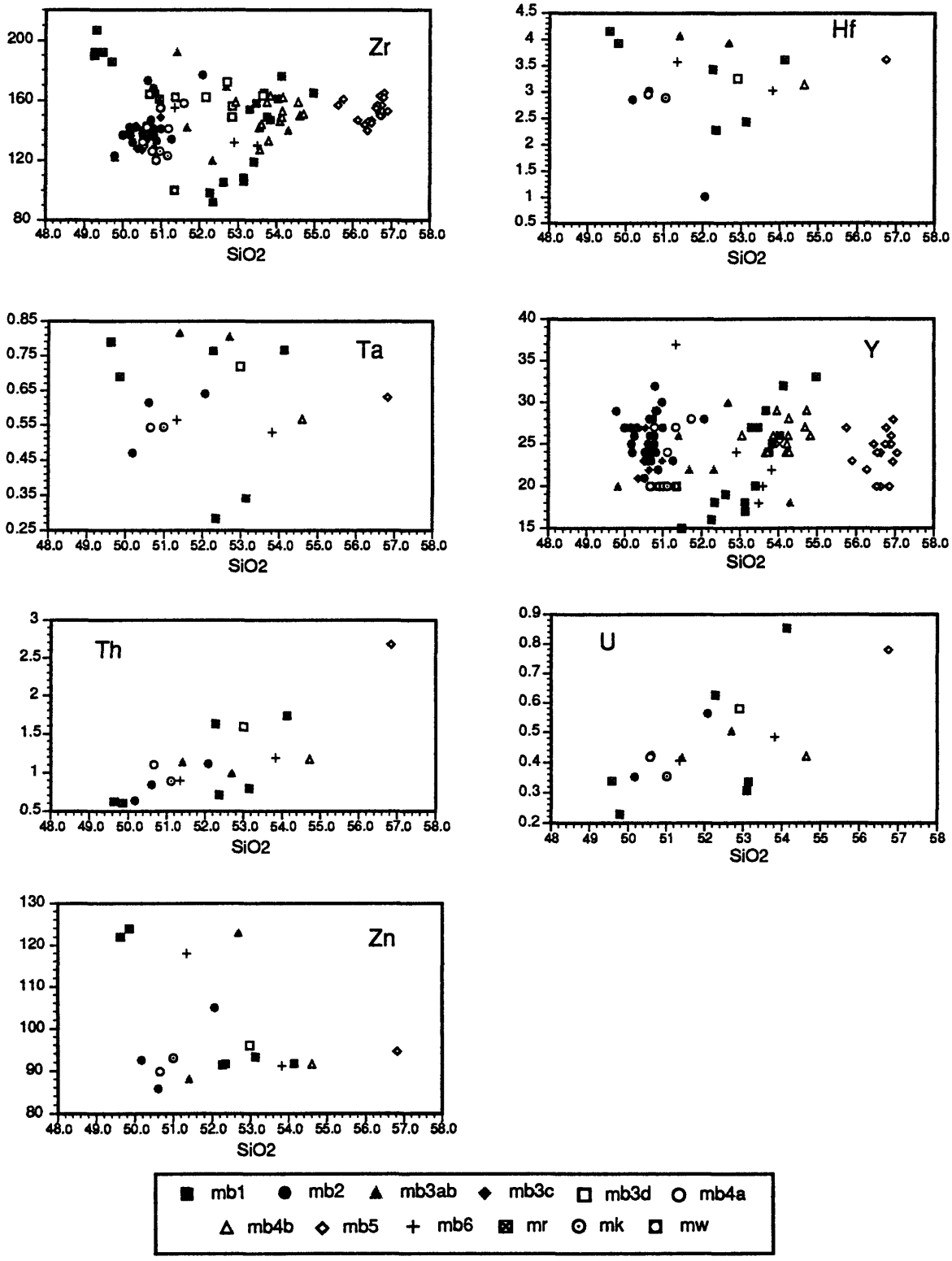

CaO and a positive correlation between Sr and $K_2O$ and Rb. The increase in Sr with increasing $SiO_2$ to about 53 percent $SiO_2$ and then leveling thereafter may reflect changes in mineral fractionation as clinopyroxene fractionation would tend to decrease CaO while increasing Sr (Sr is essentially incompatible in the clinopyroxene lattice and therefore CaO will be removed, but not Sr; Cox and others, 1981), or it may suggest mineral fractionation at different depths as the distribution coefficient of Sr is pressure dependent. As mentioned before there is the odd correlation of high Sr with the high-alumina rocks from the Sheridan segment. The most reasonable explanation may be that the correlation is fortuitous and that these rocks represent a separate batch of magma from that of the other Sheridan flows which has either experienced a different evolutionary history or has evolved from a different source area.

The Ti-group elements, Zr, Hf, and Ta, are negatively correlated with $Al_2O_3$ (fig. 12). This is surprising as Zr tends to form its own mineral rather than substitute into other minerals, and only very small amounts of aluminum are incorporated into a zircon crystal. Hafnium behaves like Zr. Thus the apparent correlation of the Ti-group elements with $Al_2O_3$ may simply be fortuitous and/or reflect different chemical source areas for different lava flows.

Rare Earth Elements

Chondrite-normalized REE spider plots (fig. 13) exhibit the following general relationships. 1) The REE patterns smoothly decrease from La to Lu, with only a minor negative Eu anomaly for the Bachelor, low-alumina Sheridan and Siah lava flows, and no Eu anomaly for the high-alumina Sheridan lava flows. 2) The light rare earth elements (LREE; La to Gd) are about three to five times more enriched than the heavy rare earth elements (HREE; Tb to Lu). 3) The basaltic andesite lava flows have higher LREE values and nearly equal to slightly lower HREE values relative to the basalt lava flows from the same vent. 4) REE patterns for all lava flows are similar with the high-alumina Sheridan basaltic-andesite lava flows having the lowest REE concentrations, and the Red Crater and Egan basalt and basaltic-andesite lava flows having the highest.

### Geochemical groups

Based on the geochemical data set, ten geochemical groups--four of basalt and six of basaltic andesite--were identified along the MBVC (table 7). Geochemical groups were defined as groups in which all samples were within 10 percent of the average of the group; new groups were formed when two or more oxides or elements differed by more than 10 percent. Thus the high-silica basaltic-andesite lava flows from the summit cone of Mount Bachelor (group X) are in a separate geochemical group from the lower-silica basaltic-andesite (group VI) and basalt (group I) lava flows that make up the Bachelor shield. Similarly, the basaltic lava flows from Egan (group IV) are distinct from the basalt-andesite flows from Egan (group V) . This definition worked well for the formation of groups I, III, IV, V, VI, VII, IX, and X, which were distinguished solely on the basis of geochemistry without regard to vent location or other considerations. Group II, however, is admittingly a mixed group containing five basalt and basaltic-andesite lava flows that simply didn't appear to belong anywhere else. Group VIII was divided from group VII on the basis that, in general, the basaltic-andesite lava flows from the central axis of the Sheridan shield (group VIII) consistently appeared slightly different geochemically (for example Ni and La) from the basaltic-andesite lava flows from the Bachelor- Kwohl segment (group VII), even though oxide or element values do not vary by more than 10 percent. In setting up the geochemical groups there was no preconceived number of groups (i.e. there is nothing magical about the number 10) nor was the purpose to assign petrogenetic relationships to the groups. It was devised simply as a means to more clearly identify petrochemical trends as well as to evaluate spatial and temporal relationships, which is difficult to do with large geochemical data bases.

There is usually good correlation between temporally related lava flows from the same vent area and the geochemical groups, although in some instances, like in the case of Egan cone, lava flows from the same vent area may fall into different geochemical groups. In

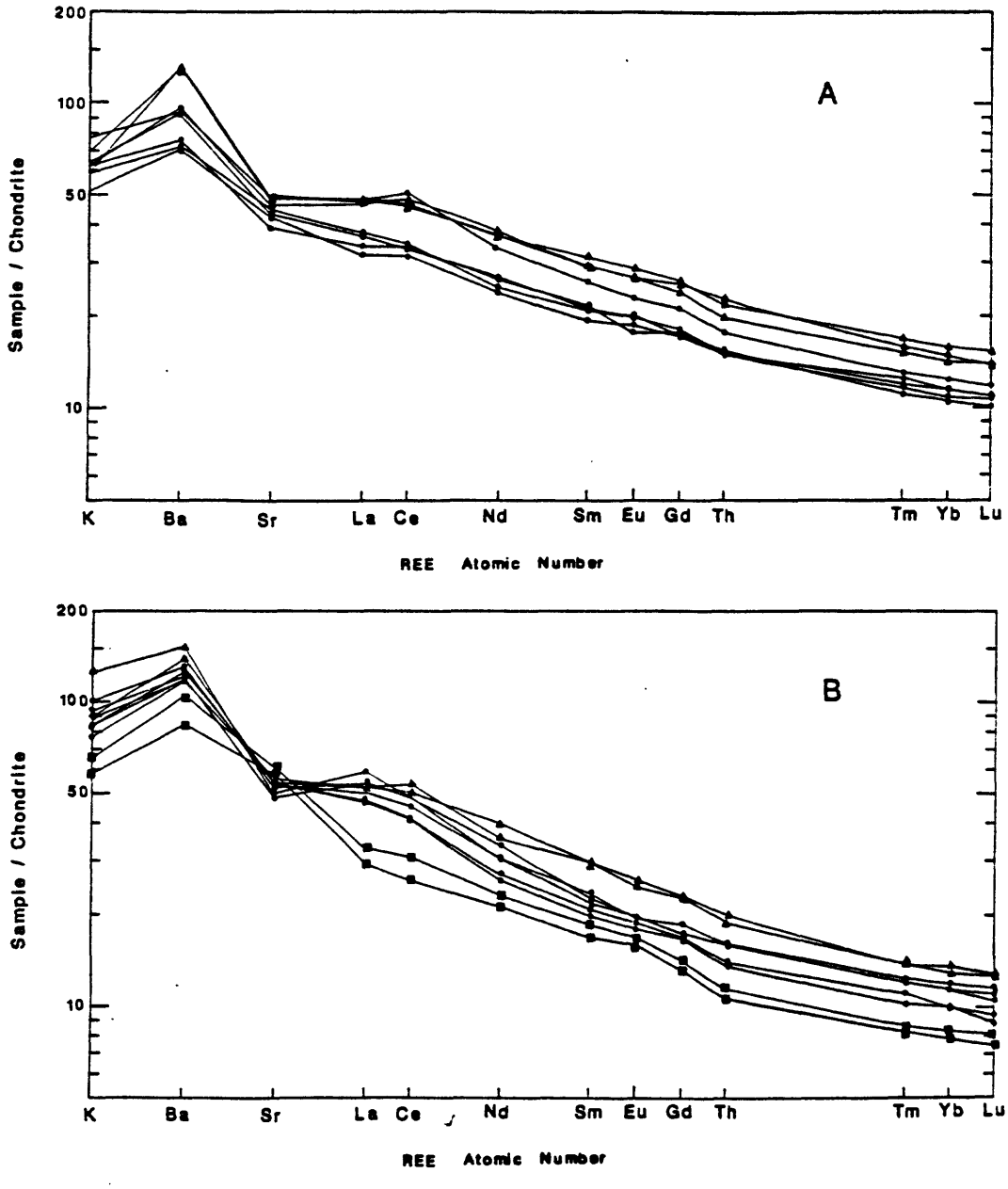


*Figure 13. Chondrite normalized trace-element patterns. A. Basalt. B. Basaltic andesite. Symbols reprsent magma types: circles - MT1; trangles - MT2; and squares - MT3. (Normalization values from Anders and Ebihara, 1982).*

*Table 7. Geochemical groups and magma types of the Mount Bachelor volcanic chain*

| | BASALT | | | | BASALTIC ANDESITE | | | | | |
|---|---|---|---|---|---|---|---|---|---|---|
| MAGMA TYPE | ——MT1—— | | —— MT 2—— | | MT 2 | MT 3 | ——————MT1—————— | | | |
| GEOCHEM. GROUP | I | II | III | IV | V | VI | VII | VIII | IX | X |
| ELEMENTS | | | | | | | | | | |
| Major (wt %) | | | | | | | | | | |
| SiO2 | 50.6± 0.31 | 52.1 ± 0.72 | 49.4 ± 0.16 | 51.1 ± 0.20 | 52.9 ± 0.43 | 52.8 ± 0.44 | 53.7 ± 0.63 | 54.0 ± 0.42 | 55.80 | 56.6 ± 0.3 |
| Al2O3 | 17.2 ± 0.13 | 17.3 ± 0.20 | 16.5 ± 0.16 | 17.2 ± 0.04 | 17.8 ± 0.23 | 18.3 ± 0.15 | 17.4 ± 0.25 | 17.4 ± 0.23 | 17.80 | 18.1 ± 0.09 |
| Fe2O3 | 9.61 ± 0.20 | 9.59 ± 0.32 | 11.74 ± 0.12 | 11.2 ± 0.11 | 10.0 ± 0.42 | 8.89 ± 0.06 | 8.64 ± 0.3 | 8.5 ± 0.08 | 7.80 | 7.78 ± 0.13 |
| MgO | 7.68 ± 0.29 | 6.94 ± 0.60 | 6.98 ± 0.17 | 538 ± 0.10 | 4.86 ± 0.37 | 5.62 ± 0.12 | 5.82 ± 0.41 | 5.14 ± 0.15 | 4.47 | 3.36 ± 0.25 |
| CaO | 9.29 ± 0.15 | 8.84 ± 0.29 | 8.67 ± 0.03 | 8.38 ± 0.07 | 8.09 ± 0.19 | 8.76 ± 0.29 | 8.37 ± 0.13 | 8.75 ± 0.24 | 8.09 | 7.59 ± 0.24 |
| Na2O | 3.27 ± 0.15 | 3.46 ± 0.15 | 3.36 ± 0.09 | 3.60 ± 0.06 | 3.61 ± 0.10 | 3.49 ± 0.08 | 3.49 ± 0.06 | 3.45 ± 0.05 | 3.54 | 3.91 ± 0.12 |
| K2O | 0.60 ± 0.06 | 0.76 ± 0.11 | 0.60 ± 0.03 | 0.65 ± 0.02 | 0.75 ± 0.04 | 0.64 ± 0.04 | 0.94 ± 0.07 | 0.96 ± 0.05 | 1.10 | 1.23 ± 0.03 |
| TiO2 | 1.32 ± 0.07 | 1.45 ± 0.13 | 1.87 ± 0.05 | 1.73 ± 0.02 | 1.49 ± 0.15 | 1.12 ± 0.01 | 1.17 ± 0.1 | 1.19 ± 0.04 | 1.04 | 1.07 ± 0.04 |
| P2O5 | 0.29 ± 0.02 | 0.38 ± 0.06 | 0.52 ± 0.02 | 0.56 ± 0.02 | 0.36 ± 0.05 | 0.23 ± 0.03 | 0.33 ± 0.04 | 0.38 ± 0.03 | 0.28 | 0.27 ± 0.01 |
| MnO | 0.15 ±0.01 | 0.15 ± 0.00 | 0.18 ± 0.00 | 0.17 ± 0.01 | 0.15 ± 0.00 | 0.13 ± 0.00 | 0.14 ± 0.01 | 0.14 ± 0.01 | 0.12 | 0.12 ± 0.00 |
| Mg# | 65 | 62 | 58 | 52 | 50 | 56 | 57 | 55 | 53 | 46 |
| No. of samples | 46 | 5 | 5 | 6 | 4 | 6 | 25 | 7 | 1 | 18 |
| Ca/Al2O3 | 0.54 | 0.51 | 0.52 | 0.49 | 0.45 | 0.48 | 0.48 | 0.50 | 0.45 | 0.42 |
| Trace and REE | | | | | | | | | | |
| Cr* | 269 ± 30 | 190 ± 8 | 216 ± 42 | 60 ± 7 | 44 ± 13 | 93 ± 13 | 140 ± 28 | 123 ± 40 | 85 | 23 ±6 |
| Ni* | 137 ± 16 | 100 ± 8 | 108 ± 14 | 56 ± 5 | 46 ± 10 | 76 ± 8 | 92 ± 17 | 58 ± 20 | 50 | 21 ± 3 |
| Co | 37.6 | | 40.5 | 34.7 | 31.3 | 33.9 | 32 | 26.9 | | 21.1 |
| Sc | 29 | | 26.8 ± .7 | 26.5 | 22.8 | 22.9 | 22.1 | 24.9 | | 19.5 |
| Ba | 245 | | 300 ± 9 | 389 | 416 | 252 | 369 | 391 | | 461 |
| Cs | 0.277 | | 0.24 ± .1 | 0.33 | 0.31 | 0.34 | 0.44 | 0.553 | | 0.954 |
| Rb* | 11.9 ± 3 | | 9.7 ± 4.4 | 9.7±1.5 | 11.5 | 17 ± 4 | 23.1 ± 4.4 | 23 ± 4 | 29 | 29 ± 4 |
| Sr* | 462 ± 28 | 531 ± 21 | 486 ± 18 | 492 ± 8 | 549 ± 27 | 630 ± 20 | 548 ±20 | 539 ± 23 | 592 | 532 ± 20 |
| La | 11.9 | | 14.8 | 15.4 | 16.2 | 9 | 15.1 | 17.8 | | 18.3 |
| Ce | 30.3 | | 37.6 | 38.6 | 41.2 | 21.1 | 35.3 | 42.6 | | 40.4 |
| Nd | 16.6 | | 22.5 | 22.7 | 23.8 | 12.9 | 17.4 | 20.2 | | 18.5 |
| Sm | 4.34 | | 5.77 | 6.2 | 5.95 | 3.33 | 4.12 | 4.86 | | 4.62 |
| Eu | 1.5 | | 1.98 | 2.13 | 1.95 | 1.18 | 1.41 | 1.54 | | 1.42 |
| Gd | 4.84 | | 6.38 | 6.89 | 6.11 | 3.45 | 4.55 | 5.24 | | 4.91 |
| Tb | 0.747 | | 0.956 | 1.05 | 0.933 | 0.509 | 0.7 | 0.806 | | 0.757 |
| Tm | 0.401 | | 0.505 | 0.55 | 0.458 | 0.273 | 0.37 | 0.43 | | 0.411 |
| Yb | 2.43 | | 3.07 | 3.4 | 2.83 | 1.66 | 2.25 | 2.65 | | 2.55 |
| Lu | 0.361 | | 0.456 | 0.501 | 0.418 | 0.242 | 0.319 | 0.397 | | 0.373 |
| Y* | 24 ±3 | 23 ± 3 | 34 ± 3 | 31 ± 3 | 24 ± 4 | 18 ± 1 | 25 ±3 | 28 ± 3 | | 24 ± 3 |
| Zr* | 138 ±9 | 165 ± 17.5 | 192 ± 7 | 149 ± 4 | 138 ± 19 | 104 ± 8 | 152 ± 10 | 161 ±8 | 161 | 152 ± 7 |
| Hf | 3.16 | | 3.94 | 3.58 | 3.94 | 2.27 | 3.15 | 3.61 | | 3.63 |
| Th | 0.81 | | 0.606 | 0.895 | 0.992 | 0.71 | 1.35 | 1.73 | | 2.68 |
| Zn* | 75 ± 5 | 83 ± 5 | 94 ± 7 | 101 ± 5 | 93 ± 4 | 80 ± 0 | 81 ± 3 | 81 ± 2 | 80 | 78 ± 6 |
| Cu* | 67 ± 7 | 60 ± 0 | 65 ± 4 | 48 ± 4 | 59 ± 2 | 62 ± 3 | 66 ± 5 | 67 ± 6 | 60 | 55 ± 8 |

*Explanation. Major element analyses determined by WDXRF (wave-length dispersive x-ray florescence spectroscopy); analyses of trace -elements denoted by * were determined by EDXRF (energy dispersive x-ray florescence spectroscopy); REE and other trace-element analyses determined by INAA (instrumental neutron activiation analysis). Mg#=(moles MgO/moles Mgo+FeO). No. of samples = number of samples averaged to determine geochemical groups and standard deviation major elements. The standard deviation for the REE and other trace elements are based on a much smaller and varying number of samples: where no statistics are recorded the sample size is one. The number of samples for a given geochemical group merely reflects sampling distribution and does not imply either a greater volume or significance of that group.*

the opposite way it is clear that most of the basalt from the central axis of the chain is broadly similar chemically regardless of vent area or temporal relation.

An advantage of viewing the data in terms of groups is that it helps bring order to the data. For example, basalt groups III and IV from Red Crater and Egan cone, respectively, have significantly lower magnesium numbers (Mg#), Cr, and Ni concentrations than the basalt from the rest of the chain, reflecting their overall lower MgO and higher $Fe_2O_3$ concentrations (table 5). Similarly they have very high $TiO_2$ concentrations with regard to the other groups. It is also more readily seen that basalt group III has higher REE values than group I basalt even though it has lower silica values. REE values for basaltic-andesite group VI, the high-alumina flows from Sheridan are the lowest of all the geochemical groups, basalt and basaltic andesite alike (fig 13; table 7).

On the basis of these relationships I have further subdivided the geochemical groups into magma types (MT1, 2 and 3). Groups I, II, VII, VIII, IX, and X fall into MT1, groups III, IV, and V (which includes both Egan basaltic andesite and mb3b from the east side of Mount Bachelor) into MT2, and group VI into MT3. In the section on petrogenesis, I will test geochemical relations between geochemical groups within the same magma type and between different magma types.

## Classification

Lava flows of the MBVC range in silica content from 49 to 57 percent $SiO_2$ and fall into the basalt (45 to 52 percent $SiO_2$) and basaltic andesite (52 to 57 percent $SiO_2$) fields on the total alkali-silica diagram (fig. 14) recommended by the IUGS (LeBas and others, 1986). This division works well for classifying the MBVC lava flows, inasmuch as the lithologically similar and spatially related lava flows that form the major part of the Sheridan Mountain, Kwohl Butte, and Mount Bachelor shields range from 52 to 55 weight percent $SiO_2$ and thus can be classified under one heading. The lava flows are clearly subalkaline.

Subdivision of the subalkaline rocks into the calc-alkaline or tholeiitic series on the basis of an iron-enrichment trend was proposed

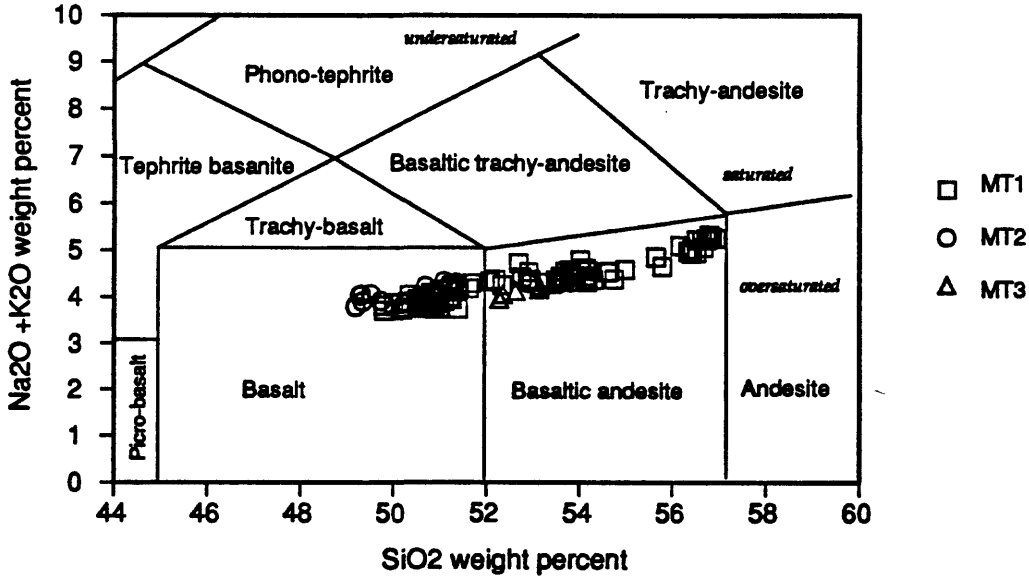


*Figure 14. Total alkali versus silica classification diagram of igneous rocks (from LeBas and others, 1986). Samples from the MBVC are plotted on a select view of the diagram from 44 to 60 wt. % SiO2. Symbols correspond to magma types: squares - MT1; circles - MT2; triangles - MT3.*

by Wager and Deer (1939) and the division commonly used to separate the two fields was defined by Irvine and Baragar (1971). No samples from the MBVC plot in the tholeiite field on an AFM diagram (fig. 15), although samples from the Red Crater chain of cones and Egan cone fall near the line. Miyashiro (1974) argued that the difference between tholeiitic and calc-alkaline suites is not necessarily defined by the presence or absence of an iron-enrichment trend, but rather is characterized by a total FeO/MgO ratio relative to either $SiO_2$ or the alkalis. A distinct advantage of the FeO/MgO vs $SiO_2$ diagram over the AFM diagram is that discrimination of calc-alkaline and tholeiitic rocks can be done on the basis of individual samples; thus an entire rock suite is not needed. For samples of the MBVC, the dividing line on a FeO/MgO vs $SiO_2$ discrimination diagram passes between the MT2 rocks and the MT1 and MT3 rocks (fig. 16); however, it should be noted that most samples plot near the line, and that samples from the summit cone of Mount Bachelor fall near or on the line.

Gill (1981) notes that in tholeiitic rocks, FeO is greater than CaO, and $P_2O_5$ generally increases with increasing $SiO_2$, at least initially. The opposite relations are present in calc-alkaline rocks. Lava flows of the groups III, IV, and V (MT2) show oxide trends that Gill (1981) ascribes to tholeiitic rocks, whereas lava flows of the other two groups (MT1 and MT3) show oxide trends that he ascribes to calc-alkaline rocks (fig. 10; table 7).

On the basis of the Miyashiro discrimination diagram and major oxide trends (CaO and FeO, and $P_2O_5$), I classify MT2 lava flows as tholeiitic (Red Crater , Egan lava, and large plagioclase mb3b flows from the east side of the Bachelor shield) and MT1 and MT3 lava flows as calc-alkaline. Although there is no noticeable Fe-enrichment trend on the Irvine and Baragar (1971) discrimination diagram (fig. 15), the MT2 geochemical groups plot closer to the tholeiite line than geochemical groups of MT1 or MT3. It should be reiterated, however, that none of the geochemical groups are strongly calc-alkaline or tholeiitic.

## Summary

In summary, the basalt (49-52 percent $SiO_2$) and low-silica basaltic-andesite (52-55 percent $SiO_2$) lava flows are generally olivine- and plagioclase-phyric, and contain olivine, plagioclase, iron-titanium oxides, and in some cases, clinopyroxene in the groundmass. The high-silica basaltic andesite lava flows (56-58 percent $SiO_2$) of the summit cone of Mount Bachelor are mineralogically unique in that they contain clinopyroxene as a phenocryst phase in addition to olivine and plagioclase, and have two clinopyroxenes in the groundmass phase. In all of the lava flows, phenocrysts are generally subhedral to euhedral and olivines lack reaction rims. In most thin sections, two plagioclase textures were noted–homogeneous and sieve-textured. In all cases, the homogeneous-textured plagioclase phenocrysts are volumetrically dominant but plagioclase phenocrysts of both textures are similar in size.

On the basis of the geochemistry, ten geochemical groups were distinguished, which are further subdivided into three magma types. Volumetrically, the majority of lava flows of the MBVC belong to MT1 which consists of basalt and basaltic andesite and encompass geochemical groups I, II, VII, VIII, IX, and X. Basalt of this magma type are the most primitive found along the MBVC and are classified as calc-alkaline.

Lava flows of MT2 include both basalt (groups III and IV from the Red Crater chain of cones and Egan cone respectively) and low-silica basaltic andesite (group V from Egan cone and mb3b from the E side of the Bachelor shield). In the field, lava flows from MT2 geochemical groups are indistinguishable from lava flows of either MT1 or MT3 geochemical groups; geochemically, however, they are more evolved. Two of the basaltic-andesite samples that make up MT2, geochemical group V (mb3b) are of the distinctive large, euhedral, plagioclase-phyric rock type discussed in the petrography section. MT2 rocks are classified as tholeiites.

Lava flows of MT3 are all low-silica basaltic andesite and comprise geochemical group VI from the Sheridan segment. They have the highest Sr and $Al_2O_3$ values and the lowest REE values of all the rocks sampled in the MBVC. Geochemical group

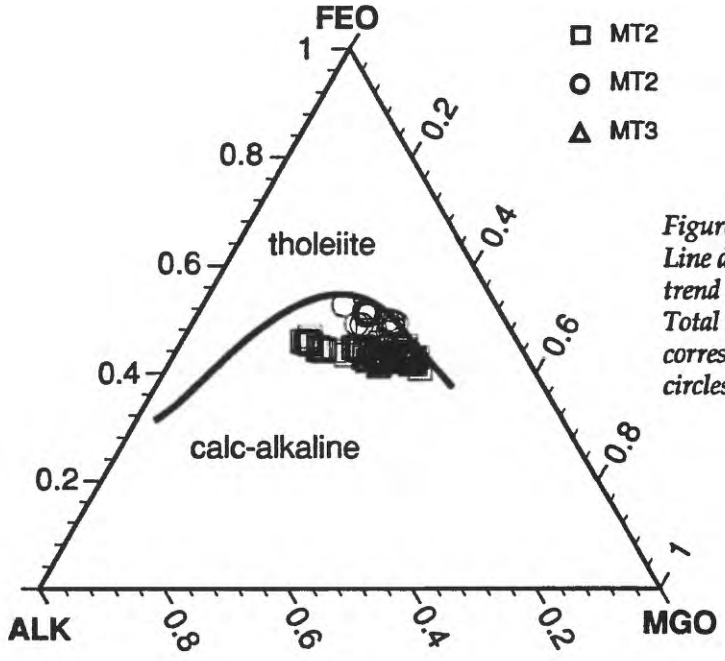


*Figure 15. A-F-M diagram of MBVC samples. Line distinguishes calc-alkaline from tholeiite trend as defined by Irvine and Baragar (1971). Total iron recalculated as FeO. Symbols correspond to magma types: squares - MT1; circles - MT2; and triangles - MT3.*

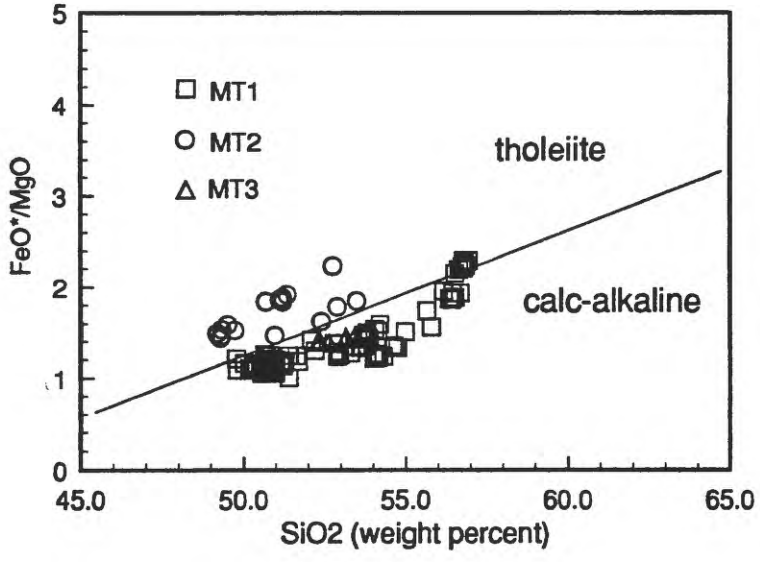


*Figure 16. Variations in FeO/MgO ratios versus silica for samples from the MBVC. Line distinguishes calc-alkaline from tholeiite trend as defined by Miyashiro (1974). Total iron recalculated as FeO. Symbols correspond to magma types: squares - MT1; circles - MT2; and triangles - MT3.*

VI includes two distinctive rock types; aphanitic lava flows, and large, euhedral, plagioclase-phyric lava flows (the latter looks the same as the MT2, geochemical group V rocks) discussed in the petrography section. These rocks, like the MT1 rocks, are classified as calc-alkaline.

## SPATIAL AND TEMPORAL RELATIONS OF MAGMA TYPES AND GEOCHEMICAL GROUPS

Spatial and temporal evolution of the MBVC determined by field mapping (Scott and Gardner, 1992) and paleomagnetic secular-variation studies are shown in relation to the ten geochemical groups and three magma types in figure 17. In general, there is good correlation between geochemical groups and mapped rock units (see fig. 2). This I believe is good supportive evidence for the validity of the geochemical groups.

Spatially, the volumetrically dominant calc-alkaline MT1, containing geochemical groups I, II, VII, VIII, IX and X, erupted mostly from vents along the central axis of the chain and from Katsuk Butte. Although vents for many of the older Bachelor-Kwohl lava flows have been buried, the distribution of shield lavas suggests that these flows were mostly erupted from vents along the axis of the chain. Vents for the volumetrically subordinate, tholeiitic MT2 lava flows from the Red Crater chain of cones and Egan cone lie either off axis or along the periphery of the MBVC. Vents for the aphanitic (mb1c) MT3, geochemical group VI lava flows from the Sheridan shield lie off axis of the chain on the west flank of the shield. However, vents for the large plagioclase-bearing MT3 lava flows (mb1a), as well as for the large plagioclase-bearing MT2 lava flows (mb3b), which have been subsequently buried, appear to have been along the axis of the chain.

The detailed spatial, temporal, and geochemical data provide useful feedback in developing a model for the evolution and development of the MBVC. Of particular note in regard to the geochemical evolution and underlying plumbing system of the MBVC are the following relationships. 1) Basalt was erupted along the entire length of the chain, whereas low-silica basaltic andesite was erupted only in the northern two-thirds, and high-silica basaltic andesite was erupted only in the northern third. Thus, the most silicic products were erupted at the north end of the MBVC which is geographically closest to the silicic highland of the Three Sisters-Broken Top area (fig. 1). 2) MT1 vents are located dominantly along the axis of the MBVC, whereas MT2 and MT3 vent locations are found dominantly along the margins or off axis of the chain. 3) MT1, group 1 basalt flows were erupted during every eruptive episode except the last (episode IV). 4) In episode III there is stratigraphic evidence to indicate the relative sequence of eruptive products. In that episode, which ranges in silica content from 50 to 57 percent $SiO_2$, eruptions became more silicic with time. 5) Lavas flows associated with the earliest eruptive episode (episode I) were vented along the entire length of the chain, whereas lava flows associated with subsequent eruptive episodes were more localized. 6) During the first and third eruptive episodes, which were volumetrically much larger than the second and fourth episodes, lava flows of several geochemical groups and magma types were extruded.

Thus, any model proposed for the geochemical evolution of the Mount Bachelor chain must accommodate, in addition to the petrologic and chemical evidence, the temporal and spatial relations of the geochemical groups and magma types. A reasonable model should explain both the uniformity of the MT1, geochemical group I basaltic chemistry through time as well as the differences between the basalt geochemical groups. In addition, the model should explain the essentially simultaneous eruptions of different geochemical groups and magma types.

## GEOCHEMICAL EVOLUTION OF THE MBVC

### Petrogenesis

In general, there are two primary stages for the differentiation of magma; one is in a source area, where partial melting imparts the initial chemical signature to a melt, and the other is in a magma chamber (or conduit), where various processes such as crystal fractionation, magma-mixing, and assimilation can modify the initial chemical signature. Processes at both stages contribute to the variety of lavas that reach the surface;

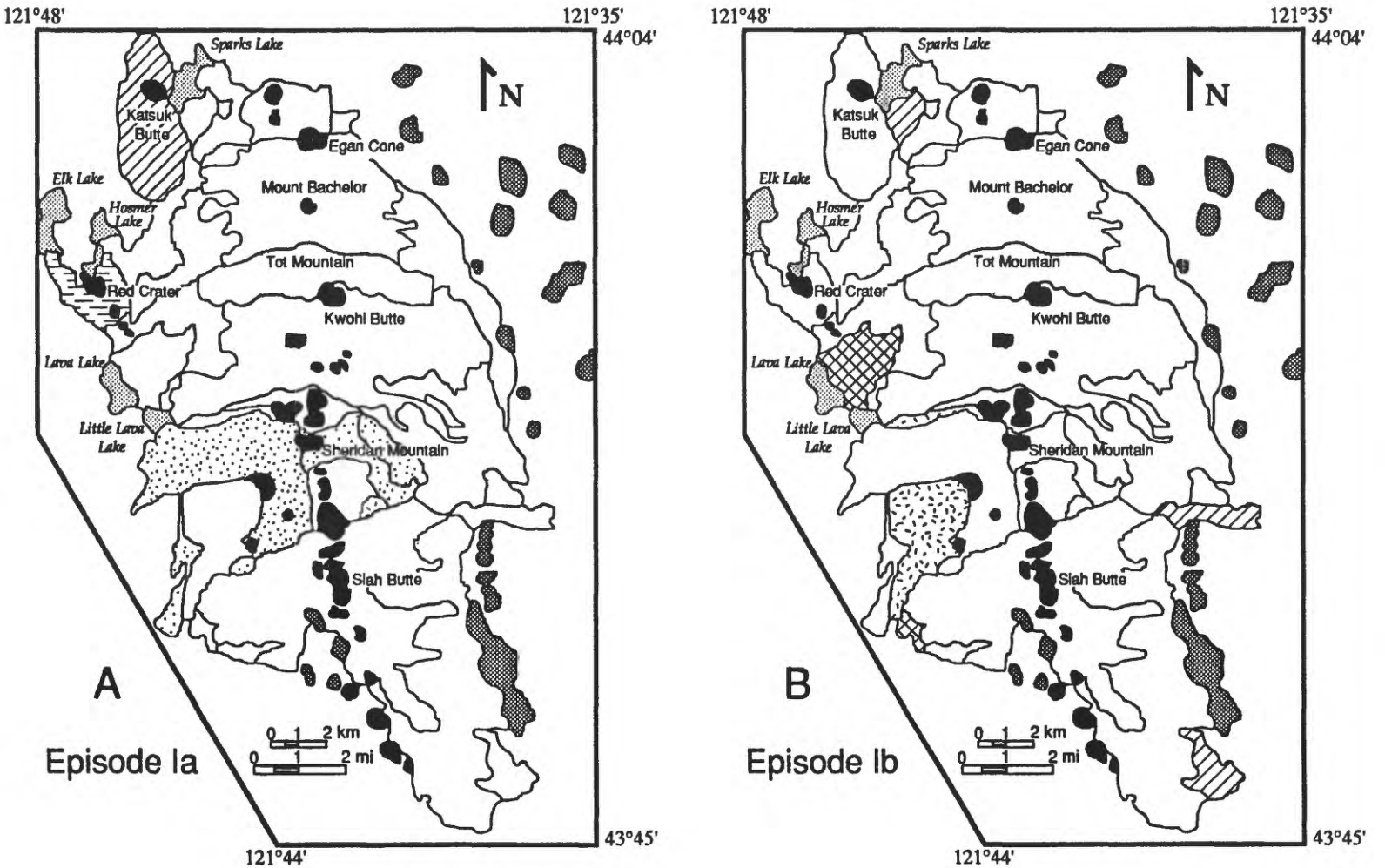


*Figure 17. Maps correlating geochemical groups with the spatial and temporal evolution of the Mount Bachelor volcanic chain. Explanation of geochemical group patterns is given after figure 17-E.*

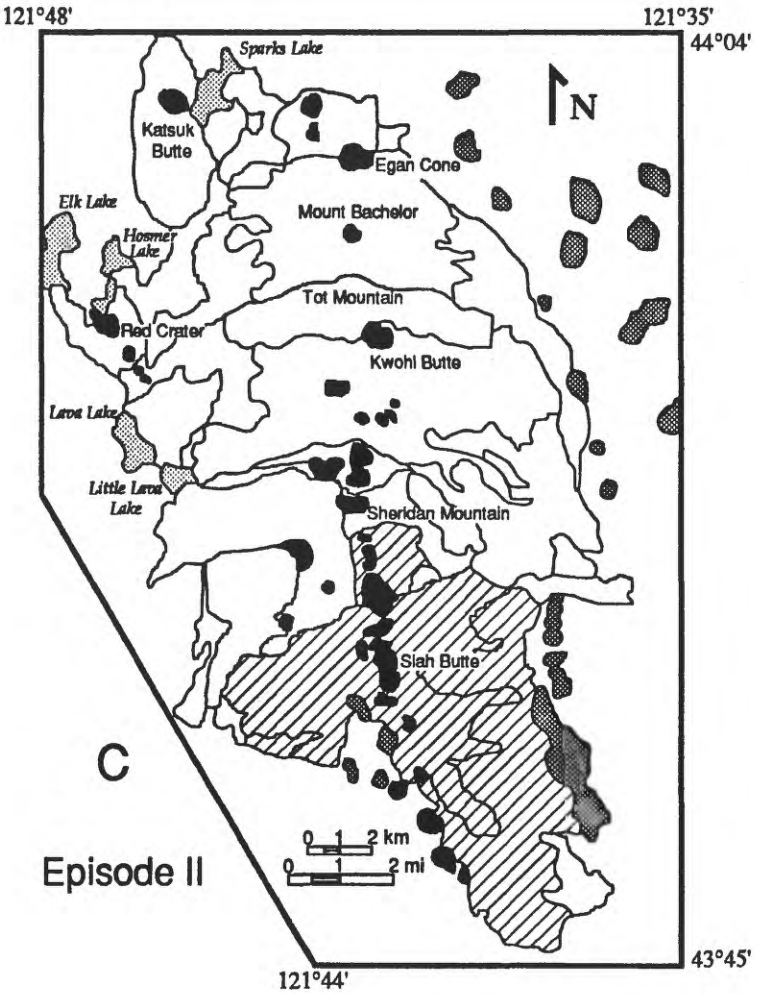


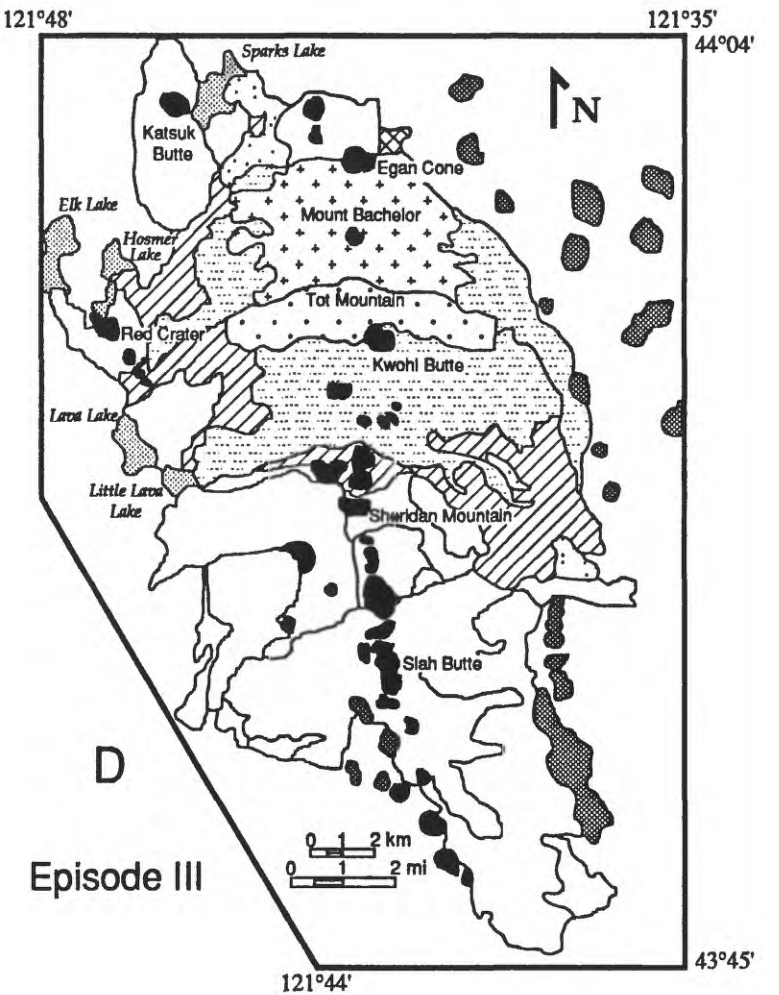


*Figure 17. continued.*

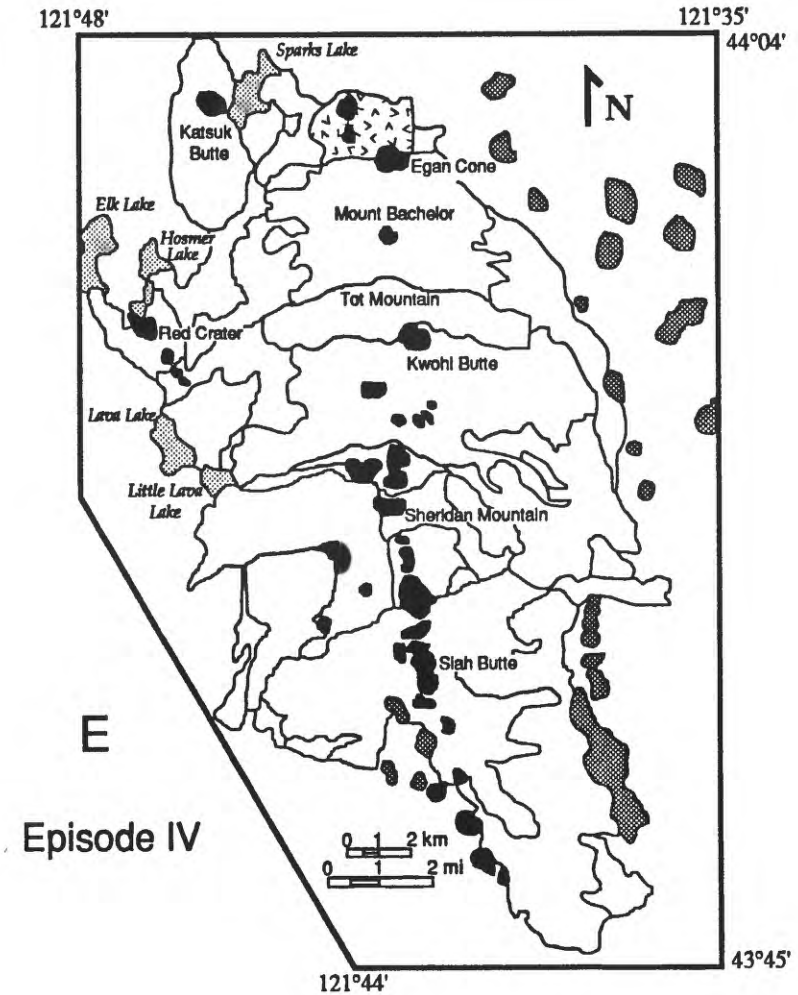


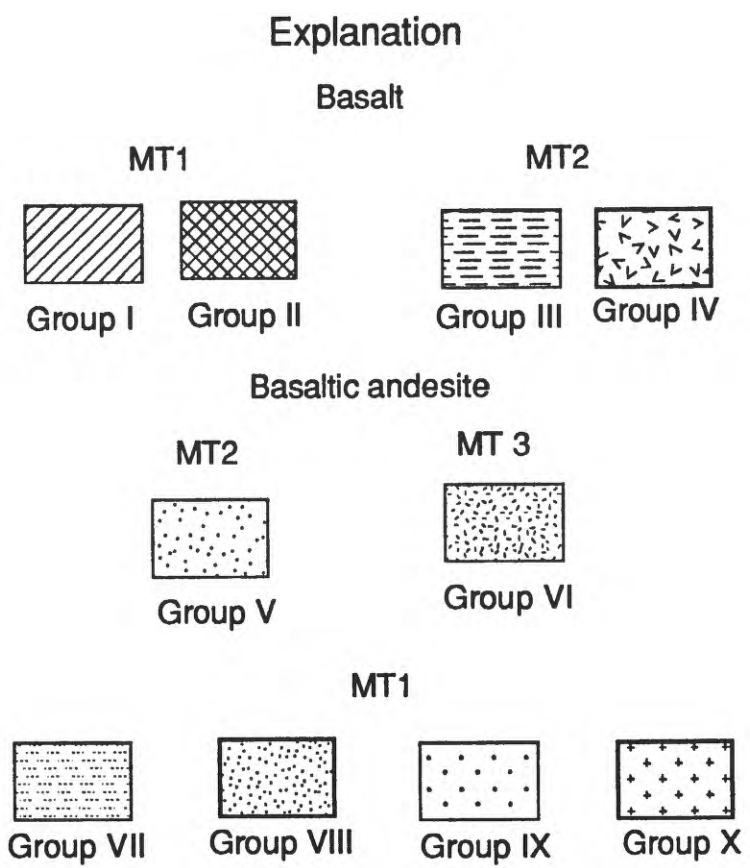


*Figure 17. continued.*

however, the degree to which that variation is due to processes acting in the source area or in the magma chamber is often difficult to assess. Partial melts from chemically different source areas typically have different REE values or patterns and dissimilar incompatible trace-element ratios. Magmas that have undergone crystal fractionation should show a progression of REE values and patterns that are consistent with mineral phases that are extracted, and parent and daughters should have similar incompatible trace-element ratios.

The purpose of this section is to evaluate the origin of the chemical diversity along the MBVC. Fundamentally, were the basaltic andesite magmas derived from the basalt magmas, or was their genesis distinct? Secondly, do the different magma types represent rocks from distinct source areas, or do they represent rocks that have followed different evolutionary paths from the same source area?

The approach to answering these questions will be to examine the major-, trace-, rare-earth element, and petrographic data to suggest potential petrologic models. These potential models will be tested using standard assimilation, crystal fractionation, and magma-mixing (AFCM) computer programs. By implication, if program compositions do not adequately explain the observed data then partial melting or distinct source areas will be invoked as the dominant control on variation.

## Major-Element Variations

Bowen (1928) argued in favor of crystal fractionation being the dominant process that links mafic and silicic magmas, a view that Gill (1981) favored for the formation of orogenic andesites. Crystal fractionation has been demonstrated to have played a major role in the differentiation of mafic lavas at Kilauea Iki, Hawaii (Wright and Fiske, 1971; Wright and others, 1976). Mineral phases that may have contributed to crystal fractionation in the MBVC lavas are, in order of decreasing volumes, plagioclase, olivine, magnetite, augite, Cr-spinel and pigeonite.

Rose and others (1980) demonstrated by means of $K_2O$-$SiO_2$ diagrams, that the evolution of composite cones within the Atitlan cauldron (Guatemala) was largely controlled by crystal fractionation of olivine and plagioclase. On a similar diagram using a moderately primitive MT1 Bachelor-segment group I basalt as a parent, most MT1 samples fall between plagioclase and olivine control lines (fig. 18), although several basalt flows from the Siah chain of cones and some from Kwohl Butte plot outside the boundaries of the fractionation lines. These flows have lower $SiO_2$ and $K_2O$ values and therefore plot below the parent composition, but their trend is similar to that of the majority of MT1 samples. Samples from MT2 and MT3 lava flows plot either outside the boundaries of the fractionation lines or between the magnetite and olivine fractionation lines.

For the MT1 samples that fall between the olivine and plagioclase control lines, the data indicates that crystal fractionation could control their evolution, but that a single mineral phase is not responsible for the variations observed. Basalt from the Red Crater chain of cones (MT2) plot to the left of the MT1 basalt which suggests that these rocks cannot be derived from MT1 basalt, but that perhaps MT1 basalt could be derived from them through fractionation of magnetite. Similarly, MT3 samples plot near the magnetite fractionation line suggesting that if they are related to MT1 and MT2 basalt, it would be by fractionation of magnetite and not the other phases.

Either clinopyroxene or plagioclase fractionation can move compositions away from olivine and magnetite control lines. The relative importance of these two phases can be assessed by examining variations in the $CaO/Al_2O_3$ ratio with increasing $SiO_2$ (none of the other mineral phases contain either oxide in amounts that would affect the ratio). Clinopyroxene $CaO/Al_2O_3$ ratios are high ($Ca/Al_{cpx}$ = 7-4); therefore clinopyroxene fractionation depletes the magma in CaO relative to $Al_2O_3$, thus lowering the ratio with increasing $SiO_2$. The opposite effect occurs with calcic plagioclase fractionation ($Ca/Al_{plag}$ = 0.5). In both the MT1 and MT2 lavas, $CaO/Al_2O_3$ ratios decrease with increasing $SiO_2$ (0.55-0.42 and 0.52-0.48 respectively; table 7) suggesting that if crystal fractionation is involved, clinopyroxene plays an important role. This does not imply, however, that the amount of clinopyroxene

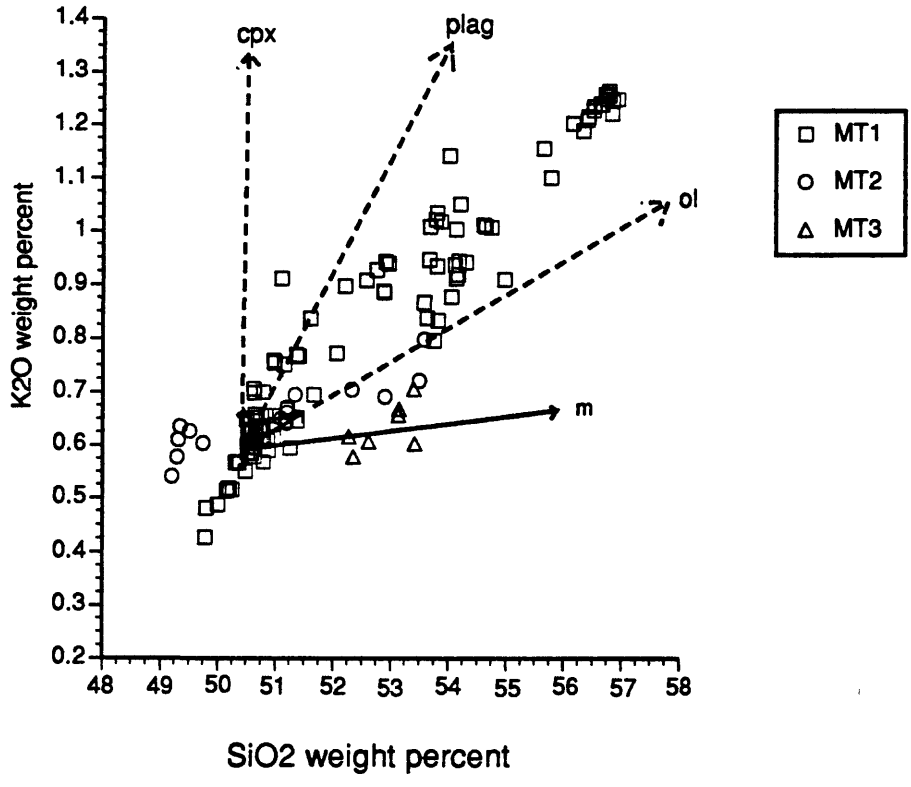


*Figure 18. K2O-SiO2 mineral fractionation diagram. The diagram shows the effects on K2O and SiO2 values of crystal fractionation of a mineral phase from a geochemical group I basaltic parent: cpx, clinopyroxene; plag, plagioclase; ol, olivine; and m, magnetite. Symbols keyed to magma types: squares - MT1; circles - MT2; and triangles - MT3. Solid lines are 10 percent crystal fractionation lines (mostly hidden by data), dashed lines are extensional traces.*

fractionation is greater than plagioclase fractionation. Cox and Devey (1987) demonstrated that when an assemblage of olivine, clinopyroxene, and plagioclase in the proportions of 15:35:50 are removed from a melt, the $CaO/Al_2O_3$ ratio decreases from 0.79 to 0.60 with 40 percent crystallization.

In a similar manner, either magnetite or olivine can move compositions away from plagioclase and clinopyroxene control lines. Evidence that both mineral phases may have contributed to crystal fractionation is that MgO and $TiO_2$, elements that favor olivine and magnetite respectively, both decrease with increasing $SiO_2$ in the MT1 and MT2 lavas.

A potential problem in invoking either clinopyroxene or magnetite crystal fractionation to account for geochemical variation in the MBVC lavas is that neither mineral is observed as a phenocryst phase in either the basalt or low-silica basaltic-andesite lava flows. Gill (1981) argues that the lack of phenocrystic magnetite is a size problem only, as magnetite crystals below phenocryst size (<0.5 mm) are still able to separate from the liquid due to their high density. Also, there is some evidence, although no consensus, that the stability field of magnetite is greater at high pressure and $fO_2$; thus magnetite fractionation could occur at depth, but not play a significant role at near-surface pressures (Gill, 1981).

Crystal fractionation of clinopyroxene at depth has also been invoked to account for the discrepancy between the chemical imprint of clinopyroxene and the lack of clinopyroxene phenocrysts (O'Donnell and Presnall, 1980). Others have suggested that sidewall crystal fractionation, or the plating of clinopyroxene onto the cooler walls of the magma chamber,

may account for the poor correlation between abundance of clinopyroxene phenocrysts observed and the amount called upon to produce viable crystal fractionation results (Dungan and Rhodes, 1978; Reagan and others, 1987).

## Trace-Element Variations

Mineral preference for certain trace elements is much more selective than for major elements; thus trace-element analysis is a sensitive tool for refining petrologic interpretations of igneous processes (see Gast, 1968; Arth, 1976; O'Hara, 1977; Allegre and others, 1977; O'Hara and Mathews, 1981; Depaolo, 1981). The final trace-element concentration in a sample is due to the original amount of the element in the source area, the extent of crystal/liquid fractionation during melting, and the extent of crystal fractionation during ascent and in a magma chamber (Gast, 1968). Crystal fractionation depletes the melt in compatible elements (those elements preferentially incorporated into the crystal relative to the melt) and enriches the melt in incompatible elements (those elements preferentially incorporated into the melt relative to the crystals). Magmas related by crystal fractionation processes should exhibit sequential enrichment in the incompatible elements and ratios between highly incompatible elements should be the same. Magmas from source areas with different compositions should have variable incompatible element ratios (O'Hara, 1977).

Normalization diagrams show the relative enrichment or depletion of elements of one sample (or geochemical group) to another; thus, they provide a simple graphical technique to test petrologic models (see Smith and Leeman, 1987). A normalization diagram for MT2, geochemical group III basalt (Red Crater) to MT1, geochemical group I basalt (fig. 19a) shows that the group III basalt flows are enriched in incompatible and, especially, rare-earth elements, and depleted in the compatible element Mg, relative to the group I basalt flows. The normalization diagram for MT2, group IV basalt (Egan cone) to MT2, group III basalt shows that these two groups have similar REE concentrations, but that other incompatible elements are enriched in the group IV lavas relative to the group III lavas (fig. 19b). Thus, by inference, the group IV lavas are also enriched in the incompatible and rare-earth elements relative to group I basalt flows. Based solely on the trace-element data, it appears that the MT2 basalt geochemical groups III and IV could be derived from MT1 geochemical group I basalt through crystal fractionation of the observed mineral phases, but not the other way around. However this is contrary to interpretations of the major-element data made on the basis of the $K_2O$-$SiO_2$ diagram (fig. 18). Group III has lower (and group IV only slightly higher) silica contents than group I, so groups I and III (and most likely I and IV) cannot be related by crystal fractionation, because none of the mineral phases observed would decrease themelt in $SiO_2$ while enriching the melt in incompatible elements. Trace-element relationships between groups III and IV , however, suggest that these two MT2 basalt groups may lie along a direct liquid line-of-descent evolutionary path or that the two groups at least evolved in a similar manner from similar parental material.

Magma type 3, basaltic andesite group VI lavas have lower incompatible and REE concentrations than either MT1, basalt group I (fig. 19c) and thus by inference MT2, basalt groups III or IV lavas. This argues against the derivation of these basaltic-andesite lavas from any of the basalt lavas sampled in the MBVC by crystal fractionation processes, as none of the mineral phases observed would deplete group VI lavas in incompatible and rare-earth elements while simultaneously increasing their silica content. Therefore, from these simple diagrams it is clear that none of the magma types are directly related to each other by simple crystal fractionation.

Comparison of MT1 basaltic andesite groups with MT1 basalt (figs. 20 a, b, and c) shows enrichment of incompatible trace-elements and LREE and either slight or no enrichment of the HREE. This is supportive evidence that the MT1 basaltic andesite groups could be derived from MT1 basalt by crystal fractionation. Comparison of normalization patterns of geochemical group VIII basaltic andesite from Sheridan Mountain with that of geochemical group VII from Mount Bachelor shows that the Sheridan Mountain basaltic andesites have slightly higher incompatible trace-element and REE values than Mount Bachelor basaltic andesite. This suggests that

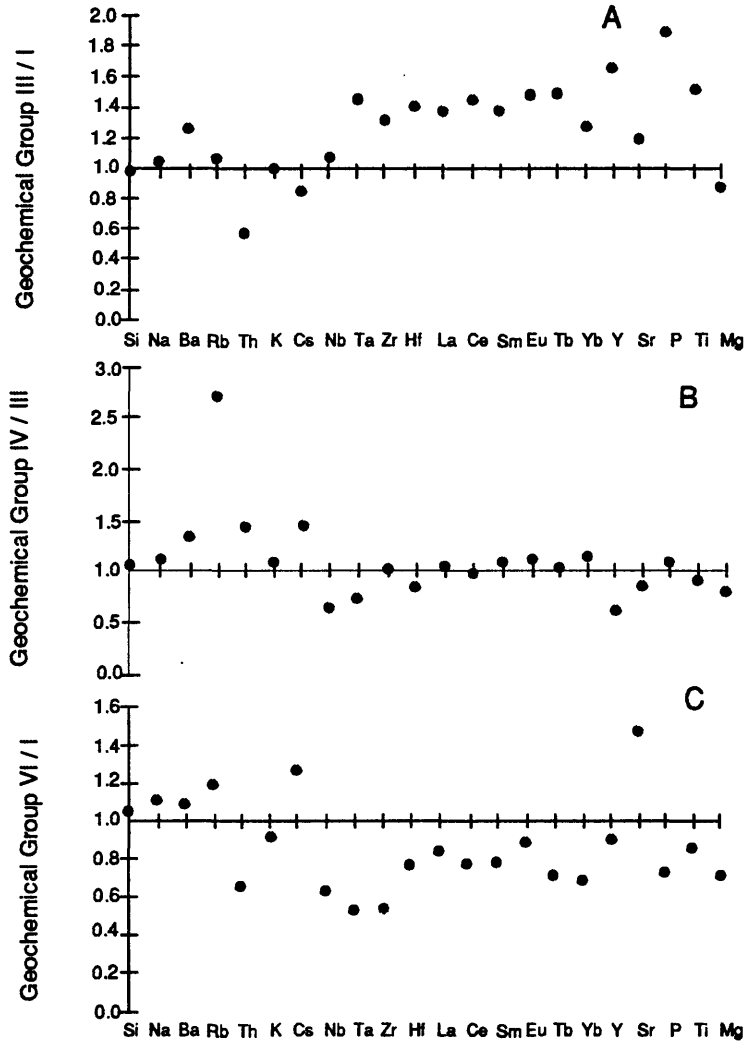


*Figure 19. Normalization diagrams. Diagrams show the relative enrichment of depletion of presumed daughter:parent values of select oxides and trace elements. A. Basalt/basalt pair of geochemical group III (PM2, Red Crater) to geochemical group I (PM1). B. Basalt/basalt pair of geochemical group IV (PM2 , Egan cone) to geochemcial group III (PM2 , Red Crater). C. Basaltic andesite/basalt pair of geochemical group VI (PM3) to basalt group I (PM1).*

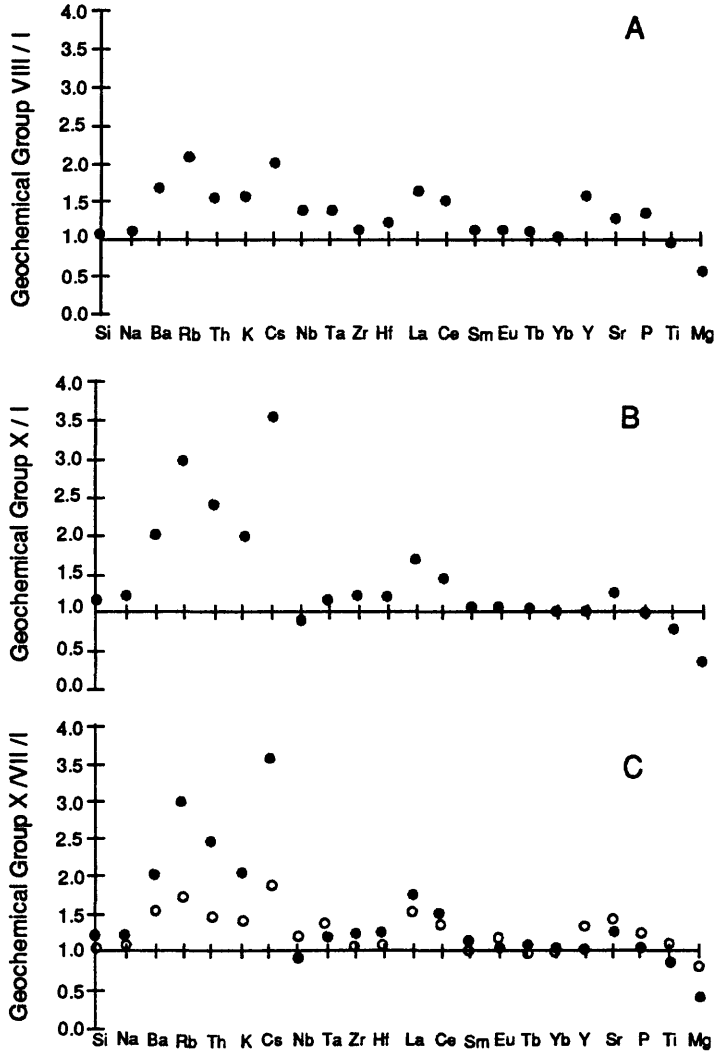


*Figure 20. Normalization diagrams. Diagrams show the relative enrichment or depletion of presumed daughter:pare nt values of select oxides and trace elements. A. Low-silica basltic andesite/basalt pair of geochemical group VIII ( PM1 - Sheridan Mountin) to geochemical group I (PM1). B. High-silica basaltic-andesite/basalt pair of geochemical group X (PM1 - Bachelor summit) to geochemical group I. C. High- and low-silica basaltic-andesite/basalt pairs; open circles group VII (PM1. Bachelor-Kwohl segment) to geochemical group I; filled circles geochemical group X to geochemical group I.*

the Sheridan Mountain (group VIII) basaltic andesite lavas had a slightly different evolutionary history than Bachelor basaltic andesite lavas (group VII).

Normalized patterns for MT1 basaltic andesite and MT1 basalt pairs show greater enrichment of K-group elements than other incompatible elements and also variable enrichment of K-group elements. Gill (1981) notes that enrichment of the K-group elements is common at convergent plate margin volcanoes and in particular that enrichment of Rb and Cs usually increases twofold or more over the range of 53-63 percent $SiO_2$ regardless of initial concentration. He also notes that reported Ba contents in orogenic andesites vary inconsistently by as much as 50 percent. Even with these inconsistencies, Gill (1981) still favors crystal fractionation as the dominant process in the formation of orogenic andesites. Smith and Leeman (1987) argue that variable enrichment of K-group elements runs counter to simple crystal fractionation models because these elements have similar, and similarly low, distribution coefficients ($K_D$s), although they admit that volatile transfer processes may account for some of the variability. The debate is beyond the scope of this work other than to point out that the K-group elements behave similarly at the MBVC as at other convergent plate margin volcanic centers.

Incompatible trace-element ratios are often used to argue for or against the differentiation of a silicic magma from a more mafic one. This is because the ratio between two incompatible elements should remain the same during crystal fractionation processes even though their absolute concentrations may vary (O'Hara, 1977; Gill, 1981; Clark, 1983). Incompatible trace-element ratios for the MBVC lavas are equivocal. Most ratios (Ba/Rb, Rb/Zr, Ce/Sm, Ta/Hf, and Th/U) show as much variation within lava flows from the same geochemical group as between lava flows from different geochemical groups and magma types (table 8). The exception is the Zr/Hf ratio, which shows little variation in MT1 and MT2 lavas, but is different for the MT3 lavas. Zirconium and Hf have such similar chemical behaviors that fractionation between them is extremely difficult. The Zr/Hf data are suggestive that the MT1 and MT2 magmas may be derived from the same source area, but may have followed different evolutionary paths and that within each magma type the basaltic andesite flows may be related to the basalt flows by crystal fractionation. It may be fortuitous (as there is only one data point) that only the MT3 sample differs significantly in ZR/Hf ratio; however, this is consistent with other evidence that suggest that the MT3 lavas may be derived from a source area distinct from that of either the MT1 or MT2 lavas.

A problem in interpreting the incompatible element ratio data is knowing what constitutes a significant difference among ratios. In the cases of Hf/Ta and Th/U differences in ratios from lava flows from the same rock unit (for example, samples 8408062 and 8507011 from the Red Crater chain and samples 8408021 and 8407053 from the Siah chain) vary by as much as 20 (Hf/Ta) to 30 percent (Th/U). If all of the calculated ratios are given a range of 20 to 30 percent of their values, then virtually all of the samples can be considered to have come from the same source. Similarly Rb values from the same flow sequence very by as much as 50 percent. That degree of variation for Rb masks any interpretation for changes in Ba/Rb or Rb/Zr ratios. Thus, the range in element concentrations from a given rock unit (or magma batch) needs to be considered when interpreting incompatible trace-element ratios.

## Petrographic Variations

Plagioclase phenocrysts are sensitive recorders of magmatic history because equilibration with changing magmatic liquids is slow (see Dungan, 1987). Four observations of plagioclase compositions and textures that are not outwardly consistent with simple crystal fractionation models are: 1) sieve-textured plagioclase phenocrysts; 2) reverse zonation; 3) increase in An values with increasing $SiO_2$ content; and 4) two populations of microphenocryst compositions in the sample from Tot Mountain.

Sieve-textured plagioclase phenocrysts have been considered the result of disequilibrium associated with magma-mixing (Dungan and Rhodes, 1978; Walker and others, 1979; Kuo and Kirkpatrick, 1982; Dungan, 1987). They are common in the MBVC lavas (although compared to homogeneous-textured plagioclase phenocrysts they represent a

*Table 8. Incompatible Element Ratios*

| Sample # | Magma type group | Ba | Rb | Ba/Rb | Zr | Rb/Zr | Hf | Hf/Zr | Ta | Ta/Hf | Ce | Sm | Ce/Sm | Th | U | Th/U |
|---|---|---|---|---|---|---|---|---|---|---|---|---|---|---|---|---|
| 8408172 | MT1/1 | 231 | 9.4 | **24.5** | 129 | **0.07** | 2.96 | **0.023** | 0.542 | **0.183** | 27.7 | 4.27 | **6.49** | 1.100 | 0.418 | **2.632** |
| 8408021 | MT1/1 | 214 | 4.9 | **44.0** | 131 | **0.04** | 2.86 | **0.022** | 0.471 | **0.165** | 25.9 | 3.89 | **6.66** | 0.630 | 0.353 | **1.785** |
| 8407053 | MT1/1 | 218 | 10.4 | **21.0** | 139 | **0.07** | 3.02 | **0.022** | 0.615 | **0.204** | 28.8 | 4.15 | **6.94** | 0.841 | 0.425 | **1.979** |
| 8409123 | MT1/1 | 278 | 11.3 | **24.6** | 132 | **0.09** | 2.89 | **0.022** | 0.544 | **0.188** | 27.2 | 4.23 | **6.43** | 0.887 | 0.354 | **2.506** |
| 8408061 | MT1/II | 285 | 10.1 | **28.2** | 181 | **0.06** | 4.07 | **0.022** | 0.817 | **0.201** | 42.1 | 5.18 | **8.13** | 1.130 | 0.417 | **2.710** |
| 8407071 | MT1/II | 352 | 15.6 | **22.6** | 173 | **0.09** | 4.02 | **0.023** | 0.640 | **0.159** | 43.5 | 5.84 | **7.45** | 1.110 | 0.562 | **1.975** |
| 8408062 | MT2/III | 291 | 10.1 | **28.8** | 169 | **0.06** | 4.17 | **0.025** | 0.792 | **0.190** | 40.1 | 5.86 | **6.84** | 0.625 | 0.341 | **1.833** |
| 8507011 | MT2/III | 310 | 7.3 | **42.4** | 166 | **0.04** | 3.94 | **0.024** | 0.691 | **0.175** | 37.6 | 5.77 | **6.52** | 0.606 | 0.231 | **2.623** |
| 8507216 | MT2/IV | 389 | 16.3 | **23.9** | 171 | **0.10** | 3.58 | **0.021** | 0.565 | **0.158** | 38.6 | 6.20 | **6.23** | 0.895 | 0.407 | **2.199** |
| 8407244 | MT2/V | 416 | 11.5 | **36.2** | 151 | **0.08** | 3.94 | **0.026** | 0.807 | **0.205** | 41.2 | 5.95 | **6.92** | 0.992 | 0.504 | **1.968** |
| 8407214 | MT3/VI | 252 | 11.2 | **22.5** | 69 | **0.16** | 2.27 | **0.033** | 0.284 | **0.125** | 21.1 | 3.33 | **6.34** | 0.710 | 0.307 | **2.313** |
| 8407064 | MT3/VI | 321 | 13.9 | **23.1** | nd | **nd** | 2.44 | **nd** | 0.341 | **0.140** | 25.5 | 3.67 | **6.95** | 0.793 | 0.336 | **2.360** |
| 8407292 | MT1/VII | 356 | 16.1 | **22.1** | 137 | **0.12** | 3.26 | **0.024** | 0.719 | **0.221** | 37.3 | 4.32 | **8.63** | 1.590 | 0.579 | **2.746** |
| 8507191 | MT1/VII | 357 | 14.4 | **24.8** | 119 | **0.12** | 3.14 | **0.026** | 0.567 | **0.181** | 33.4 | 4.15 | **8.05** | 1.170 | 0.42 | **2.786** |
| 8507222 | MT1/VII | 382 | 11.5 | **33.2** | 133 | **0.09** | 3.03 | **0.023** | 0.529 | **0.175** | 33.3 | 3.91 | **8.52** | 1.190 | 0.487 | **2.444** |
| 8507271 | MT1/VIII | 362 | 16.2 | **22.3** | 157 | **0.10** | 3.43 | **0.022** | 0.764 | **0.223** | 39.5 | 4.50 | **8.78** | 1.620 | 0.625 | **2.592** |
| 8407011 | MT1/VIII | 391 | 20.1 | **19.5** | 147 | **0.14** | 3.61 | **0.025** | 0.766 | **0.212** | 42.6 | 4.86 | **8.77** | 1.730 | 0.853 | **2.028** |
| 84091310 | MT1/X | 461 | 28.1 | **16.4** | 157 | **0.18** | 3.63 | **0.023** | 0.632 | **0.174** | 40.4 | 4.62 | **8.74** | 2.680 | 0.781 | **3.431** |

smaller proportion) and reported in both mafic and silicic lavas of the nearby Three Sisters-High Cascades mafic platform area (Clark, 1983; Hughes, 1983; Hughes and Taylor, 1986; Taylor, 1987). In the MBVC lavas, sieve-textures are usually restricted to the cores of plagioclase phenocrysts and microphenocrysts. Limited microprobe data indicate that An contents are slightly higher in the cores of these phenocrysts than in the cores of homogeneous-textured phenocrysts (table 5).

Reverse zonation was noted in the rims of a few of the plagioclase phenocrysts that were microprobed. Reverse zonation in plagioclase phenocrysts has also been considered the result of disequilibrium associated with magma mixing (see Dungan and Rhodes, 1978). However, processes other than magma mixing may account for reverse zonation such as: 1) enrichment of CaO in the melt as early-formed (high pressure) clinopyroxene dissolves back into the melt due to magma moving to lower pressure regimes (O'Donnell and Presnall, 1980); 2) CaO cation diffusivity not keeping pace with high crystal growth rates and; 3) abrupt decompression (Hirt and Nekvasil, 1988).

As noted earlier, microprobe analyses appear to document a general trend towards increasing An content with increasing whole-rock $SiO_2$ values (see fig. 7b). A similar trend was noted by Hughes and Taylor (1986) in their study of the High Cascades mafic platform rocks. They interpreted the increase in An content with increasing $SiO_2$ values as one line of evidence that the basaltic andesite in their study area were not derived from the basalt by crystal fractionation, because An contents should decrease with increasing $SiO_2$ values if crystal fractionation of plagioclase and/or clinopyroxene has occurred. However, several processes which could modify expected plagioclase content crystal fractionation trends include: 1) mixing of more mafic material into an evolving magma-chamber (O'Hara , 1977; Dungan and Rhodes, 1978); 2) changing crystallization pressure (O'Donnell and Presnell, 1980; Kuo and Kirkpatrick, 1982; Hirt and Nekvasil, 1988); or 3) changing water pressure (Grove and Baker, 1984). Another possibility is that the plagioclase phenocrysts in the most silicic rocks are xenocrystic and not phenocrystic. In the summit lavas of Mount Bachelor there is a compositional gap between phenocryst rims and groundmass cores of approximately 13 mole percent An. In all other samples the rims of the phenocrysts and cores of microphenocrysts are within a few mole percent in composition.

Two distinct groundmass populations occur in the sample from Tot Mountain (55.6 percent $SiO_2$): one about $An_{67}$ and the other about $An_{90}$ (table 5). It is difficult to envision a processes that could account for two distinct populations of late-forming similarly sized groundmass plagioclases other than magma mixing. Perhaps crystals that formed near the walls of a magma chamber or conduit, where the thermal gradient is steepest and nucleation centers are numerous, could have mixed with the less dense, more fractionated liquid that has separated due to boundary layer effects (McBirney and others, 1985; Baker and McBirney, 1985); however, this explanations seems less plausible than open-system magma mixing (O'Hara, 1977).

In summary, major-, trace, and rare-earth-element trends, mineral fractionation trends, incompatible trace-element ratios, and parent:daughter normalization patterns indicate that MT1 and MT2 basaltic andesite could be derived from MT1 and MT2 basalt respectively through crystal fractionation of the mineral phases observed. Petrographic data, however, suggest that magma mixing may also have occurred. Enrichment of the K-group elements, especially in the summit lavas from Mount Bachelor, indicates that assimilation of more silicic material may have occurred. The data also indicate, however, that the none of the magma types are directly related to each other solely by crystal fractionation processes, and that although MT1 and MT2 magmas may be from the same source area, it is likely that MT3 magmas are from a distinct source area.

### Petrologic Modeling

The simplest assumption for modeling variations along the MBVC is to assume that both parent and daughter rocks are exposed in outcrop. Although none of the MBVC basalt are primary melts, both MT1 group 1 basalt and Cayuse Crater basalt are moderately primitive as indicated by their magnesium numbers (Mg#;

66-64) and Ni concentrations (170-100 ppm). Therefore, these two basalts are potentially parental to the MT1 basaltic-andesite lavas. Similarly, MT2, group III Red Crater basalt has Mg#s (58) and Ni concentrations (107; see table 7) suggestive that it could be parental to either the group IV basalt or group V basaltic andesite. Before using these basalts as parental compositions, however, it is important to determine that the crystals and melts were in equilibrium with each other. As olivine is the earliest crystallizing phase and the dominant phenocryst phase in the basalt flows, I tested whether their compositions were in equilibrium with the melt.

Roeder and Emslie (1970) demonstrated that at 1 atmosphere, the partitioning of Mg between liquid and olivine was constant, independent of temperature, and mostly independent of oxygen fugacity. They proposed, therefore, that olivine compositions could be used to determine Mg/Fe ratios of the liquid from which they crystallized, or conversely that Mg/Fe ratios of the liquid could be used to determine the olivine compositions that would precipitate from that liquid. Furthermore, they concluded that the temperature of olivine crystallization could be deduced from whole rock compositions.

Graphically determined olivine compositions ($K_{Dol}$ = 0.30) from whole rock geochemistry (Roeder and Emslie, 1970) are generally in good agreement with olivine compositions determined by microprobe analysis (table 9). Thus, the olivines appear to be in equilibrium with their melt. Also the graphically determined olivine crystallization temperatures show a general decrease with decreasing magnesium number (table 9) which is expected if the olivines are in equilibrium.

A modified Wright-Doherty least-squares mixing program was used to model major elements. Phases extracted, phase proportions, and percent crystallization determined by major-element modeling were used for trace-element modeling using a program by Reagan and others (1987). Iron reported as $Fe_2O_3$ was

*Table 9. Graphically determined olivine crystallization temperatures and forsterite compositions (after Roeder and Emslie, 1970).*

| Sample No. | Description | MT/GG | SiO2 | Mg# | T °C (calc) | Fo (calc) | Fo obs |
|---|---|---|---|---|---|---|---|
| 8409121 | Cayuse | | 51.4 | 67 | 1217 | 86.9 | ND |
| 8408172 | Todd N | MT1/I | 50.5 | 66 | 1206 | 85.5 | ND |
| 8407123 | Siah S' vent | MT1/I | 49.8 | 63 | 1200 | 84.3 | ND |
| 8407032 | Siah ol | MT1/I | 50.7 | 64 | 1193 | 85.0 | 85 |
| 8407271 | Kwohl ol | MT1/I | 50.6 | 64 | 1200 | 85.3 | 81 |
| 8407224 | Early Bach | MT1/I | 50.4 | 65 | 1203 | 85.6 | 86 |
| 8408052 | Bach ol | MT1/I | 51.7 | 63 | 1175 | 84.6 | 82 |
| G84-19 | Red Crater | MT2/III | 49.7 | 57 | 1181 | 81.5 | 81 |
| G84-18 | Bach Big Plag | MT2/V | 52.7 | 47 | 1100 | 74.0 | 74 |
| 8407214 | Sher Big Plag | MT3/VI | 52.3 | 59 | 1136 | 82.5 | 82 |
| 8407225 | Bach int | MT1/VII | 52.9 | 62 | 1163 | 83.5 | 82 |
| 8507115 | Bach int | MT1/VII | 54.2 | 62 | 1146 | 84.5 | 83 |
| 8507254 | Tot | MT1/IX | 55.8 | 56 | 1086 | 81.5 | 82 |
| 8409139 | Bach summit | MT1/X | 56.7 | 48 | 1038 | 74.2 | 67 |
| 8409148 | Bach summit | MT1/X | 56.3 | 52 | 1059 | 78.1 | 77 |

MT/GG - magma type / geochemical group
Fo (calc) - values calculated from Roeder and Emslie (1970) diagram
T °C (calc) - values calculated from Roeder and Emslie (1970) diagram
Fo (obs) - values determined from microprobe analysis
ND - no data

calculated as FeO and the major oxides recalucated to 100 percent. I used distribution coefficients based on compilations by Hughes (1983), Clark (1983) and Reagan and others (1987) (Appendix F) to determine minimum and maximum $K_D$s for trace-element modeling.

Microprobe olivine, plagioclase, and pyroxene compositions from MBVC basalt samples were recalculated to 100 percent and used for petrologic modeling. These compositions appeared similar to compositions from similar magma types elsewhere (Deer and others, 1983; Hughes and Taylor (1986). Magnetite and apatite compositions were taken from Deer and others (1983; magnetite compositions #2 and #5, pg. 427; apatite, compositions #5 and #6, page 506). As these phases were not probed, similarity to actual compositions is unknown.

I used geochemical group compositions to model from one group to another as well as unique sample compositions to model to group compositions (i. e. a Katsuk basalt to an intermediate Bachelor, group VII composition) or to a unique sample composition. In some models I added a rhyolite composition from Rock Mesa (sample number 3s060 from Hill, 1991, pg. 221) as a potential assimilate.

For the following major-element models, Obs is the known daughter composition, Est is the modeled daughter composition and residual is the difference between the two. Phase porportions are normalized to equal 100 and the total amount of crysallization is given as 1-F (or the percent original magma). For trace element models, each model was run using both the highest permissable $K_D$ values (max) and the lowest (min). Phase proportions were taken from the major-element models. Amounts of crystallization, mixing (intrusion), assimialtion and extursion relative to crystallization are given by the ratios of mc/mo (crystallization to original magma volume), mi/mo, ma/mo, and me/mo respectively.

## Results of Major Element Modeling

Major-element crystal-fractionation modeling provides reasonable ($r2 \leq 0.1$) solutions for deriving higher silica daughter products from lower silica parents for MT2 geochemical groups (tables 10 and 12), and for MT1 basaltic andesite groups (tables 13 and 14). In all cases, solutions were best using the phases plagioclase ($An_{86}$), olivine ($Fo_{86}$), clinopyroxene ($CaO_{48}$, $MgO_{36}$, $FeO_{16}$), magnetite (#5), and apatite (#5) (table 18). For MT 2 lavas, the models best match observed compositions if the lavas are incrementally modeled from Red Crater basalt (group III) to Egan basalt (group IV) and then from Egan basalt to Egan basaltic andesite (group V), than if modeled directly from Red Crater to Egan basaltic andesite (table 11). Although residuals are low during incremental modeling, almost all of the residual is due to poor sodium modeling. In the case of modeling from Red Crater basalt to Egan basalt, the residual for sodium is slightly improved if a small amount of rhyolite is added to the system while removing the above phases. Assimilation of rhyolite does not provide reasonable solutions when modeling from either Red Crater or from Egan basalt to Egan basaltic andesite (tables 11 and 12). In these cases the model requires that plagioclase is assimilated as well, which is contrary to other petrologic and petrographic data.

For the basaltic-andesite MT 1 groups, the modeling provides reasonable solutions for evolving summit basaltic andesite (group X) from either a Sheridan (group VIII), Bachelor (group VII), or Tot (group IX) basaltic andesite, although phase proportions and total amount of crystallization differ (table 13). As with MT 2 geochemical modeling, sodium accounts for the majority of the residual. Overall residuals improve slightly if a small amount of rhyolite is added to the low-silica basaltic-andesite melts (table 14), but with or without rhyolite the residuals are <0.1; however rhyolite assimilation does not work for going from a Tot Mountain (IX) to summit (X) composition. A potential advantage of assimilating rhyolite is that it drops the amount of plagioclase cyrstallization needed and thus may explain the lack of a moderate negative europium anomaly. It also gives an explanation to the spatial observation that the largest and most silicic cones of the chain are at the north end, closest to the Silicic Highland of the Three Sisters area (fig. 1). A disadvantage of assimilating rhyolitic material is that it adds a process that may not in fact exist, and for which there is little petrographic evidence.

*Table 10. Major- and trace-element models: Red Crater basalt to Egan basalt*

A. Crystal fractionation

| Oxides | Obs | Est | Residual |
|---|---|---|---|
| SiO2 | 51.68 | 51.62 | 0.06 |
| Al2O3 | 17.39 | 17.36 | 0.03 |
| FeO | 10.22 | 10.15 | 0.07 |
| MgO | 5.44 | 5.43 | 0.01 |
| CaO | 8.48 | 8.47 | 0.00 |
| Na2O | 3.64 | 3.79 | -0.15 |
| K2O | 0.66 | 0.69 | -0.03 |
| TiO2 | 1.75 | 1.81 | -0.06 |
| P2O5 | 0.57 | 0.57 | 0.08 |
| MnO | 0.17 | 0.17 | -0.01 |

Squared resisduals 4.47E-02
F=.87
ol=37 plag=33 cpx=16 mag=11.5

B. Fractionation and assimilation

| Oxides | Obs | Est | Residual |
|---|---|---|---|
| SiO2 | 51.68 | 51.64 | 0.05 |
| Al2O3 | 17.39 | 17.39 | 0.03 |
| FeO | 10.22 | 10.14 | 0.07 |
| MgO | 5.44 | 5.42 | 0.01 |
| CaO | 8.48 | 8.46 | 0.02 |
| Na2O | 3.64 | 3.70 | -0.06 |
| K2O | 0.66 | 0.74 | -0.08 |
| TiO2 | 1.75 | 1.84 | -0.09 |
| P2O5 | 0.57 | 0.51 | 0.06 |
| MnO | 0.17 | 0.17 | 0.00 |

Squared residuals 3.08E-02
F=.91 rhy=.3
ol=41 plag=28 cpx=21 mag=9

C. Crystallization

| Elements | Max | Min | Obs |
|---|---|---|---|
| Ni | 28.4 | 83.0 | 56 ± 5 |
| Cr | 43.2 | 165.7 | 60 ± 7 |
| Sc | 27.1 | 28.5 | 26.5 |
| Ba | 344.6 | 354.8 | 389 |
| Ce | 42.4 | 42.9 | 38.6 |
| Nd | 25.3 | 25.7 | 22.7 |
| Zr | 165.6 | 169.4 | 149 ± 4 |
| Y | 37.9 | 37.9 | 31 ± 3 |
| Sr | 460.3 | 529.8 | 492 ± 8 |
| Rb | 9.8 | 10.0 | 9.7 ±1.5 |

F=.87 mc/mo=0.13

D. Assimilation

| Max | Min | Obs |
|---|---|---|
| 39.9 | 85.7 | 56 ± 5 |
| 73.2 | 174.2 | 60 ± 7 |
| 26.1 | 27.2 | 26.5 |
| 345.9 | 351.3 | 389 |
| 40.6 | 40.9 | 38.6 |
| 24 | 24.2 | 22.7 |
| 159.9 | 162 | 149 ± 4 |
| 35.9 | 35.8 | 31 ± 3 |
| 474.8 | 508.9 | 492 ± 8 |
| 11.5 | 11.6 | 9.7 ± 1.5 |

F=0.94 ma/mo=0.026
mc/mo=0.086

E. Extrusion/Intrusion

| | Max | Min | Obs |
|---|---|---|---|
| Ni | 32.8 | 85.6 | 56 ± 5 |
| Cr | 54.1 | 173.5 | 60 ± 7 |
| Sc | 26.9 | 28.3 | 26.5 |
| Ba | 337.4 | 347.4 | 389 |
| Ce | 40.1 | 40.6 | 38.6 |
| Nd | 23.9 | 24.3 | 22.7 |
| Zr | 161.8 | 165.5 | 149 ± 4 |
| Y | 34.8 | 34.8 | 31 ± 3 |
| Sr | 454.2 | 522.5 | 492 ± 8 |
| Rb | 10.4 | 10.6 | 9.7 ± 1.5 |

F=.68 me/mo=0.384
mi/mo=0.192 mc/mo=0.128

F. Assimilation/Extrusion/Intrusion

| | Max | Min | Obs |
|---|---|---|---|
| Ni | 41.8 | 87.1 | 56 ± 5 |
| Cr | 78.2 | 178.6 | 60 ± 7 |
| Sc | 26.0 | 27.1 | 26.5 |
| Ba | 341.9 | 347.4 | 389 |
| Ce | 39.2 | 39.5 | 38.6 |
| Nd | 23.2 | 23.4 | 22.7 |
| Zr | 157.7 | 159.8 | 149 ± 4 |
| Y | 34.0 | 33.9 | 31 ± 3 |
| Sr | 470.5 | 504.8 | 492 ± 8 |
| Rb | 11.9 | 12.0 | 9.7 ± 1.5 |

F=.81 ma/mo=0.026
me/mo=0.259 mi/mo=0.130
mc/mo=0.086

*Table 11. Red Crater basalt to Egan basaltic andesite*

A. Crystal fractionation

| Oxides | Obs | Est | Residual |
|---|---|---|---|
| SiO2 | 53.43 | 53.33 | 3.32 |
| Al2O3 | 17.98 | 17.93 | 1.13 |
| FeO | 9.09 | 9.02 | -1.68 |
| MgO | 4.91 | 4.9 | -2.17 |
| CaO | 8.17 | 8.18 | -0.61 |
| Na2O | 3.65 | 3.98 | 0.58 |
| K2O | 0.76 | 0.74 | 0.13 |
| TiO2 | 1.5 | 1.51 | -0.39 |
| P2O5 | 0.36 | 0.22 | -0.31 |
| MnO | 0.15 | 0.17 | -0.01 |

Squared resisduals 1.46E-01
F=.81
ol=30 plag=33 cpx=15 mag=17
ap=5

B. Fractionation and assimilation

| | Obs | Est | Residual |
|---|---|---|---|
| | 53.43 | 53.36 | 0.07 |
| | 17.98 | 17.93 | 0.04 |
| | 9.09 | 9.00 | 0.09 |
| | 4.91 | 4.89 | 0.02 |
| | 8.17 | 8.15 | 0.02 |
| | 3.65 | 3.74 | -0.09 |
| | 0.76 | 0.89 | -0.13 |
| | 1.5 | 1.59 | -0.09 |
| | 0.36 | 0.28 | 0.08 |
| | 0.15 | 0.16 | -0.01 |

Squared residuals 5.49E-02
F=.92 rhy=.99
ol=48 plag= +2 cpx=27 mag=18
ap = 7

*Table 12. Major- and trace-element models: Egan basalt to Egan basaltic andesite*

A. Crystal fractionation

| Oxides | Obs | Est | Residual |
|---|---|---|---|
| SiO2 | 53.43 | 53.42 | 0.04 |
| Al2O3 | 17.98 | 17.96 | 0.01 |
| FeO | 9.09 | 9.09 | 0.01 |
| MgO | 4.91 | 4.91 | 0.00 |
| CaO | 8.17 | 7.86 | -0.02 |
| Na2O | 3.65 | 3.65 | -0.20 |
| K2O | 0.76 | 0.76 | 0.05 |
| TiO2 | 1.5 | 1.51 | 0.06 |
| P2O5 | 0.36 | 0.36 | 0.07 |
| MnO | 0.15 | 0.15 | -0.02 |

Squared resisduals 5.23E-02
F=.94
ol=23 plag=25 cpx=11.6 mag=11.5
ap=10.6

B. Fractionation and assimilation

| | Obs | Est | Residual |
|---|---|---|---|
| | 53.43 | 53.40 | 0.02 |
| | 17.98 | 17.96 | 0.01 |
| | 9.09 | 9.08 | 0.02 |
| | 4.91 | 4.90 | 0.01 |
| | 8.17 | 8.17 | 0.00 |
| | 3.65 | 3.67 | -0.03 |
| | 0.76 | 0.81 | -0.06 |
| | 1.5 | 1.50 | 0.00 |
| | 0.36 | 0.34 | 0.30 |
| | 0.15 | 0.16 | -0.01 |

Squared residuals 5.44E-03
F=.98 rhy=4.7
ol=17 plag=+33 cpx=17 mag=40
P=26

C. Crystallization

| Elements | Max | Min | Obs |
|---|---|---|---|
| Ni | 20.8 | 49.1 | 44 ± 3 |
| Cr | 15.3 | 49.0 | 46 ± 10 |
| Sc | 23.7 | 25.9 | 22.8 |
| Ba | 406.7 | 413.3 | 416 |
| Ce | 40.6 | 41.0 | 41.2 |
| Nd | 23.8 | 24.1 | 23.8 |
| Zr | 154.4 | 157.1 | 138 ± 19 |
| Y | 32.3 | 32.4 | 24 ± 4 |
| Sr | 481.4 | 514.0 | 549 ± 27 |
| Rb | 11.6 | 11.7 | 11.5 |

F=.87 mc/mo=0.13

D. Extrusion/Intrusion

| Max | Min | Obs |
|---|---|---|
| 15.2 | 55.52 | 44 ± 3 |
| 20.2 | 75.99 | 46 ± 10 |
| 24 | 26.09 | 22.8 |
| 400.1 | 414.5 | 416 |
| 40.2 | 40.9 | 41.2 |
| 23.6 | 24.1 | 23.8 |
| 156.4 | 162.4 | 138 ± 19 |
| 31 | 31.3 | 24 ± 4 |
| 462.4 | 532 | 549 ± 27 |
| 11.2 | 11.4 | 11.5 |

F=0.72 me/mo = .38
mi/mo=0.229 mc/mo = 0.127

*Table 13. Major-element models: Low silica basaltic andesite to Bachelor high-silica basaltic andesite*

*Crystal fractionation*

A. Geochemical Group VII to X

| Oxides | Obs | Est | Residual |
|---|---|---|---|
| SiO2 | 57.03 | 57 | 0.03 |
| Al2O3 | 18.24 | 18.23 | 0.01 |
| FeO | 7.05 | 7.04 | 0.02 |
| MgO | 3.39 | 3.39 | 0.00 |
| CaO | 7.65 | 7.65 | -0.01 |
| Na2O | 3.94 | 4.11 | -0.17 |
| K2O | 1.24 | 1.16 | 0.08 |
| TiO2 | 1.08 | 1.07 | 0.01 |
| P2O5 | 0.27 | 0.22 | 0.05 |
| MnO | 0.12 | 0.13 | -0.01 |

Squared resisduals 3.82E-02
F=.82
ol=31 plag=41 cpx=18.5 mag=7.6
ap=2

B. Geochemical Group VIII to X

| Obs | Est | Residual |
|---|---|---|
| 57.03 | 57.01 | 0.01 |
| 18.24 | 18.24 | 0.00 |
| 7.05 | 7.04 | 0.01 |
| 3.39 | 3.39 | 0.00 |
| 7.65 | 7.65 | -0.01 |
| 3.94 | 4.03 | -0.09 |
| 1.24 | 1.17 | 0.07 |
| 1.08 | 1.08 | 0.00 |
| 0.27 | 0.25 | 0.02 |
| 0.12 | 0.13 | -0.01 |

Squared residuals 1.43E-02
F=.83
ol=19.5 plag=40 cpx=30.6 mag=7.7
ap=2.4

C. Geochemical Group IX to X

| Obs | Est | Residual |
|---|---|---|
| 57.03 | 57.07 | -0.04 |
| 18.24 | 18.25 | -0.02 |
| 7.05 | 7.07 | -0.02 |
| 3.39 | 3.39 | -0.01 |
| 7.65 | 7.64 | 0.00 |
| 3.94 | 3.83 | 0.11 |
| 1.24 | 1.21 | 0.03 |
| 1.08 | 1.10 | -0.02 |
| 0.27 | 0.32 | -0.05 |
| 0.12 | 0.12 | 0.00 |

Squared residuals 1.32E-02
F=.92
ol=24.7 plag=39.6 cpx=34.7 mag=1.05

D. Geochemical Group VI to X

| Oxides | Obs | Est | Residual |
|---|---|---|---|
| SiO2 | 57.03 | 57.01 | 0.01 |
| Al2O3 | 18.24 | 18.26 | -0.02 |
| FeO | 7.05 | 7.11 | -0.06 |
| MgO | 3.39 | 3.41 | -0.02 |
| CaO | 7.65 | 7.79 | -0.05 |
| Na2O | 3.94 | 4.28 | -0.34 |
| K2O | 1.24 | 0.93 | 0.31 |
| TiO2 | 1.08 | 0.93 | 0.15 |
| P2O5 | 0.27 | 0.24 | 0.03 |
| MnO | 0.12 | 0.13 | -0.01 |

Squared resisduals 2.40E-01
F=.76
ol=22.7 plag=55.4 cpx=12.7 mag=8.7
ap=0.5

E. Geochemical Group V to X

| Obs | Est | Residual |
|---|---|---|
| 57.03 | 57.03 | 0.00 |
| 18.24 | 18.25 | -0.02 |
| 7.05 | 7.09 | -0.04 |
| 3.39 | 3.41 | -0.02 |
| 7.65 | 7.68 | -0.03 |
| 3.94 | 4.19 | -0.25 |
| 1.24 | 0.96 | 0.29 |
| 1.08 | 0.99 | 0.08 |
| 0.27 | 0.26 | 0.01 |
| 0.12 | 0.14 | -0.03 |

Squared residuals 1.53E-01
F=.83
ol=24 plag=48 cpx=6.4 mag=20
ap=2

F. Geochemical Group VII to VIII

| Obs | Est | Residual |
|---|---|---|
| 54.51 | 54.50 | 0.02 |
| 17.57 | 17.56 | 0.01 |
| 7.72 | 7.72 | 0.01 |
| 5.19 | 5.19 | 0.00 |
| 8.83 | 8.84 | 0.00 |
| 3.48 | 3.56 | -0.07 |
| 0.97 | 0.96 | 0.01 |
| 1.2 | 1.19 | 0.01 |
| 0.38 | 0.36 | 0.03 |
| 0.14 | 0.14 | 0.00 |

Squared residuals 6.94E-03
F=.97
ol=75 plag=23 cpx=+97.5 mag=2.1
ap=+2.5

*Table 14. Major-element models: Low-silica basaltic andesite to Bachelor high-silica basaltic andesite*

*Crystal fractionation and assimilation*

A. Geochemical Group VII to X

| Oxides | Obs | Est | Residual |
|---|---|---|---|
| SiO2 | 57.03 | 57.02 | 0.01 |
| Al2O3 | 18.24 | 18.23 | 0.01 |
| FeO | 7.05 | 7.04 | 0.02 |
| MgO | 3.39 | 3.38 | 0.00 |
| CaO | 7.65 | 7.64 | 0.01 |
| Na2O | 3.94 | 3.95 | -0.01 |
| K2O | 1.24 | 1.24 | 0.00 |
| TiO2 | 1.08 | 1.02 | -0.04 |
| P2O5 | 0.27 | 0.26 | 0.01 |
| MnO | 0.12 | 0.13 | -0.01 |

Squared resisduals 2.25E-03
F=.88 rhy=.55
ol=40.5 plag=28.4 cpx=24.8 mag=4.6
ap=1.7

B. Geochemical Group VIII to X

| Obs | Est | Residual |
|---|---|---|
| 57.03 | 57.04 | 0.00 |
| 18.24 | 18.24 | 0.00 |
| 7.05 | 7.04 | 0.01 |
| 3.39 | 3.39 | 0.00 |
| 7.65 | 7.64 | 0.00 |
| 3.94 | 3.94 | 0.00 |
| 1.24 | 1.22 | 0.02 |
| 1.08 | 1.11 | -0.03 |
| 0.27 | 0.27 | 0.00 |
| 0.12 | 0.13 | -0.01 |

Squared residuals 1.57E-03
F=.86 rhy=.3
ol=21.6 plag=32.7 cpx=37.2 mag=6.2
ap=2.4

C. Geochemical Group IX to X

| Obs | Est | Residual |
|---|---|---|
| 57.03 | 57.06 | -0.02 |
| 18.24 | 18.25 | -0.01 |
| 7.05 | 7.07 | -0.02 |
| 3.39 | 3.39 | -0.01 |
| 7.65 | 7.65 | 0.00 |
| 3.94 | 3.22 | 0.03 |
| 1.24 | 1.17 | 0.07 |
| 1.08 | 1.07 | 0.01 |
| 0.27 | 0.30 | -0.03 |
| 0.12 | 0.12 | 0.03 |

Squared residuals 8.56E-03
F=.85
ol=16.2 plag=36.2 cpx=20.7 mag=3.4
ap=0.2 rhy=23.2

D. Geochemical Group VI to X

| Oxides | Obs | Est | Residual |
|---|---|---|---|
| SiO2 | 57.03 | 57.09 | -0.07 |
| Al2O3 | 18.24 | 18.29 | -0.05 |
| FeO | 7.05 | 7.12 | -0.08 |
| MgO | 3.39 | 3.42 | -0.03 |
| CaO | 7.65 | 7.67 | -0.03 |
| Na2O | 3.94 | 3.91 | 3.00 |
| K2O | 1.24 | 1.09 | 0.15 |
| TiO2 | 1.08 | 1.05 | 0.03 |
| P2O5 | 0.27 | 0.23 | 0.04 |
| MnO | 0.12 | 0.11 | 0.01 |

Squared resisduals 4.05E-02
F=.89 rhy=1.38
ol=39.4 plag=41.1 cpx=16.9 mag=2.6

E. Geochemical Group V to X

| Obs | Est | Residual |
|---|---|---|
| 57.03 | 57.07 | -0.04 |
| 18.24 | 18.26 | -0.02 |
| 7.05 | 7.09 | -0.03 |
| 3.39 | 3.40 | -0.01 |
| 7.65 | 7.65 | 0.00 |
| 3.94 | 3.89 | 0.05 |
| 1.24 | 1.09 | 0.15 |
| 1.08 | 1.08 | -0.01 |
| 0.27 | 0.33 | -0.06 |
| 0.12 | 0.13 | -0.01 |

Squared residuals 3.12E-02
F=.94 rhy=2.18 ap=1
ol=48.4 plag=10.6 cpx=7.3 mag=32.5

*Table 15. Major-element models: Basalt (MT1) to low-silica basaltic andesite (MT1)*

A. Crystal fractionation
Geochemical Group I to VII

| Oxides | Obs | Est | Residual |
|---|---|---|---|
| SiO2 | 54.17 | 54.09 | 0.08 |
| Al2O3 | 17.55 | 17.53 | 0.03 |
| FeO | 7.85 | 7.80 | 0.05 |
| MgO | 5.87 | 5.87 | 0.00 |
| CaO | 8.44 | 8.47 | -0.03 |
| Na2O | 3.52 | 3.92 | -0.41 |
| K2O | 0.95 | 0.82 | 0.13 |
| TiO2 | 1.18 | 1.16 | 0.02 |
| P2O5 | 0.33 | 0.20 | 0.13 |
| MnO | 0.14 | 0.15 | -0.01 |

Squared resisduals 2.11E-01
F=.78
ol=24.3 plag=47.6 cpx=16.9 mag=9.4
ap=1.8

B. Crystal fractionation
Geochemical Group I to VIII

| Obs | Est | Residual |
|---|---|---|
| 54.51 | 54.42 | 0.10 |
| 17.57 | 17.53 | 0.03 |
| 7.72 | 7.67 | 0.05 |
| 5.19 | 5.19 | 0.00 |
| 8.83 | 8.87 | -0.03 |
| 3.48 | 3.95 | -0.47 |
| 0.97 | 0.83 | 0.14 |
| 1.20 | 1.17 | 0.03 |
| 0.38 | 0.27 | 0.15 |
| 0.14 | 0.15 | -0.01 |

Squared residuals 2.73E-01
F=.77
ol=31 plag=48.2 cpx=10.1 mag=9.2
ap=1.5

C. Crystal fractionation
Cayuse to geochemical group VIII

| Obs | Est | Residual |
|---|---|---|
| 54.51 | 54.49 | 0.02 |
| 17.57 | 17.57 | -0.01 |
| 7.72 | 7.77 | -0.04 |
| 5.19 | 5.21 | -0.01 |
| 8.83 | 8.87 | -0.04 |
| 3.48 | 3.75 | -0.27 |
| 0.97 | 0.85 | 0.12 |
| 1.20 | 1.04 | 0.16 |
| 0.38 | 0.31 | 0.08 |
| 0.14 | 0.14 | 0.00 |

Squared residuals 1.22E-03
F=.88
ol=36.2 plag=39.5 cpx=18.7 mag=5.6

D. Crystal fractionation
Cayuse to individual Sheridan composition

| Oxides | Obs | Est | Residual |
|---|---|---|---|
| SiO2 | 54.45 | 54.45 | 0.00 |
| Al2O3 | 17.55 | 17.56 | -0.02 |
| FeO | 7.75 | 7.82 | -0.06 |
| MgO | 5.03 | 5.05 | -0.01 |
| CaO | 8.81 | 8.85 | -0.04 |
| Na2O | 3.63 | 3.82 | -0.19 |
| K2O | 1.01 | 0.87 | 0.14 |
| TiO2 | 1.22 | 1.07 | 0.16 |
| P2O5 | 0.4 | 0.38 | 0.02 |
| MnO | 0.14 | 0.14 | 0.00 |

Squared resisduals 8.31E-02
F=.76
ol=35.1 plag=40 cpx=20 mag=5.2

E. Fractionation and assimilation
Cayuse to individual Sheridan composition

| Oxides | Obs | Est | Residual |
|---|---|---|---|
| SiO2 | 54.45 | 54.52 | -0.07 |
| Al2O3 | 17.55 | 17.60 | -0.05 |
| FeO | 7.75 | 7.86 | -0.08 |
| MgO | 5.03 | 5.07 | -0.03 |
| CaO | 8.81 | 8.85 | -0.03 |
| Na2O | 3.63 | 3.65 | 3.00 |
| K2O | 1.01 | 0.92 | 0.15 |
| TiO2 | 1.22 | 1.11 | 0.03 |
| P2O5 | 0.40 | 0.27 | 0.04 |
| MnO | 0.14 | 0.14 | 0.01 |

Squared resisduals 6.00E-02
F=.83 rhy=0.26
ol=46.33 plag=32.5 cpx=18.7 mag=25

F. Fractionation and assimilation
Todd cone to individual Sheridan composition

| Oxides | Obs | Est | Residual |
|---|---|---|---|
| SiO2 | 54.45 | 54.38 | 0.08 |
| Al2O3 | 17.55 | 17.52 | 0.03 |
| FeO | 7.75 | 7.72 | 0.04 |
| MgO | 5.03 | 5.03 | 0.00 |
| CaO | 8.81 | 8.84 | -0.03 |
| Na2O | 3.63 | 4.00 | -0.37 |
| K2O | 1.01 | 0.88 | 0.13 |
| TiO2 | 1.22 | 1.18 | 0.03 |
| P2O5 | 0.40 | 0.28 | 0.12 |
| MnO | 0.14 | 0.14 | -0.03 |

Squared resisduals 1.83E-01
F=.75
ol=34 plag=45.6 cpx=11.7 mag=7.6
ap=1.0

It is evident from the major-element modeling that the summit basaltic andesites cannot be derived from either MT2 Egan basaltic andesite (group V) or the high-alumina Sheridan basaltic andesite (group VI; table 13D and E). Residuals become acceptable if rhyolite is added to both groups, but in the case of the Egan basaltic andesite (table 14E) phase proportions render this model unlikely.

It is also clear that the Bachelor-Kwohl (group VII) and Sheridan (group VIII) low-silica basaltic andesite are not related directly to each other by crystal fractionation processes (table 13F). This coupled with the different phase proportions needed to derive summit basaltic andesite from them supports the idea that these are distinct basaltic-andesite groups that are most likley from the same source area but have followed different evolutionary paths or are slightly different batch melts.

Overall it is difficult to derive MT1 basaltic andesite groups from MT1 group 1 basalt. Solutions are generally quite poor ($r \geq 0.25$); however, as with other models the main contributor to the high residuals is sodium (table 15). Solutions are slightly improved if individual compositions are used instead of group compositions (table 15F), and substantially improved if either rhyolite is added or if Cayuse Crater basalt is used as a parental composition (table table 15C, D, and E).

### Results of trace-element modeling

Trace-element models provide neither unique nor entirely satisfactory results. Even using a broad range of distribution coefficients and the entire range in group compositions, it is difficult in most cases to derive one group from another, or one unique composition from another, by simple crystal fractionation. Although crystal fractionation appears to drive the gross trends, it generally does not provide the finer tuning. In some cases, solutions for deriving basaltic andesite from basalt are slightly improved if extrusion rates exceed crystallization rate, and if the magma is either intruded by another composition, generally a basalt of another magma type, or if there is some assimilation of rhyolite. For example, to model from a basalt to intermediate Sheridan composition, the best solution resulted from using Cayuse basalt and intruding it with a magma similar in composition to an Egan basaltic andesite (table 17). Similarly to model from Egan basalt to Egan basaltic andesite the model is improved somewhat if extrusion rates are greater than crystallization rates and if the magma is intruded with a MT1 Katsuk basalt. In this case however, it is hard to argue that this solution is much better than the solution for straight crystallization.

In the case of modeling from low-silica basaltic andesite to summit high-silica basaltic andesite, simple crystal fractionation works moderately well (table 16). The models indicate that summit lavas are best derived from a Bachelor-Kwohl (VII) parent rather than from a Sheridan (VIII) parent. For some elements differences between the model and observed are decreased if rhyolite is assimilated, although the overall solution is not uniquely improved by mixing, extrusion or assimilation.

### Discussion

Results of major and trace-element modeling do not support a model of simple, closed-system crystal fractionation of a single basaltic parent to derive the variations in MBVC lava chemistry. On the other hand, the results provide permissive evidence that crystal fractionation of different basaltic parents coupled with extrusion and magma mixing can account for much of the variations seen within the basalt and low-silica basaltic-andesite groups. Only in deriving the summit lavas from a low-silica basaltic-andesite parent does closed-system crystal fractionation appear viable; however equally good results are obtained by assimilating rhyolite. In most other cases, assimilation of a rhyolitic composition does not uniquely improve trace-element solutions and in some cases makes them worse. For the summit rocks, assimilation of rhyolite would move compositions towards the tholeiite field and may explain the difference between phenocryst and groundmass compositions. However, no silicic inclusions were seen anywhere in the field and no clearly xenocrystic crystals were detected. Thus, whether rhyolite plays a role in the evolution of the summit rocks remains equivocal.

For deriving MT1 basaltic andesite from MT1 basalt, the major-element models

*Table 16. Trace element models - low-silica basaltic andesite to Bachelor summit*

intermediate Bach to summit
A. Crystal fractionation

| Elements | Max | Min | Obs |
|---|---|---|---|
| Ni | 16.46 | 65.5 | 23 ± 6 |
| Cr | 18.02 | 98.7 | 21 ± 3 |
| Sc | 22.86 | 23.4 | 19.5 |
| Ba | 428.2 | 447.4 | 461 |
| Ce | 41.79 | 42.6 | 40.4 |
| Nd | 20.47 | 20.9 | 18.5 |
| Zr | 166.1 | 170.7 | 152±7 |
| Y | 25.58 | 25.6 | 24±3 |
| Sr | 494.27 | 614.6 | 532±30 |
| Rb | 27.16 | 28.0 | 29 ± 4 |

F=.82 mc/mo=0.18

intermediate Bach to summit
B. Fractionation and assimilation

| Max | Min | Obs |
|---|---|---|
| 23.71 | 65.53 | 23 ± 6 |
| 33.24 | 101.78 | 21 ± 3 |
| 21.02 | 21.4 | 19.5 |
| 435.5 | 443.1 | 461 |
| 39.39 | 39.76 | 40.4 |
| 19.11 | 19.36 | 18.5 |
| 157.77 | 160.36 | 152±7 |
| 23.76 | 23.76 | 24±3 |
| 521.73 | 573.7 | 532±30 |
| 29.53 | 29.85 | 29 ± 4 |

F=0.94 ma/mo=0.06
mc/mo=0.12

intermediate Bach to summit
C. Assimilation/extrusion

| | Max | Min | Obs |
|---|---|---|---|
| Ni | 13.5 | 56.8 | 23 ± 6 |
| Cr | 18.2 | 89.0 | 21 ± 3 |
| Sc | 20.6 | 21.1 | 19.5 |
| Ba | 464.4 | 475.8 | 461 |
| Ce | 41.2 | 41.7 | 40.4 |
| Nd | 19.9 | 20.2 | 18.5 |
| Zr | 164.6 | 168.4 | 152±7 |
| Y | 24.5 | 24.5 | 24±3 |
| Sr | 511.2 | 584.7 | 532±30 |
| Rb | 22.5 | 22.9 | 29 ± 4 |

F=.54 ma/mo=0.07
me/mo=0.394 mc/mo=0.13

Sheridan to summit
D. Crystal fractionation

| Max | Min | Obs |
|---|---|---|
| 14.5 | 42.7 | 23 ± 6 |
| 10.2 | 71.1 | 21 ± 3 |
| 24.8 | 25.5 | 19.5 |
| 432.0 | 451.8 | 461 |
| 47.9 | 48.9 | 40.4 |
| 23.4 | 24.0 | 18.5 |
| 184.5 | 190.5 | 152±7 |
| 31.6 | 31.6 | 24±3 |
| 492.0 | 600.9 | 532±30 |
| 21.1 | 21.6 | 29 ± 4 |

F=.83 mc/mo=0.17

Sheridan to summit
E. Assimilation

| | Max | Min | Obs |
|---|---|---|---|
| Ni | 17.8 | 42.8 | 23 ± 6 |
| Cr | 15.4 | 73.2 | 21 ± 3 |
| Sc | 23.5 | 24.2 | 19.5 |
| Ba | 439.0 | 451.1 | 461 |
| Ce | 46.0 | 46.7 | 40.4 |
| Nd | 22.4 | 22.8 | 18.5 |
| Zr | 178.3 | 182.9 | 152±7 |
| Y | 30.1 | 30.1 | 24±3 |
| Sr | 506.0 | 574.7 | 532±30 |
| Rb | 23.3 | 23.7 | 29 ± 4 |

F=.905 ma/mo=0.04
mc/mo=0.136

*Table 17. Trace element models - MT1 basalt to MT1 basaltic andesite*

Group I to Sheridan (Group 8)
A. Crystal fractionation

| Elements | Max | Min | Obs |
|---|---|---|---|
| Ni | 16.9 | 97.0 | 58±20 |
| Cr | 32.08 | 209.7 | 123±40 |
| Sc | 30.36 | 30.8 | 24.9 |
| Ba | 283.7 | 302.7 | 391 |
| Ce | 34.31 | 35.1 | 42.6 |
| Nd | 19.48 | 20.0 | 20.2 |
| Zr | 167.3 | 172.6 | 161±8 |
| Y | 29.91 | 29.8 | 28±3 |
| Sr | 378.94 | 527.0 | 539±23 |
| Rb | 14.15 | 14.6 | 20.1 |

F=.77 mc/mo=0.23

Cayuse to Sheridan (Group 8)
B. Crystal fractionation

| Max | Min | Obs |
|---|---|---|
| 11.54 | 87.53 | 58±20 |
| 22.42 | 269.26 | 123±40 |
| 28.44 | 29.19 | 24.9 |
| 207.92 | 220.23 | 391 |
| 26.19 | 26.81 | 42.6 |
| 13.82 | 14.23 | 20.2 |
| 126.82 | 131.77 | 161±8 |
| 21.69 | 21.67 | 28±3 |
| 387.59 | 508.06 | 539±23 |
| 13.59 | 14.05 | 20.1 |

F=0.78 mc/mo=0.22

Cayuse to Sheridan 51
C. Crystal fractionation

| | Max | Min | Obs |
|---|---|---|---|
| Ni | 20.4 | 96.7 | 49 |
| Cr | 28.4 | 251.0 | 95 |
| Sc | 27.5 | 28.6 | 24.9 |
| Ba | 208.4 | 220.3 | 391 |
| Ce | 26.1 | 26.8 | 42.6 |
| Nd | 13.7 | 14.2 | 20.2 |
| Zr | 127.5 | 132.1 | 147 |
| Y | 21.4 | 21.4 | 25 |
| Sr | 389.7 | 507.6 | 510 |
| Rb | 13.6 | 14.1 | 20 |

F=.78 mc/mo=0.22

Cayuse to Sheridan 51/Group 8
D. Extrusion/intrusion

| Max | Min | Obs | Obs |
|---|---|---|---|
| 24.0 | 70.5 | 49 | 58±20 |
| 25.8 | 143.9 | 95 | 123±40 |
| 24.4 | 27.3 | 24.9 | 24.9 |
| 321.0 | 332.3 | 391 | 391 |
| 34.7 | 35.2 | 42.6 | 42.6 |
| 19.5 | 19.9 | 20.2 | 20.2 |
| 158.5 | 162.2 | 147 | 161±8 |
| 31.1 | 1.1 | 25 | 28±3 |
| 438.9 | 526.1 | 510 | 539±23 |
| 15.9 | 16.2 | 20 | 20.1 |

F=.78 me/mo=.66
mi/mo=.66 mc/mo=.22

Cayuse to Sheridan 51
E. Assimilation

| | Max | Min | Obs |
|---|---|---|---|
| Ni | 33.9 | 100.5 | 49 |
| Cr | 68.0 | 279.4 | 95 |
| Sc | 23.4 | 26.3 | 24.9 |
| Ba | 232.7 | 238.4 | 391 |
| Ce | 25.0 | 25.4 | 42.6 |
| Nd | 12.9 | 13.2 | 20.2 |
| Zr | 121.6 | 124.1 | 147 |
| Y | 19.8 | 19.8 | 25 |
| Sr | 415.9 | 470.5 | 510 |
| Rb | 17.0 | 17.2 | 20 |

F=.91 ma/mo=0.055
mc/mo=0.145

point to a Cayuse-like basalt rather than a Bachelor basalt as a more likely parent largely because sodium residuals are substantially reduced when Cayuse basalt is used. Differences are less dramatic when modeling trace-element data, and indeed the low Ba content of the Cayuse basalt makes that element in particular difficult to model. Regardless, neither a Cayuse nor any MBVC basalt can produce any of the MT1 basaltic andesite solely through crystal fractionation. Modeling solutions improve when crystal fractionation is coupled with extrusion rates exceeding crystallization rates and mixing of the MT1 parental magma with MT2 basalt or basaltic andesite. Similarly, MT2 Egan basaltic andesite is slightly better modeled as crystal fractionation of Egan basalt coupled again with extrusion and mixing, this time with MT1 basalt.

The validity of mixing magma types is only explored inferentially here. MT1 and MT2 basalts are indistinguishable in the field as both have essentially the same phenocryst assemblage, percent crystallinity, vesicularity, and flow expression (thickness of flow, length, etc.). Microprobe analyses show similar phase compositions (with MT2 phases being slightly more evolved than MT1), and olivine crystallization temperatures differ only slightly. Thus physically mixing MT1 and MT2 basaltic magmas is probably reasonable provided their flow paths intersect.

Although again the evidence is inferential, it is known from the paleomagnetic data that both magma types were erupted during episodes I and III, and thus the possibility of conduit intersection is at least reasonable. Petrographic evidence for mixing is primarily represented by sieve-textured plagioclase phenocrysts. In the two MT1 thin sections in which there is probe data for both sieve-textured and non-sieve textured phenocrysts, the phenocryst cores are sieve-textured and are more calcic than cores of non-sieved phenocrysts. Perhaps this reflects quenching of hotter MT1 magma after commingling with the MT2 magmas. The only other case in which both sieve-textured and non-sieve textured phenocrysts were probed was for a MT3 magma and in this case the sieve-textured core has a lower An content than non-sieve textured cores. One can speculate that if this rock mixed with a MT1 magma this would be the relationship one would expect, but as there is only one geochemical group for the MT3, ideas on mixing cannot be tested. More speculative perhaps is that most major and trace elements the MBVC basalts lie intermediate between Cayuse and Red Crater compositions and thus may already be the result of magma mixing (table 19).

Results from the models presented here indicate that MT3 group VI basaltic andesite cannot be derived from either a MT1 or MT2 basalt through crystal fractionation, magma mixing, nor assimilation of any of the rock types exposed along the MBVC. The lack of a parental basalt for the group VI basaltic andesites may be one of exposure (i.e. the parental basalt for this group may not have vented to the surface or may have been buried by younger lava flows) or incorrect correlation of parent:daughter products. The latter explanation seems unlikely as none of the basaltic geochemical groups have REE values as low as geochemical group VI (fig. 13). Another possibility is that these basaltic andesites are not derived from any of the basalts but represent 'near-primary' basaltic-andesite melts as suggested by Hughes (1983) and Hughes and Taylor (1986) from a source area probably distinct from the basalts

My interpretation of the petrochemical data is different than those of Sutton (1974), Clark (1983), Hughes (1983), and Hughes and Taylor (1986) who have all argued against the derivation of basaltic andesite and more silicic products from contemporaneous basalt for nearby central Oregon High Cascades areas. In particular, Sutton (1974) at Mount Jefferson and Clark (1983) at South Sister argued against the derivation of the more silicic magmas from basalt primarily because ratios of highly excluded incompatible elements varied considerably with increasing $SiO_2$. As mentioned above, magmas related by crystal fractionation processes should have the same incompatible element ratios. However, it is shown that incompatible ratio pairs from the MBVC often vary widely within a given rock unit and as such neither support nor refute either crystal fractionation or partial melting as the dominant process.

Petrologic studies of the High Cascades mafic platform just to the north of the MBVC (Taylor, 1978; Taylor, 1981; Hughes, 1983; Hughes and Taylor, 1986; Taylor 1987) are the

*Table 18. Averaging of Red Crater and Cayuse compositions and comparing the average with group I compositions*

| | Red Crater | Cayuse | Red Crater and Cayuse | group 1 |
|---|---|---|---|---|
| SiO2 | 49.5 | 51.4 | 50.45 | 50.6 ± 0.31 |
| Al2O3 | 16.6 | 16.6 | 16.6 | 17.2 ± 0.13 |
| FeTO3 | 11.91 | 9.31 | 10.61 | 9.61 ± 0.20 |
| MgO | 6.71 | 8.37 | 7.54 | 7.68 ± 0.29 |
| CaO | 8.63 | 9.2 | 8.915 | 9.29 ± 0.15 |
| Na2O | 3.43 | 3.09 | 3.26 | 3.27 ± 0.15 |
| K2O | 0.63 | 0.64 | 0.635 | 0.60 ± 0.06 |
| TiO2 | 1.9 | 1.06 | 1.48 | 1.32 ± 0.07 |
| P2O5 | 0.53 | 0.22 | 0.375 | 0.29 ±0.02 |
| MnO | 0.18 | 0.15 | 0.165 | 0.15 ± 0.01 |
| | | | | |
| Nb | 14 | 12 | 13 | 12.2 ± 0.8 |
| Rb | 6 | 14 | 10 | 11.3±2.9 |
| Sr | 492 | 428 | 460 | 461±28 |
| Zr | 192 | 100 | 146 | 135±10 |
| | | | | |
| Ba | 291 | 173 | 232 | 235±29 |
| Co | 39.7 | 39.74 | 39.72 | 38.4±1.6 |
| Ni | 131 | 148 | 139.5 | 140±16 |
| Cr | 172 | 451 | 311.5 | 270±30 |
| Cs | 0.228 | 0.6 | 0.414 | 0.27±0.02 |
| Hf | 4.17 | 2.3 | 3.235 | 2.93±0.07 |
| Rb | 10.1 | 11 | 10.55 | 11.3±2.9 |
| Ta | 0.792 | 0.48 | 0.636 | 0.543±0.07 |
| Th | 0.625 | 1.2 | 0.9125 | 0.86±0.19 |
| U | 0.341 | 0.5 | 0.4205 | 0.386±0.04 |
| Zn | 122 | 54 | 88 | 77±5 |
| Zr | 169 | 105 | 137 | 135±10 |
| Sc | 26.1 | 27.74 | 26.92 | 27.2±0.83 |

most relevant to this study both because of proximity and because the rock suite is composed almost entirely of basalt and basaltic andesite. On the basis of REE and trace-element data, Hughes (1983) delineated two basaltic andesite series: a North Sister (NS) and Mount Washington (MW) series. It was concluded that neither series could be derived from the mafic platform basalt, but rather that they represented near-primary magmas derived from a source area distinct from that of the basalt (Hughes, 1983; Hughes and Taylor, 1986). In support of this conclusion, Hughes and Taylor (1986) noted that phenocryst compositions for the two main phases, olivine and plagioclase, were more mafic in the basaltic andesite than in the basalt. They suggested that the implications of the petrochemical disparity between the High Cascades basalt and basaltic andesite may signify differences in primary magma production in a changing tectono-magmatic regime from one of primarily compressional calc-alkaline magmatism to one of primarily extensional tholeiitic basaltic magmatism (Hughes, 1983; Hughes and Taylor, 1986).

The rocks of the MBVC represent a much shorter time frame and a smaller area than do the rocks of the High Cascades mafic platform; however, similarities and differences between the two suites of rocks should be addressed. Phenocryst assemblages for both suites are similar, although some of the mafic platform rocks have orthopyroxene, which is not present in the rocks of the MBVC. Like the rocks of the mafic platform, MBVC plagioclase compositions appear to become more anorthitic with increasing $SiO_2$; unlike the mafic platform rocks, however, MBVC olivine compositions within a given magma type decrease with increasing $SiO_2$. The contrast in plagioclase and olivine behaviors in the MBVC suite suggests that the apparent increase in anorthite is probably related to processes acting on the magma, such as the influence of volatiles, magma mixing, or decompression, rather than to differences in the source area. The hypothesis that the increase in An content is due to magma modifying processes is supported by the following two lines of evidence. 1) In the Tot Mountain lavas, groundmass plagioclase compositions form two distinct clusters, one which has An values similar to phenocryst core compositions, and the other which has An values similar to rim compositions. It is difficult to interpret the presence of the two phases to processes other than magma mixing. 2) In the summit lavas of Mount Bachelor, plagioclase phenocrysts and groundmass phases do not appear to be in equilibrium as phenocryst rim and groundmass core compositions differ by 15 mole percent An, which suggests sudden decompression, magma-mixing, or assimilation.

REE patterns for MBVC rocks are similar to the mafic platform rocks (Hughes, 1983; Hughes and Taylor, 1986). REE values for the MBVC MT1 basalts are similar to the 'normal' basalt values for the mafic platform, and MBVC basaltic andesite MT1 and MT2, and MT3 REE values correspond to the mafic platform Mount Washington and North Sister values, respectively. Petrologic models for the MBVC suite indicate that nothing in the REE signatures of either the MT1 and MT2 assemblages precludes the derivation of the basaltic andesites from the basalts. However, based on REE data, the MT3, North Sister-like basaltic andesites cannot be derived from any of the basalt exposed in either the MBVC area or in the mafic platform area (Hughes and Taylor, 1986). The low REE values, different Hf/Zr incompatible trace-element ratios, and distinctive trend on the $K_2O$-$SiO_2$ diagram suggest that the MT3 geochemical group VI rocks are likely derived from a source area different from either the MT1 or MT2 rocks. The idea that the MT3 basaltic andesites may represent cumulates, or conversely, resorption of plagioclase into the melt based on their lack of an Eu anomaly (fig. 13) does not appear reasonable, because some MT3 basaltic andesite lava flows are aphanitic and others contain large euhedral phenocrysts of plagioclase that show no evidence of resorption. Thus, the basaltic andesite of geochemical group VI, like the North Sister basaltic andesite of the mafic platform, may represent 'near-primary' basaltic andesite as suggested by Hughes (1983).

MBVC basalts and basaltic andesite were erupted within the same tectonic framework. The symmetric distribution of the MT1 lava flows suggests that the vents for basalt and the basaltic andesite, if not the same, were in close spatial association. Furthermore, temporal

information interpreted from paleomagnetic data indicates that both calc-alkaline and tholeiitic basalt and basaltic andesite were erupted essentially simultaneously. Most MBVC lavas are calc-alkaline and compositionally less evolved than the contemporaneous smaller volume MBVC tholeiite lavas. Observations from the MBVC, therefore, do not support the idea of a tectonically changing regime as advanced by Hughes and Taylor (1986).

Petrologic studies of the MBVC suggest that magma that fed the MBVC system came from at least two chemically distinct source areas. The MT3 geochemical group VI lavas have Hf/Zr incompatible trace-element ratios and REE values that are distinct from those of either MT1 or MT2 geochemical group lavas. Thus the elevated $Al_2O_3$ and Sr values on the variation diagrams can be ascribed to a group of lava flows that are chemically unrelated to the rest of the MBVC lava flows.

Although the MT1 and MT2 lavas form distinct trends on most variation diagrams, differ in REE abundances, and are classified as calc-alkaline and tholeiitic respectively, there are no compelling reasons to consider that these two magma types come from different source areas. Highly excluded incompatible element ratios do not vary within error ranges for the two assemblages and they fall within the same general group on the $K_2O$-$SiO_2$ diagram. Experimental and theoretical work by Grove and Byran (1983) and Grove and Kinzler (1986) has led these workers to postulate that the differences between calc-alkaline and tholeiitic magma trends arise from the depth and pressure at which crystal fractionation takes place rather than from differences in source area. They propose that tholeiitic magmas arise from one-stage near surface crystal fractionation and that calc-alkaline magmas from two stage crystal fractionation at depth and near surface. The MT1 and MT2 rocks have similar mineral constituents, but major-element model phase proportions differ substantially in deriving basaltic andesite from basalt for each magma type. Thus, although the MT2 and MT1 series may have a similar parental magma, they appear to have taken substantially different evolutionary paths, perhaps similar to those proposed by Grove and Bryan (1983) and Grove and Kinzler (1986).

Subtle variations in geochemical group I basaltic lava flows may represent discrete batches of partial melt from the same source area. This, coupled with petrographic evidence of magma mixing (e.g. sieve-textured plagioclase phenocrysts and two groundmass plagioclase populations in Tot Mountain rocks) may, in part, explain some of the poor fits in the petrologic models. Continual replenishment of a magma chamber or conduit zone that is concurrently undergoing crystal fractionation may make it impossible to ever match parental and daughter products satisfactorily, even using widely ranging distribution coefficients.

Combined spatial, temporal, and petrologic data indicate that the MBVC was most likely underlain by more than one magma chamber or conduit. Within the resolution of the paleomagnetic data, MT1 geochemical groups erupted coevally with MT2 and MT3 geochemical groups. It would be difficult to keep thermally similar magmas (olivine phenocryst temperatures do not differ significantly between the magma types; table 5-1) distinct if they were all erupting from the same chamber. The spatial distribution of MT1 vents occupying the central axis and the MT2 and MT3 vents lying off axis and along the margins of the MBVC also lend support to the idea of multiple magma conduits. Although highly speculative, I consider the possibility that the early plumbing system was largely a network of conduits or conduit zones that may have allowed easy mixing of various basaltic magmas and was subject to almost constant recharge, but that only in evolving the more silicic basaltic andesite magmas did a 'magma chamber' develop where closed system processes then may have dominated.

The models here have purposely dealt with only surface observations and 'surface' processes. I have not attempted to characterize the source regions for the magma or magmas, but have only presented what appears to be reasonable solutions that integrates known spatial, temporal and geochemical data. Furthermore, I have given the models the widest possible latitude in distribution coefficients to see if AFC processes are remotely possible. I think the data presented indicate that these processes are responsible for much of

the gross character of the geochemical data, and intuitively perhaps make the most sense. Obviously, more stringent analysis of the REE data is needed to determine if hypotheses presented here fall within our present understanding of REE systematics or not. The range of distribution coefficients used in this study needs to be critically evaluated especially as more high-temperature and high-pressure experimental petrology is done. Thermodynamic considerations regarding the degree of crystallization and magma mixing need to be addressed. Finally, isotopic studies are needed to determine the extent, if any, of crustal interaction, or the extent of source heterogeneity (see Bullen and Clynne, 1987).

## SUMMARY

In summary, the following observations and conclusions regarding the eruptive history and the chemical evolution of the Mount Bachelor volcanic chain have been made.

1) Paleomagnetic secular-variation data indicate that growth of the Mount Bachelor volcanic chain was episodic. Four eruptive episodes are distinguished by paleomagnetic directions and vent locations.

2) Early eruptive activity, assigned to eruptive episode I, was focused in the central part of the chain along the Sheridan segment. Eruptive activity shifted to the south of the chain along the Siah segment during episode II and then to the north of the chain along the Bachelor segment during episodes III and IV. Major hiatuses in eruptive activity occurred between episodes I and II and between episodes III and IV. Coeval with eruptive episode I, Sheridan-segment eruptions, were eruptions from vents of the Red Crater chain of cones and Katsuk Butte along the northwest margin of the chain, as well as minor eruptions from the southern part of the chain along the Siah segment.

3) Paleomagnetic data coupled with field and chemical data show that lithologically and chemically similar lava flows are not necessarily temporally related, and that lithologically similar lava flows are not necessarily chemically related. For example, the lithologically and chemically similar lava flows of the Siah segment were erupted during two different time periods; minor eruptions occurred during episode I, but most of the Siah-segment lava flows vented during episode II. Similarly, the lithologically distinct big plagioclase lava flows (mb1a and mb3b) were erupted during different episodes, and were evolved from disparate magmas; one tholeiitic (mb3b) and the other calc-alkaline (mb1a).

4) Differences in chemistry are subtle, but ten geochemical groups, four of basalt and six of basaltic andesite composition, are distinguished by WDXRF whole-rock major-element and EDXRF trace-element analyses.

5) Two distinct magma types, MT1 consisting of geochemical groups I II, VII, VIII, IX, and X, and MT2 consisting of geochemical groups III, IV, and V, are evident in major- and trace-element silica-variation diagrams. Both magma types are composed of basalt and basaltic andesite geochemical groups. A third magma type, MT3 consisting solely of basaltic andesite geochemical group VI, is distinguished on the basis of REE data and elevated Sr and $Al_2O_3$ values.

6) MT1 and MT3 rocks are classified as calc-alkaline and MT2 rocks as tholeiite using the classification scheme of Miyashiro (1974) and major-element relationships discussed by Gill (1981).

7) Petrologic models that derive basaltic andesite from basalt by crystal fractionation of the mineral assemblage of olivine, plagioclase, clinopyroxene and magnetite, show good correlation between observed and modeled values for the major elements. However, observed and modeled values for the trace elements do not always show good correlation and indicate that other processes are likely involved. One difficulty in modeling is in matching the correct parent and daughter products. In open-systems that are constantly being replenished this may be almost impossible to do.

8) MT1 basaltic andesite appears derived from MT1 basalt through combined processes of open-system crystal fractionation, high extrusion rates, and perhaps magma mixing with a MT2 magma. This interpretation does not violate any trends observed on silica-variation diagrams, $K_2O$-$SiO_2$ mineral fractionation plots, basalt normalization diagrams, or incompatible-element ratios, and is consistent with the petrographic evidence.

MT2 basaltic andesite was derived from MT2 basalt by similar processes.

9) Although the MT1 and MT2 lava flows do not appear to be related by near surface processes, similarities in REE patterns, incompatible trace-element ratios, and $K_2O$-$SiO_2$ mineral fractionation trends suggest that they may have shared a common source, but have followed different evolutionary paths (see Grove and Baker, 1983).

10) No basalt in the MBVC area is parental to the MT3 basaltic andesite. REE, incompatible trace element ratios, and mineral fractionation trends all suggest that MT3 lavas come from a different source area than either the MT1 or MT2 lavas, and may represent 'near-primary' basaltic andesite as postulated by Hughes and Taylor (1986).

11) Combined spatial, temporal and geochemical data show that rocks of several distinctly different geochemical groups from more than one magma type were emplaced during a given eruptive episode. Furthermore, vents for the volumetrically dominant calc-alkaline MT1 lava flows are located along the central axis of the MBVC, whereas vents for the smaller volume tholeiite MT2 and calc-alkaline MT3 lava flows are located along the periphery, or off the main axis, of the chain. The combined data suggest that the MBVC was underlain by several small magma chambers or conduit zones tapping distinct magma sources.

12) The model proposed for the evolution of the MBVC requires discrete batches of partial melt, from at least two different source areas. It is speculated that the MBVC was underlain by several small magma chambers or more likely a series of conduit zones that fed simultaneous eruptions of magmas from different sources or from magmas that followed different evolutionary paths. The magma underwent continual crystal fractionation and was periodically replenished with new melts, each of which may represent a different degree of partial melting . In addition, magma from different magma chambers or conduits, may have mixed, and minor assimilation of silicic material may have occurred. Early in the history of the MBVC, magma from any of the three magma types could have vented anywhere along chain, but the growth of the MT1 plumbing system prevented further venting of MT2 and MT3 magmas along the central axis. It is further speculated that closed-system crystal fractionation may have only developed once enough magma ponded to form a magma chamber of a certain threshold size.

## ACKNOWLEDGEMENTS

This report essentially constitutes my Master's Thesis which was done at the University of Colorado - Boulder, and was funded by the Volcanic Hazards Project of the U. S. Geological Survey. Edward Larson and John Drexler at the University encouraged me to broaden my scope from working on just a paleomagnetic investigation to include the chemistry of the rocks as well. The combined approach certainly made the project more interesting for me and I thank them for their support and encouragement in trying to make me more multidimensional. Primary acknowledgement goes to two individuals without whose guidance this project would not have been completed. Richard Hoblitt introduced me to the discipline of paleomagnetism and what I have learned about paleomagnetic sampling, secular variation, and interpretation I owe largely to him. And I am indebted to William Scott, who introduced me to both the obvious and subtle aspects of looking at black rocks in the field, instilled in me an appreciation for the importance of good geologic mapping, and who patiently saw me through all aspects of this project. I also thank Dave Sherrod and Mike Clynne for their excellent reviews of the manuscript; any problems remaining are solely the responsibility of the author.

## REFERENCES CITED


Allegre, C. J., Treuil, Michel, Minster, Jean-Francois, Minster, Bernard, and Alberede, Francis, 1977, Systematic use of trace element in igneous process: Contributions to Mineralogy and Petrology, v. 60, p. 57-75.

Anders, Edward, and Ebihara, Mitsuru, 1982, Solar-system abundances of the elements: Geochemica et Cosmochimica Acta, v. 46, p. 2363-2380.

Arth, J. G., 1976, Behavior of trace elements during magmatic processes - A summary of theoretical models and their applications: U. S. Geological Survey Journal of Research, v. 4, no. 1, p 41-47.

Bowen, N.L., 1928, The evolution of the igneous rocks: (reprinted 1956) New York, Dover, 332 p.

Bacon, C. R., 1983, Eruptive history of Mount Mazama and Crater Lake caldera, Cascade Range, U.S.A.: Journal of Volcanology and Geothermal Research, v. 18, p. 57-115.

Bullen, T. D., and Clynne, M.A., 1987, Isotopic diversity at Lassen Volcanic Center, southern Cascade Range, California [abs.]: Transactions, American Geophysical Union, v. 68, no. 44, p. 1526.

Baedecker, P.A., ed., 1987, Methods for geochemical analysis: U. S. Geological Survey Bulletin, 1770, 80 pgs.

Baedecker, P. A., and McKowen, D. M., 1987, Instrumental neutron activation analysis of geological samples, in Baedecker, P. A., ed., Methods for geochemical analysis: U. S. Geological Survey Bulletin 1770, Chapter H.

Baker, B. H., and McBirney, A. R., 1985, Liquid fractionation: Part III: Geochemistry of zoned magams and the compositional effects of liquid fractionation: Journal of Volcanolgy and Geothermal Research, v. 24, p. 55-81.

Champion, D. E., 1980, Holocene geomagnetic secular variation in the western United States: Implications for the global geomagnetic field: U. S. Geological Survey Open-File Report 80-824, 277 p.

Clark, J. G., 1983, Geology and petrology of South Sister Volcano, High Cascade Range, Oregon: Eugene, University of Oregon, Ph.D. dissertation, 235 p.

Conrey, R.M., 1991, Geology and petrology of the Mt. Jefferson area, High Cascades Range, Oregon: Pullman, Washington State University, Ph.D. dissertation, 357 pgs.

Conrey, R.M., and Sherrod, D.R., 1988, Stratigraphy of drill holes and geochemistry of surface rocks, Breitenbush Hot Springs, 15-minute Quadrangle, Cascade Range, in Sherrod, D. R., ed., Geology and Geothermal Resources of the Breitenbush-Austin Hot Springs area, Clackamas and Marion counties, Oregon: State of Oregon, Department of Geology and Mineral Industries Open-File Report O-88-5, p. 15-29.

Cox, K.G., and Devey, C.W., 1987, Factionation processes in Deccan Traps magma: Comments on the paper G. Sen - Mineralogy and petrogenesis of the Deccan Trap lava flows around Mahabaleshwar, India: Journal of Petrology, v. 28, pt. 1, p. 235-238.

Cox, K.G., Bell, J.D., and Pankhurst, R.J., 1981, The interpretation of igneous rocks (3rd ed.): London, George Allen and Unwin, 450 p.

Deer, W.A., Howie, R.A., and Zussman, J., 1983, An introduction to the rock-forming minerals (14th ed.): London, Longman House, 528 p.

DePaolo, D. J., 1981, Trace element and isotopic effects of combined wallrock assimilation and fractional crystallization: Earth and Planetary Science Letters, v. 53, p. 182-202.

Dungan, M.A., Rhodes, J. M., 1978, Residual glasses and melt inclusions in basalts from DSDP Legs 45 and 46: Evidence for magma mixing: Contributions of Mineralogy and Petrology, v. 67, p. 417-431.

Dungan, M.A., 1987, Open system magmatic evolution of the Taos Plateau Volcanic field, northern New Mexico: II. The genesis of cryptic hybrids: Journal of Petrology, v. 28, no. 5, p.955-977.

Fisher, R. A., 1953, Dispersion on a sphere: Proceedings of the Royal Society of London, A217, p. 295-305.

Gast, P.W., 1968, Trace element fractionation and the origin of tholeiitic and alkaline magma types: Geochemica et Cosmochimica Acta: v. 32, p. 1057-1086.

Gill, J.B., 1981, Orogenic andesites and plate tectonics: New York, Springer-Verlag, 385 p.

Grove, T.L., and Bryan, W.B., 1983, Fractionation of pyroxene-phryic MORB at low pressures: An experimental study: Contributions to Mineralogy and Petrology, v. 84, p. 293-309.

Grove, T.L., and Baker, M.B., 1984, Phase equilibrium controls on the tholeiitic and calc-alkaline differentiation trends: Journal of Geophysical Research, v. 89, no. B5, p. 3253-3274.

Grove, Timothy L., and Kinzler, Rosamond J., 1986, Petrogenesis of andesites: Annual Review of Earth and Planetary Science Letters, v. 14, p. 3253-3274.

Hill, B.E., 1985, Petrology of the Bend Pumice and Tumulo Tuff, a Pleistocene Cascade eruption involving magma mixing: Corvallis, Oregon State University, MS thesis, 101 p.

Hill, B.E., 1991, Petrogenesis of compositionally distinct silicic volcanoes in the Three Sisters region of the Oregon Cascade Range: The effects of crustal extension on the development of continental arc silicic magmatism: Corvallis, Oregon State University, Ph.D. dissertation, 235 p.

Hirt, William, and Nekvasil, Hanna, 1988, An investigation of the role of deompression in the development of calcic zones in plagioclase crystallization from felsic magmas [abs]: Geological Society of America Abstracts with Programs, v. 20, p. A249.

Hoblitt, R.P., Reynolds, R.L., and Larson, E.E., 1985, Suitability of nonwelded pyroclastic-flow deposits for studies of magnetic secular variation: A test based on deposits emplaced at Mount St. Helens, Washington, 1980: Geology, v. 4, p. 242-245.

Hughes, S.S., 1983, Petrochemical evolution of High Cascade volcanic rocks in the Three Sisters region, Oregon: Corvallis, Oregon State University, Ph.D. dissertation, 198 p.

Hughes, Scott, S., and Taylor, E.M., 1986, Geochemistry, petrogenesis and tectonic implications High Cascade mafic platform lavas: Geological Society of America Bulletin, v. 97, p. 1024-1036.

Irvine, T.N., 1967, Chromium spinel as a petrographic indicator, part 2. Petrologic applications: Canadian Journal of Earth Sciences, v. 4, p. 71-103.

Irvine, T.N., and Baragar, W.R., 1971, A guide to the chemical classification of the common volcanic rocks: Canadian Journal of Earth Sciences, v. 8, p. 523-548.

Johnson, R.G., and King, B.S., 1987, Energy dispersive X-ray flourescence spectroscopy, in Baedecker, P. A., ed., Methods for geochemical analysis: U.S. Geological Survey Bulletin 1770, Chapter F.

Kuntz, M.A., Champion, D.E., Spiker, E.C., and Lefebvre, R.H., 1986, Contrasting magma types and steady-state, volume-predictable, basaltic volcanism along the Great Rift, Idaho: Geological Society of American Bulletin, v. 97, p. 579-594.

Kuo, Lung-Chuan, and Kirkpatrick, R. J., 1982, Pre-eruption history of phyric basalts from DSDP Legs 45 and 46: Evidence from morphology and zoning patterns in plagioclase: Contributions to Mineralogy and Petrology, v. 79, p. 13-27.

Le Bas, M.J., Le Maitre, R.W., Streckeisen, A., and Zanettin, B., 1986, A chemical classification of volcanic rocks based on the total alklai-silica diagram: Journal of Petrology, v. 27, p. 745-750.

Mankinen, E.A., Gromme, C.S., Dalrymple, G.B., Lanphere, M.A., and Bailey, R.A., 1986, Paleomagnetism and K-Ar ages of volcanic rocks from Long Valley caldera, California: Journal of Geophysical Research, v. 91, p. 633-652.

McBirney, A.R., Baker, B.H., and Nilson, R.H., 1985, Liquid fractionation. Part I: Basic principles and experimental simulations: Journal of Volcanology and Geothermal Research, v. 24, p. 1-24.

McBirney,A.R., 1978, Volcanic evolution of the Cascade Range: Annual Review of Earth and Planetary Science Letters, v. 6. p. 437-456.

Miyashiro, A., 1974, Volcanic rock series in islands arcs and active continental margins: American Journal of Science, v. 274, p. 321-355.

O'Donnell, T.H., and Presnall, D.C., 1980, Chemical variations of the glass and mineral phases in basalts dredged from 25°-30° N along the mid-Atlantic Ridge: American Journal of Science, v. 280-A, p. 845-868.

O'Hara, M.J., 1977, Geochemical evolution during fractional crystallization of a periodically refilled magma chamber: Nature, v. 266, p. 503-507.

O'Hara, M. J., and Mathews, R.E., 1981, Geochemical evolution in an advancing, periodically replenished, periodically tapped, continuously fractionated magma chamber: Royal Geological Society of London, v. 138, p. 237-277.

Porter, S.C., Pierce, K.L., and Hamilton, T.D., 1983, Late Wisconsin mount glaciaiton in the western United States, in Porter, S. C., ed., Late-Quaternary environments of the United States, v. 1, The late Pleistocene: University of Minnetsota Press, p. 71-111.

Reagan, M.K., Gill, J.B., Malavassi, Eduardo, and Garcia, M.O., 1987, Changes in magma composition at Arenal volcano, Costa Rica, 1968-1985: Real-time monitoring of open-system differentiation: Bulletin of Volcanology, v. 49, p. 415-434.

Roeder, P.L., and Emslie, R.F., 1970, Olivine-liquid equilibrium: Contributions to Mineralogy and Petrology, v. 29, p. 275-289.

Rose, W.I., Jr., Penfield, G.T., Drexler, J.W., and Larson, P.B., 1980, Geochemistry of the Andesite flank lavas of three composite cones within the Atitlan Cauldron, Guatemala: Bulletin of Volcanologique, v. 43, n. 1, p. 131-153.

Sarna-Wojcicki, A.M., Meyer, C.E., Nakata, J.K., Scott, W.E., Hill, B.E., Slate, J.L., and Russell, P.C., 1989, Age and correlation of mid-Quaternary ash beds and tuffs in the vicinity of Bend, Oregon, in Scott, W. E., Gardner, C. A., and Sarna-Wojcicki, A. M., eds., Guidebook for field trip to the Mount Bachelor-South Sister-Bend area, central Oregon High Cascades: U. S. Geological Survey Open-File Report 89-645, p. 55-63.

Scott, W.E., 1977, Quaternary glaciation and volcanism, Metolius River area, Oregon: Geological Society of America Bulletin, v. 88 p. 113-124.

Scott, W.E., 1987, Holocene rhyodacite eruptions on the flanks of South Sister volcano, Oregon, in Fink, J.H., ed. Geological Society of America Special Paper 212: Geological Society of America, p. 35-53.

Scott, W.E., 1989, Temporal relations between eurptions of Mount Bacelor volcanic chain and fluctuations of late Quaternary glaciers, in Scott, W.E., Gardner, C.A., and Sarna-Wojcicki, A.M., eds., Guidebook for field trip to the Mount Bachelor-South Sister-Bend area, central Oregon High Cascades: U.S. Geological Survey Open-File Report 89-645, p. 10-19.

Scott, W.E., and Gardner, C.A., 1985, Late Pleistocene-Early Holocene development of the Bachelor Butte volcanic zone, Cascade Range, Oregon [abs]: Transactions of the American Geophysical Union, v. 64, p. 1141.

Scott, W.E., and Gardner, C.A., 1989, Road log for day 2 –Southern part of the Mount Bachelor volcanic chain and late Holocene rhyolite eruptions at South Sister, in Scott, W.E., Gardner, C.A., and Sarna-Wojcicki, A.M., eds., Guidebook for field trip to the Mount Bachelor-South Sister-Bend area, central Oregon High Cascades: U. S. Geological Survey Open-File Report 89-645, p. 36-49.

Scott, W.E., and Gardner, C.A., 1992, Geologic map of the Mount Bachelor volcanic chain and surrounding area, Cascade Range, Oregon: U. S. Geological Survey Miscellaneous Inversitgations Map I-1967, scale 1:50,000.

Smith, D.R., and Leeman, W.P., 1987, Petrogensis of Mount St. Helenes dacitic magmas: Journal of Geophysical Research, v. 92, no. B10, p. 10,313-10,334.

Sutton, K.G., 1974, Geology of Mt. Jefferson: Corvallis, Oregon State University, Ph.D. dissertation, 120 p.

Taggert, J.E., Jr., Lindsay, J.R., Scott, B., Vivat, D.A., Bartel, A., and Stewart, K., 1987, Analysis of geologic materials by wave-length dispersive X-ray fluorescence spectroscopy, in Baedecker, P.A., ed., Methods for geochemical analysis: U. S. Geological Survey Bulletin 1770, Chapter E.

Tarling, D.H., 1983, Paleomagnetism: London, Chapman and Hall Ltd, 369 p.

Taylor, E.M., 1978, Field Geology of S. W. Broken Top quadrangle, Oregon: Department of Geology and Mineral Industries Special Paper 2, 50 p.

Taylor, E.M., 1981, Central High Cascade roadside geology, Bend, Sisters, McKenzie Pall, and Santiam Pass, Oregon, in Johnston, D.A., and Donnelly-Nolan, J., eds., Guides to some volcanic terranes in Washington, Idaho, and northern California: U.S. Geological Survey Circular 838, p. 55-83.

Taylor, E.M., 1987, Field Geology of the northwest quarter of the Broken Top 15' quadrangle, Deschutes County, Oregon: Oregon Department of Geology and Mineral Industries Special Paper 21, 20 p.

Wadge, G., 1982, Steady state volcanism - Evidence from eruption histories o f polygenetic volcanoes: Journal of Geophysical Research, v. 87, no. B5, p. 4035-4049.

Wager, L.R., and Deer, W. A., 1939, The petrology of the Skaergaard intrusion, Kanderlaugssuag, East Greenland: Medd Groenl 105, v. 4.

Walker, D., Shibata, T., and DeLong, S. E., 1979, Abyssal tholeiites from the oceanographer fracture zone II: Phase equilibrium and mixing: Contributions to Mineralogy and Petrology, v. 70, p. 111-175.

White, C.M., and McBirney, A.R., 1978, Some quantitative aspects of orogenic volcanism in the Oregon Cascades: in Smith, R. B., and Eaton, G. P., eds. Geological Survey of America, Memoir 152, p. 369-388.

Williams, Howell, 1944, Volcanoes of the Three Sisters region, Oregon Cascades: University of California Publications, Bulletin of the Departmetn of Geological Sciences, p. 37-83.

Wright, T.L., and Fiske, R.S., 1971, Origin of the differentiated and hybrid lavas of Kilauea Volcano, Hawaii: Journal of Petrology, v. 12, p. 1-65.

Wright, T.L., Peck, D.L., and Shaw, H.R., 1976, Kilauea Lava Lakes: Natural laboratories for study of cooling, crystallization and differentiation of basaltic magma: American Geophysical Union Monograph, vol. 19, p. 375-390.

# APPENDICES

A. Representative microprobe analyses for olivine, plagioclase, and clinopyroxene

B. Spinel microprobe analyses

C. Chemical analyses

D. Analytical limits of detection and accuracy for the major and trace elements

E. INAA analyses

F. Distribution coefficents used for trace-element modeling

## Appendix A. Representative microprobe analyses. Olivine.

| Sample/SiO2 | G84-19/49.7 | S84072 24/50.4 | | | | S840727-1/50.6 | | | S840703-2/50.7 | | |
|---|---|---|---|---|---|---|---|---|---|---|---|
| pheno or groundmass? | mpheno | gm | gm | pheno | pheno | pheno | gm | pheno | pheno | pheno | pheno | gm |
| c=center; r=rim | c | | | r | c | nc | | c | r | r | c | |
| weight per. oxides | | | | | | | | | | | | |
| MgO | 42.25 | 27.25 | 40.08 | 41.04 | 44.21 | 42.95 | 35.79 | 42.61 | 40.17 | 45.34 | 46.36 | 33.28 |
| SiO2 | 39.27 | 36.49 | 38.38 | 39.02 | 40.68 | 39.26 | 39.56 | 39.59 | 37.74 | 41.68 | 42.2 | 37.68 |
| CaO | 0.27 | 0.35 | 0.36 | 0.38 | 0.25 | 0.24 | 0.48 | 0.22 | 0.26 | 0 | 0 | 0 |
| TiO2 | 0 | 0.18 | 0.17 | 0 | 0 | 0 | 0.31 | 0.12 | 0.16 | 0 | 0 | 0 |
| MnO | 0 | 0 | 0.49 | 0.49 | 0.38 | 0.37 | 0 | 0 | 0 | 0 | 0 | 0 |
| FeO | 17.71 | 32.97 | 18.72 | 18.15 | 13.88 | 15.89 | 23.59 | 17.34 | 17.76 | 16.82 | 15.1 | 27.56 |
| NiO | 0.67 | 0.64 | 0.58 | 0.54 | 0.73 | 0.68 | 0.56 | 0.69 | 0.55 | 0 | 0 | 0 |
| total | 100.17 | 97.88 | 98.78 | 99.62 | 100.13 | 99.39 | 100.29 | 100.57 | 96.64 | 103.84 | 103.66 | 98.52 |
| Cations in formula | | | | | | | | | | | | |
| MgO | 1.6028 | 1.1415 | 1.5549 | 1.5722 | 1.6469 | 1.6317 | 1.3892 | 1.6061 | 1.5843 | 1.6463 | 1.6638 | 1.3405 |
| SiO2 | 0.9996 | 1.0256 | 0.9988 | 1.0027 | 1.0168 | 1.0005 | 1.0301 | 1.0012 | 0.9986 | 1.0056 | 1.0161 | 1.0183 |
| CaO | 0.0074 | 0.0105 | 0.0101 | 0.0103 | 0.0068 | 0.0067 | 0.0133 | 0.006 | 0.0075 | 0 | 0 | 0 |
| TiO2 | 0 | 0.0037 | 0.0034 | 0 | 0 | 0 | 0.006 | 0.0024 | 0.0032 | 0 | 0 | 0 |
| MnO | 0 | 0 | 0.0109 | 0.0107 | 0.0081 | 0.0079 | 0 | 0 | 0 | 0 | 0 | 0 |
| FeO | 0.377 | 0.7749 | 0.4075 | 0.3901 | 0.29 | 0.3388 | 0.5137 | 0.3667 | 0.3929 | 0.3426 | 0.3041 | 0.6228 |
| NiO | 0.0136 | 0.0144 | 0.0121 | 0.0112 | 0.0147 | 0.014 | 0.0117 | 0.0141 | 0.0118 | 0 | 0 | 0 |
| total | 3.0004 | 2.9706 | 2.9977 | 2.9972 | 2.9833 | 2.9996 | 2.964 | 2.9965 | 2.9983 | 2.9945 | 2.984 | 2.9816 |
| stoichiometry | | | | | | | | | | | | |
| SiO2 | 1.9992 | 2.0512 | 1.9976 | 2.0054 | 2.0336 | 2.001 | 2.0602 | 2.0024 | 1.9972 | 2.0112 | 2.0322 | 2.0366 |
| other cations | 2.0008 | 1.945 | 1.9989 | 1.9945 | 1.9665 | 1.9991 | 1.9339 | 1.9953 | 1.9997 | 1.9889 | 1.9679 | 1.9633 |
| total | 4 | 3.9962 | 3.9965 | 3.9999 | 4.0001 | 4.0001 | 3.9941 | 3.9977 | 3.9969 | 4.0001 | 4.0001 | 3.9999 |
| forsterite | 81 | 60 | 79 | 80 | 85 | 83 | 73 | 81 | 80 | 83 | 85 | 68 |
| fayalite | 19 | 40 | 21 | 20 | 15 | 17 | 27 | 19 | 20 | 17 | 15 | 32 |

Appendix A. (continued). Olivine.

| Sample/SiO2 | S850711-5/54.2 | | | S840725-4/55.8 | | | | S840914-8/56.3 | | | S840913-9/56.7 | |
|---|---|---|---|---|---|---|---|---|---|---|---|---|
| pheno or groundmass? c=center; r=rim | gm | pheno c | pheno r | pheno nc | pheno r | mpheno | gm | mpheno nc | mpheno r | gm | pheno c | pheno r |
| weight per. oxides | | | | | | | | | | | | |
| MgO | 40.74 | 43.8 | 43.2 | 42.66 | 41.01 | 37.53 | 35.95 | 38.83 | 33.24 | 31.23 | 32.52 | 30.02 |
| SiO2 | 39.73 | 40.35 | 40.52 | 40.06 | 39.88 | 38.26 | 38.2 | 38.53 | 37.46 | 37.55 | 37.96 | 37.44 |
| CaO | 0.22 | 0.23 | 0.14 | 0.2 | 0.19 | 0.39 | 0.28 | 0.19 | 0.31 | 0.43 | 0.23 | 0.26 |
| TiO2 | 0.14 | 0.14 | 0.14 | 0.19 | 0.19 | 0.15 | 0 | 0 | 0 | 0.14 | 0.19 | 0.23 |
| MnO | 0.3 | 0.4 | 0.41 | 0.37 | 0.34 | 0.4 | 0.4 | 0.47 | 0.57 | 0.57 | 0.59 | 0.69 |
| FeO | 19.75 | 16.12 | 16.42 | 16.9 | 18.37 | 22.3 | 23.97 | 21.41 | 27.83 | 29.98 | 28.48 | 31.07 |
| NiO | 0.55 | 0.49 | 0.56 | 0.78 | 0.64 | 0.31 | 0.61 | 0.56 | 0.62 | 0.43 | 0.38 | 0.42 |
| total | 101.43 | 101.53 | 101.39 | 101.16 | 100.62 | 99.34 | 99.41 | 99.99 | 100.03 | 100.33 | 100.35 | 100.13 |
| Cations in formula | | | | | | | | | | | | |
| MgO | 1.5388 | 1.6256 | 1.6069 | 1.5967 | 1.5521 | 1.4688 | 1.418 | 1.5042 | 1.3296 | 1.2562 | 1.2965 | 1.2164 |
| SiO2 | 1.0068 | 1.0046 | 1.0107 | 1.006 | 1.0126 | 1.0046 | 1.0108 | 1.0015 | 1.0052 | 1.0133 | 1.0154 | 1.0176 |
| CaO | 0.006 | 0.0061 | 0.0037 | 0.0054 | 0.0051 | 0.0109 | 0.0079 | 0.0053 | 0.009 | 0.0124 | 0.0066 | 0.0076 |
| TiO2 | 0.0026 | 0.0025 | 0.0027 | 0.0037 | 0.0035 | 0.0029 | 0 | 0 | 0 | 0.0029 | 0.0038 | 0.0047 |
| MnO | 0.0064 | 0.0085 | 0.0088 | 0.0079 | 0.0074 | 0.0089 | 0.0091 | 0.0102 | 0.0129 | 0.0131 | 0.0134 | 0.0158 |
| FeO | 0.4186 | 0.3356 | 0.3426 | 0.3549 | 0.3901 | 0.4898 | 0.5305 | 0.4654 | 0.6246 | 0.6765 | 0.637 | 0.7062 |
| NiO | 0.0112 | 0.0099 | 0.0112 | 0.0158 | 0.013 | 0.0066 | 0.0131 | 0.0118 | 0.0135 | 0.0094 | 0.0081 | 0.0093 |
| total | 2.9904 | 2.9928 | 2.9866 | 2.9904 | 2.9838 | 2.9925 | 2.9894 | 2.9984 | 2.9948 | 2.9838 | 2.9808 | 2.9776 |
| stoichiometry | | | | | | | | | | | | |
| SiO2 | 2.0136 | 2.0092 | 2.0214 | 2.012 | 2.0252 | 2.0092 | 2.0216 | 2.003 | 2.0104 | 2.0266 | 2.0308 | 2.0352 |
| other cations | 1.9836 | 1.9882 | 1.9759 | 1.9844 | 1.9712 | 1.9879 | 1.9786 | 1.9969 | 1.9896 | 1.9705 | 1.9654 | 1.96 |
| total | 3.9972 | 3.9974 | 3.9973 | 3.9964 | 3.9964 | 3.9971 | 4.0002 | 3.9999 | 4 | 3.9971 | 3.9962 | 3.9952 |
| forsterite | 79 | 83 | 82 | 82 | 80 | 75 | 73 | 76 | 68 | 65 | 67 | 63 |
| fayalite | 21 | 17 | 18 | 18 | 20 | 25 | 27 | 24 | 32 | 35 | 33 | 37 |

Appendix A. (continued). Olivine.

| Sample/SiO2 | S840805-2/51.7 | | | S840721-4/52.3 | | G84-18/52.7 | | S840722-5/52.9 | | | | |
|---|---|---|---|---|---|---|---|---|---|---|---|---|
| pheno or groundmass? | pheno | pheno | gm | gm | gm | mpheno | gm | gm | pheno | pheno | pheno | pheno |
| c=center; r=rim | r | c | | | | nc | | c | c | r | c | r |
| weight per. oxides | | | | | | | | | | | | |
| MgO | 40.74 | 38.03 | 37.61 | 37.66 | 42.68 | 36.1 | 32.01 | 40.71 | 42.81 | 37.94 | 43.8 | 43.2 |
| SiO2 | 39.35 | 39.1 | 38.04 | 39.87 | 39.5 | 38.64 | 37.43 | 39.34 | 39.92 | 38.73 | 40.35 | 40.52 |
| CaO | 0 | 0 | 0 | 0 | 0.27 | 0 | 0 | 0 | 0 | 0 | 0.23 | 0.14 |
| TiO2 | 0.13 | 0.25 | 0.26 | 0 | 0.14 | 0.14 | 0.31 | 0 | 0 | 0 | 0.14 | 0.14 |
| MnO | 0.31 | 0.53 | 0.51 | 0.51 | 0.33 | 0.57 | 0.59 | 0.54 | 0.31 | 0.59 | 0.4 | 0.41 |
| FeO | 19.69 | 22.9 | 22.32 | 23.94 | 16.79 | 26 | 29.86 | 19.48 | 17.31 | 22.05 | 16.12 | 16.42 |
| NiO | 0.6 | 0.49 | 0.47 | 0 | 0 | 0 | 0 | 0 | 0 | 0 | 0.49 | 0.56 |
| total | 100.82 | 101.3 | 99.21 | 101.98 | 99.71 | 101.45 | 100.2 | 100.07 | 100.35 | 99.31 | 101.53 | 101.39 |
| Cations in formula | | | | | | | | | | | | |
| MgO | 1.5488 | 1.4603 | 1.4753 | 1.4362 | 1.6161 | 1.4019 | 1.2851 | 1.5549 | 1.6114 | 1.4789 | 1.6256 | 1.6069 |
| SiO2 | 1.0037 | 1.0074 | 1.001 | 1.0202 | 1.0036 | 1.0069 | 1.0082 | 1.008 | 1.0082 | 1.0129 | 1.0046 | 1.0107 |
| CaO | 0 | 0 | 0 | 0 | 0.0074 | 0 | 0 | 0 | 0 | 0 | 0.0061 | 0.0037 |
| TiO2 | 0.0025 | 0.0049 | 0.0052 | 0 | 0.0028 | 0.0027 | 0.0062 | 0 | 0 | 0 | 0.0025 | 0.0027 |
| MnO | 0.0065 | 0.0115 | 0.0113 | 0.011 | 0.0072 | 0.0126 | 0.0134 | 0.0116 | 0.0066 | 0.013 | 0.0085 | 0.0088 |
| FeO | 0.4199 | 0.4934 | 0.4912 | 0.5123 | 0.3567 | 0.5665 | 0.6728 | 0.4175 | 0.3656 | 0.4823 | 0.3356 | 0.3426 |
| NiO | 0.0122 | 0.0101 | 0.0098 | 0 | 0 | 0 | 0 | 0 | 0 | 0 | 0.0099 | 0.0112 |
| total | 2.9936 | 2.9876 | 2.9938 | 2.9797 | 2.9938 | 2.9906 | 2.9857 | 2.992 | 2.9918 | 2.9871 | 2.9928 | 2.9866 |
| stoichiometry | | | | | | | | | | | | |
| SiO2 | 2.0074 | 2.0148 | 2.002 | 2.0404 | 2.0072 | 2.0138 | 2.0164 | 2.016 | 2.0164 | 2.0258 | 2.0092 | 2.0214 |
| other cations | 1.9899 | 1.9802 | 1.9928 | 1.9595 | 1.9902 | 1.9837 | 1.9775 | 1.984 | 1.9836 | 1.9742 | 1.9882 | 1.9759 |
| total | 3.9973 | 3.995 | 3.9948 | 3.9999 | 3.9974 | 3.9975 | 3.9939 | 4 | 4 | 4 | 3.9974 | 3.9973 |
| forsterite | 79 | 75 | 75 | 74 | 82 | 71 | 66 | 79 | 82 | 75 | 83 | 82 |
| fayalite | 21 | 25 | 25 | 26 | 18 | 29 | 34 | 21 | 18 | 25 | 17 | 18 |

Appendix A. (continued). Plagioclase.

| Sample # | G84-19 | S840722-4 | S840727-1 | | | | S840703-2 | | | | S03-2 cont | S850805-2 | |
|---|---|---|---|---|---|---|---|---|---|---|---|---|---|
| pheno or groundmass? c=center; r=rim s=sieve;cl=clean | mpheno | pheno nc | pheno c-s | pheno nr-s | mpheno c-cl | gm | pheno c | pheno nr | pheno r | gm | gm | pheno c | pheno nr |
| weight per. oxides | | | | | | | | | | | | | |
| Na2O | 3.23 | 2.38 | 0.77 | 1.26 | 2.97 | 3.47 | 2.7 | 2.08 | 1.59 | 2.55 | 3.58 | 1.99 | 2.59 |
| Al2O3 | 29.18 | 30.46 | 34.25 | 33.87 | 30.24 | 29.33 | 31.96 | 32.77 | 33.56 | 31.56 | 30.06 | 31.61 | 27.96 |
| SiO2 | 50.67 | 48.92 | 46.88 | 47.31 | 51.11 | 51.71 | 50.88 | 49.57 | 49.36 | 50.73 | 54.29 | 49.22 | 52.98 |
| K2O | 0.26 | 0.16 | 0.08 | 0.12 | 0.17 | 0.21 | 0.15 | 0.17 | 0.16 | 0.13 | 0.3 | 0.22 | 0.4 |
| CaO | 12.82 | 13.98 | 17.37 | 16.96 | 13.24 | 12.54 | 14.85 | 16.06 | 16.54 | 14.39 | 12.43 | 15.72 | 12.96 |
| FeO | 0.91 | 0.71 | 0.81 | 0.91 | 0.77 | 1.07 | 0.75 | 0.61 | 0.54 | 0.77 | 0.73 | 0.78 | 2.61 |
| total | 97.07 | 96.61 | 100.16 | 100.43 | 98.5 | 98.33 | 101.29 | 101.26 | 101.75 | 100.13 | 101.39 | 99.54 | 99.5 |
| Cations in formula | | | | | | | | | | | | | |
| Na2O | 0.2931 | 0.2176 | 0.0683 | 0.1117 | 0.2653 | 0.3103 | 0.2363 | 0.1821 | 0.1384 | 0.2245 | 0.3097 | 0.1773 | 0.231 |
| Al2O3 | 1.6115 | 1.6927 | 1.8515 | 1.8277 | 1.6405 | 1.5944 | 1.6977 | 1.7464 | 1.7788 | 1.6919 | 1.5806 | 1.7143 | 1.509 |
| SiO2 | 2.3746 | 2.3065 | 2.1508 | 2.1661 | 2.3521 | 2.3851 | 2.2929 | 2.2416 | 2.2204 | 2.3078 | 2.422 | 2.2645 | 2.4353 |
| K2O | 0.0153 | 0.0099 | 0.0046 | 0.007 | 0.0097 | 0.0125 | 0.0087 | 0.0096 | 0.0091 | 0.0075 | 0.0172 | 0.0138 | 0.0236 |
| CaO | 0.6437 | 0.7062 | 0.8536 | 0.8321 | 0.6529 | 0.6198 | 0.7169 | 0.7783 | 0.7969 | 0.7014 | 0.5942 | 0.7748 | 0.6383 |
| FeO | 0.0356 | 0.0281 | 0.0312 | 0.0348 | 0.0297 | 0.0413 | 0.0282 | 0.023 | 0.0204 | 0.0292 | 0.0273 | 0.0298 | 0.1003 |
| total | 4.9738 | 4.961 | 4.96 | 4.9794 | 4.9502 | 4.9634 | 4.9807 | 4.981 | 4.964 | 4.9623 | 4.951 | 4.9745 | 4.9375 |
| Stoichiometry | | | | | | | | | | | | | |
| SiO2 + Al2O3 | 15.944 | 15.997 | 16.009 | 15.975 | 15.97 | 15.918 | 15.962 | 15.952 | 15.997 | 15.999 | 16.01 | 15.915 | 15.777 |
| all other cations | 3.9508 | 3.8472 | 3.8308 | 3.9424 | 3.8304 | 3.9356 | 3.9604 | 3.972 | 3.8592 | 3.8504 | 3.7936 | 3.9828 | 3.9728 |
| total | 19.895 | 19.844 | 19.84 | 19.918 | 19.801 | 19.854 | 19.923 | 19.924 | 19.856 | 19.849 | 19.804 | 19.898 | 19.75 |
| Anorthite | 68 | 76 | 92 | 88 | 70 | 66 | 75 | 80 | 84 | 75 | 65 | 80 | 71 |
| Orthoclase | 2 | 1 | 0 | 1 | 1 | 1 | 1 | 1 | 1 | 1 | 2 | 1 | 3 |
| Albite | 31 | 23 | 7 | 12 | 29 | 33 | 25 | 19 | 15 | 24 | 34 | 18 | 26 |

Appendix A. (continued). Plagioclase.

| Sample # | (05-2) cont | S84-721-4 | | | G84-18 | | | | S840722-5 | | | | S850711-5 | |
|---|---|---|---|---|---|---|---|---|---|---|---|---|---|---|
| pheno or groundmass? c=center; r=rim s=sieve;cl=clean | mpheno nr | pheno nc | pheno r | gm | mpheno c | pheno c | pheno r | gm | pheno c-s | pheno r-s | pheno c-cl | pheno r-cl | pheno c-s | pheno r-s |
| weight per. oxides | | | | | | | | | | | | | | |
| Na2O | 3.54 | 3.14 | 2.69 | 3.54 | 2.23 | 3.73 | 2.46 | 2.94 | 1.82 | 2.3 | 2.74 | 1.78 | 1.32 | 2.36 |
| Al2O3 | 28.63 | 30.39 | 30.68 | 30.26 | 31.45 | 30 | 31.16 | 30.66 | 33.14 | 31.78 | 29.33 | 32.15 | 33.44 | 30.68 |
| SiO2 | 54.27 | 52.97 | 51.89 | 51.97 | 49.31 | 53.28 | 51.39 | 52.37 | 48.6 | 49.39 | 51.14 | 48.34 | 47.24 | 50.84 |
| K2O | 0.32 | 0.5 | 0.16 | 0.14 | 0.16 | 0.19 | 0.15 | 0.2 | 0.17 | 0.17 | 0.24 | 0.23 | 0.12 | 0.23 |
| CaO | 11.38 | 12.82 | 13.54 | 13.46 | 15.01 | 12.34 | 14.38 | 13.69 | 16.08 | 15.48 | 13.52 | 15.73 | 17.08 | 14.11 |
| FeO | 0.87 | 0.6 | 0.53 | 0.89 | 0.85 | 0.64 | 0.88 | 0.87 | 0.78 | 0.71 | 0.68 | 0.85 | 0.83 | 0.84 |
| total | 99.01 | 100.42 | 99.49 | 100.26 | 99.01 | 100.18 | 100.42 | 100.73 | 100.59 | 99.83 | 97.65 | 99.08 | 100.03 | 99.06 |
| Cations in formula | | | | | | | | | | | | | | |
| Na2O | 0.3129 | 0.2746 | 0.2377 | 0.3118 | 0.1992 | 0.3265 | 0.216 | 0.2574 | 0.1612 | 0.2046 | 0.2472 | 0.1601 | 0.1177 | 0.2099 |
| Al2O3 | 1.5363 | 1.6179 | 1.6465 | 1.6201 | 1.7113 | 1.5974 | 1.6648 | 1.6304 | 1.78 | 1.717 | 1.6079 | 1.7525 | 1.8125 | 1.6607 |
| SiO2 | 2.4708 | 2.3927 | 2.3631 | 2.3606 | 2.2766 | 2.4068 | 2.3294 | 2.3627 | 2.15 | 2.2647 | 2.3786 | 2.236 | 2.1725 | 2.3353 |
| K2O | 0.0188 | 0.0143 | 0.009 | 0.0079 | 0.0094 | 0.0109 | 0.0085 | 0.0117 | 0.0098 | 0.01 | 0.0142 | 0.0133 | 0.0072 | 0.0136 |
| CaO | 0.5553 | 0.6205 | 0.6604 | 0.6549 | 0.7428 | 0.5975 | 0.6983 | 0.6619 | 0.7849 | 0.7606 | 0.6737 | 0.7798 | 0.8418 | 0.6945 |
| FeO | 0.033 | 0.0288 | 0.0203 | 0.0337 | 0.0327 | 0.0241 | 0.0335 | 0.0327 | 0.0295 | 0.0272 | 0.0265 | 0.0328 | 0.032 | 0.0321 |
| total | 4.9271 | 4.9488 | 4.937 | 4.989 | 4.972 | 4.9632 | 4.9505 | 4.9568 | 4.9154 | 4.9841 | 4.9481 | 4.9745 | 4.9837 | 4.9461 |
| Stoichiometry | | | | | | | | | | | | | | |
| SiO2 + Al2O3 | 16.028 | 16.042 | 16.038 | 15.923 | 15.952 | 16.017 | 15.977 | 15.972 | 15.72 | 15.927 | 15.946 | 15.954 | 15.94 | 15.984 |
| all other cations | 3.68 | 3.7528 | 3.7096 | 4.0332 | 3.9364 | 3.836 | 3.8252 | 3.8548 | 3.9416 | 4.0096 | 3.8464 | 3.944 | 3.9948 | 3.8004 |
| total | 19.708 | 19.795 | 19.748 | 19.956 | 19.888 | 19.853 | 19.802 | 19.827 | 19.662 | 19.936 | 19.792 | 19.898 | 19.935 | 19.784 |
| Anorthite | 63 | 68 | 73 | 67 | 78 | 64 | 76 | 71 | 82 | 78 | 72 | 82 | 87 | 76 |
| Orthoclase | 2 | 2 | 1 | 1 | 1 | 1 | 1 | 1 | 1 | 1 | 2 | 1 | 1 | 1 |
| Albite | 35 | 30 | 26 | 32 | 21 | 35 | 23 | 28 | 17 | 21 | 26 | 17 | 12 | 23 |

Appendix A. (continued). Plagioclase.

| Sample # | (11-5) | | S840725-4 | | | | S840914-8 | | | | S84013-9 | | |
|---|---|---|---|---|---|---|---|---|---|---|---|---|---|
| pheno or groundmass? c=center; r=rim s=sieve;cl=clean | cont pheno c-cl | gm | mpheno c | mpheno c | mpheno c | mpheno r | pheno c | pheno r | micro c | micro r | pheno c | pheno r | gm |
| weight per. oxides | | | | | | | | | | | | | |
| Na2O | 2.08 | 3.23 | 1.13 | 3.99 | 0.97 | 2.56 | 1.35 | 2.88 | 4.19 | 4.39 | 2.02 | 2.84 | 3.96 |
| Al2O3 | 31.91 | 29.14 | 33.76 | 27.98 | 33.28 | 29.7 | 33.3 | 29.61 | 26.24 | 27 | 32.01 | 30.53 | 28.05 |
| SiO2 | 50.03 | 54.28 | 47.6 | 53.69 | 46.94 | 52.54 | 46.81 | 50.93 | 55.19 | 55.22 | 47.96 | 45.34 | 53.22 |
| K2O | 0.23 | 0.33 | 0.13 | 0.32 | 0.15 | 0.31 | 0.18 | 0.29 | 0.43 | 0.46 | 0.19 | 0.13 | 0.39 |
| CaO | 15.18 | 12.33 | 16.88 | 11.32 | 16.97 | 13.32 | 16.92 | 13.33 | 9.99 | 9.75 | 15.94 | 15.59 | 11.37 |
| FeO | 0.69 | 0.8 | 0.55 | 0.78 | 0 | 0 | 0.75 | 0.8 | 0.96 | 1.06 | 0.8 | 0.78 | 0.99 |
| total | 100.12 | 100.11 | 100.05 | 98.08 | 98.31 | 98.43 | 99.31 | 97.84 | 97 | 97.88 | 98.92 | 95.21 | 97.98 |
| Cations in formula | | | | | | | | | | | | | |
| Na2O | 0.1837 | 0.2829 | 0.1001 | 0.3563 | 0.0877 | 0.2273 | 0.1214 | 0.2597 | 0.3757 | 0.391 | 0.1815 | 0.2671 | 0.355 |
| Al2O3 | 1.7147 | 1.5497 | 1.8229 | 1.5186 | 1.8249 | 1.6046 | 1.8183 | 1.6218 | 1.4309 | 1.4604 | 1.7515 | 1.7465 | 1.5276 |
| SiO2 | 2.2809 | 2.4492 | 2.181 | 2.4729 | 2.1841 | 2.4083 | 2.1687 | 2.367 | 2.5537 | 2.5338 | 2.2261 | 2.2002 | 2.4592 |
| K2O | 0.0137 | 0.0189 | 0.0076 | 0.0187 | 0.0092 | 0.018 | 0.0109 | 0.0171 | 0.0255 | 0.0271 | 0.0113 | 0.0081 | 0.023 |
| CaO | 0.7412 | 0.5959 | 0.8288 | 0.5586 | 0.8461 | 0.6539 | 0.8397 | 0.6639 | 0.4952 | 0.4792 | 0.7929 | 0.8106 | 0.5631 |
| FeO | 0.0263 | 0.0303 | 0.021 | 0.0302 | 0 | 0 | 0.0292 | 0.031 | 0.0372 | 0.0406 | 0.0312 | 0.0317 | 0.0382 |
| total | 4.9605 | 4.9269 | 4.9614 | 4.9553 | 4.952 | 4.9121 | 4.9882 | 4.9605 | 4.9182 | 4.9321 | 4.9945 | 5.0642 | 4.9661 |
| Stoichiometry | | | | | | | | | | | | | |
| SiO2 + Al2O3 | 15.982 | 15.996 | 16.016 | 15.966 | 16.036 | 16.052 | 15.948 | 15.955 | 15.938 | 15.977 | 15.91 | 15.787 | 15.947 |
| all other cations | 3.8596 | 3.712 | 3.83 | 3.8552 | 3.772 | 3.5968 | 4.0048 | 3.8868 | 3.7344 | 3.7516 | 4.0676 | 4.47 | 3.9172 |
| total | 19.842 | 19.708 | 19.846 | 19.821 | 19.808 | 19.648 | 19.953 | 19.842 | 19.673 | 19.728 | 19.978 | 20.257 | 19.864 |
| Anorthite | 79 | 66 | 88 | 60 | 90 | 73 | 86 | 71 | 55 | 53 | 80 | 75 | 60 |
| Orthoclase | 1 | 2 | 1 | 2 | 1 | 2 | 1 | 2 | 3 | 3 | 1 | 1 | 2 |
| Albite | 20 | 32 | 11 | 38 | 9 | 25 | 12 | 28 | 42 | 44 | 18 | 25 | 38 |

Appendix A. (continued). Clinopyroxene.

| Sample No. | G84-19 | S840703-2 | 840722-5 | 840725-4 | | 840713-9 | | 840914-8 | |
|---|---|---|---|---|---|---|---|---|---|
| pheno or gm | gm | gm | gm | mpheno | gm | pheno | gm | gm | gm |
| Oxide percent | | | | | | | | | |
| MgO | 13.44 | 14.36 | 16.84 | 25.16 | 14.96 | 14.3 | 19.06 | 16.14 | 22.6 |
| Al2O3 | 3.21 | 3.57 | 1.88 | 0.9 | 1.39 | 2.49 | 0.66 | 2.85 | 0.75 |
| SiO2 | 47.98 | 50.54 | 50.92 | 53.15 | 50.97 | 49.43 | 51.06 | 50.99 | 50.64 |
| CaO | 19.89 | 20.91 | 17.15 | 2.42 | 18.16 | 20.31 | 4.83 | 20.54 | 2.34 |
| TiO2 | 2.02 | 0 | 0.89 | 0.48 | 0 | 0.93 | 0.63 | 0.64 | 0.71 |
| FeO | 10.71 | 8.7 | 10.09 | 15.71 | 11.11 | 9.5 | 21.38 | 7.45 | 18.62 |
| Total | 97.25 | 98.08 | 97.77 | 97.82 | 96.59 | 96.96 | 97.62 | 98.61 | 95.66 |
| Cations | | | | | | | | | |
| MgO | 0.7755 | 0.8106 | 0.9478 | 1.3851 | 0.8586 | 0.8202 | 1.0891 | 0.8995 | 1.2967 |
| Al2O3 | 0.1466 | 0.1592 | 0.0838 | 0.0391 | 0.0632 | 0.1128 | 0.0297 | 0.1255 | 0.034 |
| SiO2 | 1.8577 | 1.9134 | 1.9233 | 1.9629 | 1.9628 | 1.9021 | 1.9573 | 1.906 | 1.9491 |
| CaO | 0.825 | 0.8483 | 0.6941 | 0.0959 | 0.7491 | 0.8373 | 0.1983 | 0.8227 | 0.0965 |
| TiO2 | 0.0587 | 0 | 0.0252 | 0.0134 | 0 | 0.027 | 0.0181 | 0.018 | 0.0204 |
| FeO | 0.3469 | 0.2755 | 0.3187 | 0.4845 | 0.3576 | 0.3057 | 0.6855 | 0.2331 | 0.5992 |
| Total | 4.0104 | 4.007 | 3.9929 | 3.9809 | 3.9913 | 4.0051 | 3.978 | 4.0048 | 3.9959 |
| Stoichiometry | | | | | | | | | |
| SiO2+Al2O3 | 2.0043 | 2.0726 | 2.0071 | 2.002 | 2.026 | 2.0149 | 1.987 | 2.0315 | 1.9831 |
| all other cati | 2.0061 | 1.9344 | 1.9858 | 1.9789 | 1.9653 | 1.9902 | 1.991 | 1.9733 | 2.0128 |
| Fs | 18 | 14 | 16 | 25 | 18 | 16 | 35 | 12 | 30 |
| En | 40 | 42 | 48 | 70 | 44 | 42 | 55 | 46 | 65 |
| Wo | 42 | 44 | 35 | 5 | 38 | 43 | 10 | 42 | 5 |

Appendix A. (continued). Clinopyroxene

| Sample No. | G84-19 | S840703-2 | 840722-5 | 840725-4 | | 840713-9 | | 840914-8 | |
|---|---|---|---|---|---|---|---|---|---|
| pheno or gm | gm | gm | gm | mpheno | gm | pheno | gm | gm | gm |
| Oxide percent | | | | | | | | | |
| MgO | 13.44 | 14.36 | 16.84 | 25.16 | 14.96 | 14.3 | 19.06 | 16.14 | 22.6 |
| Al2O3 | 3.21 | 3.57 | 1.88 | 0.9 | 1.39 | 2.49 | 0.66 | 2.85 | 0.75 |
| SiO2 | 47.98 | 50.54 | 50.92 | 53.15 | 50.97 | 49.43 | 51.06 | 50.99 | 50.64 |
| CaO | 19.89 | 20.91 | 17.15 | 2.42 | 18.16 | 20.31 | 4.83 | 20.54 | 2.34 |
| TiO2 | 2.02 | 0 | 0.89 | 0.48 | 0 | 0.93 | 0.63 | 0.64 | 0.71 |
| FeO | 10.71 | 8.7 | 10.09 | 15.71 | 11.11 | 9.5 | 21.38 | 7.45 | 18.62 |
| Total | 97.25 | 98.08 | 97.77 | 97.82 | 96.59 | 96.96 | 97.62 | 98.61 | 95.66 |
| Cations | | | | | | | | | |
| MgO | 0.7755 | 0.8106 | 0.9478 | 1.3851 | 0.8586 | 0.8202 | 1.0891 | 0.8995 | 1.2967 |
| Al2O3 | 0.1466 | 0.1592 | 0.0838 | 0.0391 | 0.0632 | 0.1128 | 0.0297 | 0.1255 | 0.034 |
| SiO2 | 1.8577 | 1.9134 | 1.9233 | 1.9629 | 1.9628 | 1.9021 | 1.9573 | 1.906 | 1.9491 |
| CaO | 0.825 | 0.8483 | 0.6941 | 0.0959 | 0.7491 | 0.8373 | 0.1983 | 0.8227 | 0.0965 |
| TiO2 | 0.0587 | 0 | 0.0252 | 0.0134 | 0 | 0.027 | 0.0181 | 0.018 | 0.0204 |
| FeO | 0.3469 | 0.2755 | 0.3187 | 0.4845 | 0.3576 | 0.3057 | 0.6855 | 0.2331 | 0.5992 |
| Total | 4.0104 | 4.007 | 3.9929 | 3.9809 | 3.9913 | 4.0051 | 3.978 | 4.0048 | 3.9959 |
| Stoichiometry | | | | | | | | | |
| SiO2+Al2O3 | 2.0043 | 2.0726 | 2.0071 | 2.002 | 2.026 | 2.0149 | 1.987 | 2.0315 | 1.9831 |
| other cations | 2.0061 | 1.9344 | 1.9858 | 1.9789 | 1.9653 | 1.9902 | 1.991 | 1.9733 | 2.0128 |
| Fs | 18 | 14 | 16 | 25 | 18 | 16 | 35 | 12 | 30 |
| En | 40 | 42 | 48 | 70 | 44 | 42 | 55 | 46 | 65 |
| Wo | 42 | 44 | 35 | 5 | 38 | 43 | 10 | 42 | 5 |

Appendix B. Spinel microprobe analyses.

| Sample No. | G84-19a | b | 8407224a | b | 8407271a | b |
|---|---|---|---|---|---|---|
| Elements | | | | | | |
| MgO | 8.94 | 7.73 | 12.60 | 12.53 | 9.56 | 9.25 |
| Al2O3 | 24.00 | 23.40 | 41.29 | 45.13 | 31.51 | 32.74 |
| TiO2 | 2.26 | 2.26 | 0.88 | 0.98 | 2.01 | 1.93 |
| Cr2O3 | 25.19 | 25.19 | 24.25 | 20.49 | 26.49 | 25.67 |
| MnO | 0.00 | 0.00 | 0.00 | 0.00 | 0.00 | 0.00 |
| FeO | 36.46 | 36.59 | 24.65 | 25.68 | 34.22 | 33.88 |
| total | 96.85 | 95.17 | 103.67 | 104.81 | 103.79 | 103.47 |
| normalized to 100 percent | | | | | | |
| MgO | 9.23 | 8.12 | 12.15 | 11.95 | 9.21 | 8.94 |
| Al2O3 | 24.78 | 24.59 | 39.83 | 43.06 | 30.36 | 31.64 |
| TiO2 | 2.33 | 2.37 | 0.85 | 0.94 | 1.94 | 1.87 |
| Cr2O3 | 26.01 | 26.47 | 23.39 | 19.55 | 25.52 | 24.81 |
| MnO | 0.00 | 0.00 | 0.00 | 0.00 | 0.00 | 0.00 |
| FeO | 37.65 | 38.45 | 23.78 | 24.50 | 32.97 | 32.74 |
| FeO | 21.46 | 23.07 | 19.50 | 20.58 | 22.75 | 22.92 |
| Fe2O3 | 16.19 | 15.38 | 4.28 | 3.92 | 10.22 | 9.82 |
| cations | | | | | | |
| Mg | 0.23 | 0.20 | 0.30 | 0.30 | 0.23 | 0.22 |
| Al | 0.49 | 0.48 | 0.78 | 0.84 | 0.60 | 0.62 |
| Ti | 0.03 | 0.03 | 0.01 | 0.01 | 0.02 | 0.02 |
| Cr | 0.34 | 0.35 | 0.31 | 0.26 | 0.34 | 0.33 |
| Mn | 0.00 | 0.00 | 0.00 | 0.00 | 0.00 | 0.00 |
| Fe 2+ | 0.30 | 0.32 | 0.27 | 0.29 | 0.32 | 0.32 |
| Fe 3+ | 0.20 | 0.19 | 0.05 | 0.05 | 0.13 | 0.12 |
| total | 1.59 | 1.58 | 1.73 | 1.75 | 1.63 | 1.63 |
| cations based on 32 oxygens | | | | | | |
| Mg | 3.46 | 3.07 | 4.19 | 4.08 | 3.37 | 3.26 |
| Al | 7.35 | 7.35 | 10.86 | 11.61 | 8.78 | 9.11 |
| Ti | 0.44 | 0.45 | 0.15 | 0.16 | 0.36 | 0.34 |
| Cr | 5.17 | 5.31 | 4.28 | 3.54 | 4.95 | 4.79 |
| Mn | 0.00 | 0.00 | 0.00 | 0.00 | 0.00 | 0.00 |
| Fe 2+ | 4.51 | 4.89 | 3.77 | 3.94 | 4.67 | 4.68 |
| Fe 3+ | 3.06 | 2.93 | 0.75 | 0.68 | 1.89 | 1.81 |
| Stochiometry | | | | | | |
| Al, Cr, and Fe3+, Ti | 16.03 | 16.04 | 16.04 | 15.98 | 15.97 | 16.06 |
| Mg, Fe 2+, and Mn | 7.97 | 7.96 | 7.96 | 8.02 | 8.03 | 7.94 |
| Mg/Mg +Fe2+ | 0.43 | 0.39 | 0.53 | 0.51 | 0.42 | 0.41 |
| Al/Al + Cr | 0.59 | 0.58 | 0.72 | 0.77 | 0.64 | 0.66 |
| Fe3+/Cr+Al+ Fe3+ | 0.20 | 0.19 | 0.05 | 0.04 | 0.12 | 0.11 |

Appendix B. (continued).

| Sample No. | 8408052a | | b 8407115a | b | | c 8407254a |
|---|---|---|---|---|---|---|
| Elements | | | | | | |
| MgO | 14.08 | 13.97 | 12.08 | 12.79 | 10.81 | 7.04 |
| Al2O3 | 31.75 | 31.04 | 33.56 | 34.04 | 30.02 | 12.16 |
| TiO2 | 1.43 | 1.49 | 1.29 | 2.78 | 1.55 | 6.03 |
| Cr2O3 | 24.98 | 25.04 | 28.74 | 31.88 | 29.81 | 25.16 |
| MnO | 0.36 | 0.31 | 0.00 | 0.00 | 0.00 | 0.00 |
| FeO | 25.57 | 25.57 | 27.53 | 30.26 | 29.98 | 47.27 |
| total | 98.17 | 97.42 | 103.20 | 111.75 | 102.17 | 97.66 |
| normalized to 100 percent | | | | | | |
| MgO | 14.34 | 14.34 | 11.71 | 11.45 | 10.58 | 7.21 |
| Al2O3 | 32.34 | 31.86 | 32.52 | 30.46 | 29.38 | 12.45 |
| TiO2 | 1.46 | 1.53 | 1.25 | 2.49 | 1.52 | 6.17 |
| Cr2O3 | 25.45 | 25.70 | 27.85 | 28.53 | 29.18 | 25.76 |
| MnO | 0.37 | 0.32 | 0.00 | 0.00 | 0.00 | 0.00 |
| FeO | 26.05 | 26.25 | 26.68 | 27.08 | 29.34 | 48.40 |
| FeO | 14.85 | 14.96 | 19.21 | 18.95 | 20.54 | 22.27 |
| Fe2O3 | 11.20 | 11.29 | 7.47 | 8.12 | 8.80 | 26.14 |
| cations | | | | | | |
| Mg | 0.36 | 0.36 | 0.29 | 0.28 | 0.26 | 0.18 |
| Al | 0.63 | 0.62 | 0.64 | 0.60 | 0.58 | 0.24 |
| Ti | 0.02 | 0.02 | 0.02 | 0.03 | 0.02 | 0.08 |
| Cr | 0.33 | 0.34 | 0.37 | 0.38 | 0.38 | 0.34 |
| Mn | 0.01 | 0.00 | 0.00 | 0.00 | 0.00 | 0.00 |
| Fe 2+ | 0.21 | 0.21 | 0.27 | 0.26 | 0.29 | 0.31 |
| Fe 3+ | 0.14 | 0.14 | 0.09 | 0.10 | 0.11 | 0.33 |
| total | 1.70 | 1.69 | 1.67 | 1.65 | 1.64 | 1.48 |
| cations based on 32 oxygens | | | | | | |
| Mg | 5.04 | 5.05 | 4.17 | 4.12 | 3.85 | 2.91 |
| Al | 8.98 | 8.86 | 9.16 | 8.67 | 8.45 | 3.97 |
| Ti | 0.26 | 0.27 | 0.22 | 0.45 | 0.28 | 1.26 |
| Cr | 4.74 | 4.80 | 5.26 | 5.45 | 5.63 | 5.51 |
| Mn | 0.07 | 0.06 | 0.00 | 0.00 | 0.00 | 0.00 |
| Fe 2+ | 2.93 | 2.95 | 3.84 | 3.83 | 4.19 | 5.04 |
| Fe 3+ | 1.99 | 2.00 | 1.34 | 1.48 | 1.62 | 5.32 |
| Stochiometry | | | | | | |
| Al, Cr, and Fe3+, Ti | 15.97 | 15.94 | 15.99 | 16.05 | 15.96 | 16.06 |
| Mg, Fe 2+, and Mn | 8.04 | 8.06 | 8.01 | 7.95 | 8.03 | 7.94 |
| Mg/Mg +Fe2+ | 0.63 | 0.63 | 0.52 | 0.52 | 0.48 | 0.37 |
| Al/Al + Cr | 0.65 | 0.65 | 0.64 | 0.61 | 0.60 | 0.42 |
| Fe3+/Cr+Al+ Fe3+ | 0.13 | 0.13 | 0.09 | 0.09 | 0.10 | 0.36 |

Appendix B. (continued).

| Sample No. | (254)b cont | c | d | e | f | g | h |
|---|---|---|---|---|---|---|---|
| Elements | | | | | | | |
| MgO | 11.71 | 11.24 | 7.43 | 7.74 | 10.85 | 10.93 | 7.16 |
| Al2O3 | 34.36 | 31.66 | 21.66 | 22.43 | 32.59 | 31.65 | 22.38 |
| TiO2 | 1.51 | 1.72 | 2.67 | 2.35 | 1.68 | 1.82 | 2.36 |
| Cr2O3 | 27.69 | 26.47 | 24.25 | 25.91 | 27.92 | 28.07 | 25.89 |
| MnO | 0.00 | 0.00 | 0.00 | 0.00 | 0.37 | 0.41 | 0.48 |
| FeO | 30.66 | 32.23 | 42.58 | 42.04 | 33.54 | 33.25 | 41.75 |
| total | 105.93 | 103.32 | 98.59 | 100.47 | 106.95 | 106.13 | 100.02 |
| normalized to 100 percent | | | | | | | |
| MgO | 11.05 | 10.88 | 7.54 | 7.70 | 10.14 | 10.30 | 7.16 |
| Al2O3 | 32.44 | 30.64 | 21.97 | 22.33 | 30.47 | 29.82 | 22.38 |
| TiO2 | 1.43 | 1.66 | 2.71 | 2.34 | 1.57 | 1.71 | 2.36 |
| Cr2O3 | 26.14 | 25.62 | 24.60 | 25.79 | 26.10 | 26.45 | 25.88 |
| MnO | 0.00 | 0.00 | 0.00 | 0.00 | 0.35 | 0.39 | 0.48 |
| FeO | 28.94 | 31.19 | 43.19 | 41.84 | 31.35 | 31.33 | 41.74 |
| FeO | 20.26 | 20.28 | 23.32 | 23.85 | 20.69 | 20.68 | 23.79 |
| Fe2O3 | 8.68 | 10.92 | 19.87 | 17.99 | 10.66 | 10.65 | 17.95 |
| cations | | | | | | | |
| Mg | 0.27 | 0.27 | 0.19 | 0.19 | 0.25 | 0.26 | 0.18 |
| Al | 0.64 | 0.60 | 0.43 | 0.44 | 0.60 | 0.58 | 0.44 |
| Ti | 0.02 | 0.02 | 0.03 | 0.03 | 0.02 | 0.02 | 0.03 |
| Cr | 0.34 | 0.34 | 0.32 | 0.34 | 0.34 | 0.35 | 0.34 |
| Mn | 0.00 | 0.00 | 0.00 | 0.00 | 0.00 | 0.01 | 0.01 |
| Fe 2+ | 0.28 | 0.28 | 0.32 | 0.33 | 0.29 | 0.29 | 0.33 |
| Fe 3+ | 0.11 | 0.14 | 0.25 | 0.23 | 0.13 | 0.13 | 0.22 |
| total | 1.66 | 1.65 | 1.55 | 1.55 | 1.64 | 1.64 | 1.55 |
| cations based on 32 oxygens | | | | | | | |
| Mg | 3.96 | 3.93 | 2.90 | 2.95 | 3.69 | 3.75 | 2.75 |
| Al | 9.18 | 8.75 | 6.68 | 6.76 | 8.75 | 8.58 | 6.80 |
| Ti | 0.26 | 0.30 | 0.53 | 0.45 | 0.29 | 0.31 | 0.46 |
| Cr | 4.96 | 4.91 | 5.02 | 5.24 | 5.03 | 5.10 | 5.28 |
| Mn | 0.00 | 0.00 | 0.00 | 0.00 | 0.07 | 0.08 | 0.10 |
| Fe 2+ | 4.07 | 4.11 | 5.03 | 5.12 | 4.22 | 4.22 | 5.13 |
| Fe 3+ | 1.57 | 1.99 | 3.86 | 3.48 | 1.96 | 1.96 | 3.48 |
| Stochiometry | | | | | | | |
| Al, Cr, and Fe3+, Ti | 15.97 | 15.96 | 16.07 | 15.93 | 16.03 | 15.95 | 16.02 |
| Mg, Fe 2+, and Mn | 8.03 | 8.04 | 7.93 | 8.07 | 7.97 | 8.05 | 7.99 |
| Mg/Mg +Fe2+ | 0.49 | 0.49 | 0.37 | 0.37 | 0.47 | 0.47 | 0.35 |
| Al/Al + Cr | 0.65 | 0.64 | 0.57 | 0.56 | 0.64 | 0.63 | 0.56 |
| Fe3+/Cr+Al+ Fe3+ | 0.10 | 0.13 | 0.25 | 0.22 | 0.12 | 0.13 | 0.22 |

*Appendix C. Chemical Analyses*

| Sample No. | 8407214 | 8507271 | 8407223 | 84-16 | 8407061 | 85-7 | 8508013 | 8408051 | 8407281 | 8407215 | 8508012 | 8407011 | 8407066 | 8407064 | 8407024 |
|---|---|---|---|---|---|---|---|---|---|---|---|---|---|---|---|
| Map Unit | mb1a | mb1a | mb1a | mb1a | mb1b | mb1b | mb1b | mb1b | mb1b | mb1b | mb1b | mb1b | mb1c | mb1c | mb1c |
| SiO2 | 52.3 | 53.8 | 52.3 | 53.8 | 53.3 | 51.1 | 53.8 | 53.5 | 53.7 | 54.0 | 55.0 | 54.1 | 52.6 | 53.1 | 53.4 |
| Al2O3 | 18.5 | 17.4 | 18.3 | 17.4 | 17.2 | 17.3 | 17.4 | 17.3 | 17.5 | 17.4 | 17.3 | 17.3 | 18.5 | 18.3 | 18.1 |
| FeTO3 | 8.95 | 8.51 | 8.98 | 8.44 | 8.97 | 9.44 | 8.54 | 8.92 | 8.58 | 8.54 | 8.33 | 8.53 | 8.84 | 8.83 | 8.83 |
| MgO | 5.72 | 5.28 | 5.78 | 5.18 | 6.33 | 7.33 | 5.28 | 5.98 | 5.24 | 4.99 | 4.96 | 5.06 | 5.71 | 5.54 | 5.49 |
| CaO | 9.03 | 8.90 | 9.22 | 8.88 | 8.27 | 9.27 | 8.88 | 8.23 | 8.95 | 8.74 | 8.21 | 8.69 | 8.78 | 8.57 | 8.40 |
| Na2O | 3.47 | 3.49 | 3.33 | 3.58 | 3.49 | 3.29 | 3.48 | 3.48 | 3.48 | 3.60 | 3.55 | 3.59 | 3.50 | 3.50 | 3.56 |
| K2O | 0.58 | 0.93 | 0.61 | 0.91 | 0.79 | 0.60 | 0.95 | 0.88 | 0.91 | 1.00 | 1.04 | 1.01 | 0.61 | 0.66 | 0.70 |
| TiO2 | 1.10 | 1.18 | 1.12 | 1.18 | 1.14 | 1.30 | 1.20 | 1.16 | 1.24 | 1.21 | 1.10 | 1.22 | 1.12 | 1.13 | 1.14 |
| P2O5 | 0.20 | 0.35 | 0.20 | 0.35 | 0.39 | 0.28 | 0.36 | 0.41 | 0.34 | 0.40 | 0.39 | 0.39 | 0.23 | 0.24 | 0.27 |
| MnO | 0.13 | 0.14 | 0.13 | 0.13 | 0.15 | 0.15 | 0.14 | 0.15 | 0.14 | 0.14 | 0.14 | 0.14 | 0.13 | 0.13 | 0.13 |
| FeO | | 6.39 | 6.04 | 6.37 | | 6.47 | 6.26 | 5.80 | | | 5.60 | | | | |
| H2O+ | | 0.26 | 0.38 | 0.21 | | <0.01 | 0.34 | 0.44 | | | 0.40 | | | | |
| H2O- | | 0.05 | 0.01 | 0.15 | | 0.26 | 0.07 | 0.05 | | | 0.04 | | | | |
| CO2 | | <0.01 | <0.01 | <0.01 | | <0.01 | <0.01 | <0.01 | | | <0.01 | | | | |
| Nb | <10 | 11 | <10 | 15 | 13 | 12 | 11 | 11 | 17 | 12 | 14 | 18 | <10 | 11 | 11 |
| Pb | 16 | 19 | 15 | 17 | 22 | 10 | 16 | 21 | 25 | 20 | 27 | 29 | 14 | 21 | 19 |
| Sr | 605 | 510 | 602 | 490 | 585 | 440 | 517 | 540 | 515 | 510 | 546 | 545 | 634 | 639 | 656 |
| Zr | 92 | 147 | 98 | 150 | 154 | 140 | 149 | 158 | 165 | 161 | 165 | 176 | 105 | 108 | 119 |
| Y | 18 | 25 | 16 | 22 | 27 | 20 | 24 | 27 | 29 | 26 | 33 | 32 | 19 | 18 | 20 |
| Cu | 60 | 75 | 65 | 80 | 60 | 75 | | 60 | | 70 | 75 | 70 | | 60 | 65 |
| Ni | 70 | 60 | 75 | 50 | 90 | 140 | | 80 | | 40 | 50 | 35 | | 70 | 80 |
| Zn | 70 | 80 | 70 | 80 | 80 | 80 | | 85 | | 80 | 80 | 85 | | 80 | 80 |
| Cr | 80 | 125 | 80 | 110 | 190 | 200 | | 165 | | 110 | 95 | 100 | | 100 | 110 |
| Ba | 252 | | 362 | | | | | | | | | 391 | | 321 | |
| Co | 33.9 | | 28.3 | | | | | | | | | 26.9 | | 31.7 | |
| Ni | 91.8 | | 39 | | | | | | | | | 48.6 | | 85.9 | |
| Cr | 64.2 | | 93.5 | | | | | | | | | 95.2 | | 88.6 | |
| Cs | 0.34 | | 0.548 | | | | | | | | | 0.553 | | 0.338 | |
| Hf | 2.27 | | 3.43 | | | | | | | | | 3.61 | | 2.44 | |
| Pb | 11.2 | | 16.2 | | | | | | | | | 20.1 | | 13.9 | |
| Ta | 0.284 | | 0.764 | | | | | | | | | 0.766 | | 0.341 | |
| Th | 0.71 | | 1.62 | | | | | | | | | 1.73 | | 0.793 | |
| U | 0.307 | | 0.625 | | | | | | | | | 0.853 | | 0.336 | |
| Zn | 91.6 | | 91.3 | | | | | | | | | 91.7 | | 93.3 | |
| Zr | 69 | | 157 | | | | | | | | | 147 | | | |
| Sc | 22.9 | | 26.1 | | | | | | | | | 24.9 | | 22 | |
| Latitude | 43 53 41 | 43 53 50 | 43 53 02 | 43 53 00 | 43 56 01 | 43 53 00 | 43 54 18 | 43 54 08 | 43 54 40 | 43 53 23 | 43 52 40 | 43 53 15 | 43 52 15 | 43 52 05 | 43 54 45 |
| Longitude | 121 41 25 | 121 40 54 | 121 39 16 | 121 38 42 | 121 45 03 | 121 40 48 | 121 42 43 | 121 45 25 | 121 39 48 | 121 41 33 | 121 41 12 | 121 14 02 | 121 44 00 | 121 44 25 | 121 42 15 |

*Appendix C.*

| Sample No. | 8407062 | 8407242 | 8407071 | 8408024 | 8408023 | 8407191 | 8407193 | 8407216 | 8407101 | 8509052 | 8507062 | 8408015 | 8408032 | 8407194 | 8407052 |
|---|---|---|---|---|---|---|---|---|---|---|---|---|---|---|---|
| Map Unit | mb1c | mb2a | mb2a? | mb2a | mb2b | mb2b | mb2b | mb2b | mb2b | mb2b | mb2b | mb2b | mb2b | mb2b | mb2b |
| SiO2 | 53.2 | 51.0 | 52.1 | 50.8 | 50.0 | 50.3 | 50.2 | 51.3 | 50.9 | 50.7 | 51.0 | 50.8 | 50.8 | 50.2 | 50.7 |
| Al2O3 | 18.2 | 17.2 | 17.2 | 17.1 | 17.3 | 17.2 | 17.2 | 17.5 | 17.2 | 17.1 | 17.0 | 17.0 | 17.2 | 17.3 | 17.1 |
| FeTO3 | 8.88 | 9.61 | 9.86 | 9.67 | 10.00 | 9.83 | 9.81 | 9.28 | 9.55 | 9.46 | 9.35 | 9.46 | 9.48 | 9.83 | 9.42 |
| MgO | 5.49 | 7.18 | 6.24 | 7.18 | 7.75 | 7.98 | 7.96 | 7.11 | 7.78 | 7.89 | 8.01 | 7.83 | 7.68 | 8.03 | 8.05 |
| CaO | 8.53 | 9.26 | 8.28 | 9.29 | 9.29 | 9.25 | 9.24 | 9.24 | 9.15 | 9.23 | 9.30 | 9.39 | 9.17 | 9.21 | 9.34 |
| Na2O | 3.55 | 3.23 | 3.54 | 3.35 | 3.38 | 3.24 | 3.33 | 3.34 | 3.13 | 3.34 | 3.12 | 3.21 | 3.42 | 3.19 | 3.16 |
| K2O | 0.67 | 0.65 | 0.77 | 0.65 | 0.49 | 0.51 | 0.51 | 0.59 | 0.61 | 0.60 | 0.61 | 0.61 | 0.60 | 0.52 | 0.62 |
| TiO2 | 1.13 | 1.44 | 1.42 | 1.41 | 1.35 | 1.29 | 1.30 | 1.25 | 1.27 | 1.24 | 1.00 | 1.29 | 1.27 | 1.30 | 1.26 |
| P2O5 | 0.25 | 0.32 | 0.45 | 0.32 | 0.28 | 0.28 | 0.28 | 0.27 | 0.28 | 0.29 | 0.27 | 0.30 | 0.29 | 0.28 | 0.29 |
| MnO | 0.13 | 0.15 | 0.16 | 0.15 | 0.15 | 0.15 | 0.16 | 0.14 | 0.15 | 0.15 | 0.15 | 0.15 | 0.15 | 0.15 | 0.15 |
| FeO | | | | | | | | | 6.26 | | 6.28 | | | | |
| H2O+ | | | | | | | | | 0.35 | | 0.22 | | | | |
| H2O- | | | | | | | | | 0.01 | | 0.02 | | | | |
| CO2 | | | | | | | | | <0.01 | | <0.01 | | | | |
| Nb | <10 | 14 | 12 | 15 | 12 | 11 | 10 | <10 | <10 | | 13 | 12 | 13 | 10 | 12 |
| Pb | 17 | 18 | 16 | 18 | 12 | 10 | <10 | 10 | 12 | | 16 | 10 | 11 | <10 | 12 |
| Sr | 642 | 474 | 568 | 479 | 452 | 446 | 448 | 467 | 455 | | 475 | 462 | 485 | 435 | 486 |
| Zr | 106 | 155 | 177 | 165 | 137 | 132 | 139 | 134 | 133 | | 141 | 137 | 138 | 137 | 140 |
| Y | 17 | 27 | 28 | 29 | 27 | 26 | 27 | 23 | 22 | | 30 | 24 | 26 | 24 | 23 |
| Cu | | | 60 | 60 | | | | | 60 | | 60 | | | | |
| Ni | | | 100 | 110 | | | | | 140 | | 150 | | | | |
| Zn | | | 90 | 80 | | | | | 70 | | 70 | | | | |
| Cr | | | 190 | 220 | | | | | 280 | | 320 | | | | |
| Ba | | | 352 | | | | | | | | | | | | |
| Co | | | 34.6 | | | | | | | | | | | | |
| Ni | | | 116 | | | | | | | | | | | | |
| Cr | | | 164 | | | | | | | | | | | | |
| Cs | | | 0.461 | | | | | | | | | | | | |
| Hf | | | 1.02 | | | | | | | | | | | | |
| Pb | | | 15.6 | | | | | | | | | | | | |
| Ta | | | 0.64 | | | | | | | | | | | | |
| Th | | | 1.11 | | | | | | | | | | | | |
| U | | | 0.562 | | | | | | | | | | | | |
| Zn | | | 105 | | | | | | | | | | | | |
| Zr | | | 173 | | | | | | | | | | | | |
| Sc | | | 23.6 | | | | | | | | | | | | |
| Latitude | 43 51 43 | 43 52 43 | 43 50 38 | 43 48 03 | 43 39 35 | 43 47 43 | 43 46 45 | 43 54 50 | 43 52 28 | 43 52 15 | 43 50 07 | 43 49 45 | 43 51 17 | 43 38 41 | 43 50 15 |
| Longitude | 121 44 11 | 121 36 27 | 121 43 50 | 121 36 26 | 121 39 20 | 121 38 23 | 121 36 43 | 121 40 57 | 121 40 22 | 121 37 47 | 121 36 43 | 121 36 46 | 121 38 37 | 121 37 30 | 121 43 40 |

*Appendix C.*

| Sample No. | 8408021 | 8407123 | 8407192 | 8407026 | 8507272 | 8407073 | 8407196 | 8408014 | 8407033 | 8508031 | 8407053 | 8407032 | 8407057 | 8407025 | 8408022 |
|---|---|---|---|---|---|---|---|---|---|---|---|---|---|---|---|
| Map Unit | mb2b | mb2b | mb2b | mb2b | mb2b | mb2c | mb2c | mb2c | mb2c | mb2c | mb2c | mb2c | mb2c | mb2c | mb2c |
| SiO2 | 50.2 | 49.8 | 50.3 | 50.8 | 50.8 | 50.7 | 50.8 | 50.6 | 50.5 | 50.6 | 50.6 | 50.7 | 50.5 | 50.6 | 50.7 |
| Al2O3 | 17.3 | 17.4 | 17.1 | 17.2 | 17.1 | 17.2 | 17.2 | 17.3 | 17.3 | 17.2 | 17.2 | 17.2 | 17.1 | 17.0 | 17.2 |
| FeTO3 | 9.81 | 10.29 | 9.76 | 9.53 | 9.83 | 9.62 | 9.42 | 9.42 | 9.64 | 9.61 | 9.50 | 9.54 | 9.63 | 9.97 | 9.56 |
| MgO | 8.04 | 7.64 | 8.09 | 7.76 | 7.05 | 7.41 | 7.64 | 7.66 | 7.49 | 7.37 | 7.60 | 7.47 | 7.49 | 7.11 | 7.22 |
| CaO | 9.29 | 9.29 | 9.16 | 9.15 | 9.24 | 9.39 | 9.46 | 9.46 | 9.49 | 9.47 | 9.48 | 9.46 | 9.49 | 9.27 | 9.54 |
| Na2O | 3.20 | 3.38 | 3.32 | 3.21 | 3.38 | 3.22 | 3.18 | 3.24 | 3.17 | 3.27 | 3.20 | 3.25 | 3.30 | 3.23 | 3.36 |
| K2O | 0.52 | 0.43 | 0.57 | 0.57 | 0.70 | 0.64 | 0.61 | 0.60 | 0.60 | 0.62 | 0.59 | 0.59 | 0.65 | 0.70 | 0.61 |
| TiO2 | 1.29 | 1.37 | 1.30 | 1.35 | 1.46 | 1.37 | 1.30 | 1.30 | 1.37 | 1.38 | 1.36 | 1.33 | 1.34 | 1.52 | 1.36 |
| P2O5 | 0.28 | 0.24 | 0.28 | 0.29 | 0.34 | 0.31 | 0.29 | 0.30 | 0.30 | 0.31 | 0.30 | 0.30 | 0.31 | 0.36 | 0.31 |
| MnO | 0.15 | 0.16 | 0.15 | 0.15 | 0.15 | 0.15 | 0.15 | 0.15 | 0.15 | 0.15 | 0.15 | 0.15 | 0.15 | 0.16 | 0.15 |
| FeO | | | | | 6.58 | 7.11 | 6.84 | | 6.13 | 6.34 | | | 6.48 | 6.77 | |
| H2O+ | | | | | 0.35 | 0.36 | 0.25 | | 0.41 | 0.33 | | | 0.39 | 0.30 | |
| H2O- | | | | | 0.08 | <0.01 | <0.01 | | <0.01 | 0.06 | | | <0.01 | <0.01 | |
| CO2 | | | | | <0.01 | <0.01 | 0.01 | | <0.01 | <0.01 | | | <0.01 | 0.01 | |
| Nb | 11 | 11 | 10 | 12 | 17 | 15 | 11 | 12 | 11 | 11 | 12 | 13 | <10 | 12 | 14 |
| Rb | 9 | 11 | 13 | 13 | 19 | 19 | 14 | 10 | 13 | 15 | 10 | 11 | <10 | 18 | 12 |
| Sr | 453 | 426 | 450 | 493 | 479 | 462 | 453 | 469 | 457 | 481 | 472 | 485 | 452 | 454 | 472 |
| Zr | 142 | 123 | 142 | 141 | 168 | 147 | 136 | 141 | 140 | 143 | 137 | 140 | 138 | 173 | 140 |
| Y | 25 | 29 | 27 | 29 | 32 | 28 | 25 | 23 | 23 | 25 | 24 | 24 | 21 | 28 | 26 |
| Cu | 70 | | 60 | 75 | | | | | 60 | 75 | | | | 65 | |
| Ni | 140 | | 145 | 150 | | | | | 115 | 120 | | | | 100 | |
| Zn | 80 | | 70 | 80 | | | | | 70 | 70 | | | | 80 | |
| Cr | 300 | | 285 | 290 | | | | | 215 | 200 | | | | 190 | |
| Ba | 214 | | | | | | | | | | 218 | | | | |
| Co | 40 | | | | | | | | | | 39.1 | | | | |
| Ni | 153 | | | | | | | | | | 136 | | | | |
| Cr | 241 | | | | | | | | | | 211 | | | | |
| Cs | 0.244 | | | | | | | | | | 0.299 | | | | |
| Hf | 2.86 | | | | | | | | | | 3.02 | | | | |
| Rb | 4.86 | | | | | | | | | | 10.4 | | | | |
| Ta | 0.471 | | | | | | | | | | 0.615 | | | | |
| Th | 0.63 | | | | | | | | | | 0.841 | | | | |
| U | 0.353 | | | | | | | | | | 0.425 | | | | |
| Zn | 92.6 | | | | | | | | | | 85.9 | | | | |
| Zr | 131 | | | | | | | | | | 139 | | | | |
| Sc | 26.6 | | | | | | | | | | 28.3 | | | | |
| Latitude | 43 48 40 | 43 47 40 | 43 48 57 | 43 52 12 | 43 53 20 | 43 51 30 | 43 51 07 | 43 51 07 | 43 51 32 | 43 50 50 | 43 50 40 | 43 52 11 | 43 51 07 | 43 55 03 | 43 49 15 |
| Longitude | 121 38 03 | 121 38 43 | 121 36 48 | 121 40 27 | 121 41 13 | 121 43 47 | 121 39 05 | 121 37 28 | 121 40 10 | 121 44 00 | 121 43 40 | 121 40 17 | 121 41 33 | 121 41 55 | 121 39 09 |

*Appendix C.*

| Sample No. | 8407034 | 8407243 | 8407075 | 8407102 | 8407197 | 8608241 | 8408061 | 8608243 | 8608234 | 8408052 | 8407231 | 8407244 | 8507102 | 8408065 | 8507092 |
|---|---|---|---|---|---|---|---|---|---|---|---|---|---|---|---|
| Map Unit | mb2c | mb2c | mb2c | mb2c | mb2c | mb3a? | mb3a | mb4a | mb3a? | mb3a? | mb3b | mb3b | mb3c | mb3c | mb3c |
| SiO2 | 50.5 | 50.6 | 50.7 | 50.7 | 50.6 | 49.8 | 51.4 | 50.8 | 54.3 | 51.7 | 52.3 | 52.7 | 50.5 | 50.3 | 50.6 |
| Al2O3 | 17.1 | 17.2 | 17.2 | 17.1 | 17.1 | 17.2 | 17.0 | 17.0 | 17.2 | 17.5 | 18.0 | 17.4 | 17.4 | 17.3 | 17.0 |
| FeTO3 | 9.48 | 9.55 | 9.61 | 9.65 | 9.51 | 10.00 | 9.50 | 9.39 | 8.42 | 9.11 | 9.80 | 10.76 | 9.66 | 9.76 | 9.67 |
| MgO | 7.80 | 7.56 | 7.34 | 7.61 | 7.87 | 8.25 | 6.86 | 7.81 | 6.12 | 6.91 | 5.28 | 4.27 | 7.68 | 7.70 | 7.85 |
| CaO | 9.48 | 9.47 | 9.39 | 9.32 | 9.39 | 9.41 | 8.92 | 9.42 | 8.30 | 8.80 | 8.36 | 7.83 | 9.06 | 9.06 | 9.03 |
| Na2O | 3.26 | 3.27 | 3.34 | 3.21 | 3.17 | 3.21 | 3.39 | 3.23 | 3.42 | 3.59 | 3.53 | 3.81 | 3.31 | 3.46 | 3.30 |
| K2O | 0.58 | 0.59 | 0.64 | 0.63 | 0.58 | 0.48 | 0.77 | 0.63 | 0.94 | 0.69 | 0.70 | 0.90 | 0.61 | 0.57 | 0.70 |
| TiO2 | 1.30 | 1.31 | 1.37 | 1.36 | 1.35 | 1.34 | 1.60 | 1.27 | 1.08 | 1.31 | 1.51 | 1.72 | 1.33 | 1.36 | 1.40 |
| P2O5 | 0.30 | 0.30 | 0.32 | 0.32 | 0.29 | 0.24 | 0.40 | 0.27 | 0.30 | 0.32 | 0.30 | 0.43 | 0.27 | 0.28 | 0.30 |
| MnO | 0.15 | 0.15 | 0.15 | 0.15 | 0.15 | 0.15 | 0.15 | 0.15 | 0.13 | 0.14 | 0.15 | 0.16 | 0.15 | 0.15 | 0.15 |
| FeO | | | | 6.90 | | | | | | | | | 6.43 | | 6.37 |
| H2O+ | | | | 0.29 | | | | | | | | | 0.33 | | 0.18 |
| H2O- | | | | 0.04 | | | | | | | | | 0.04 | | 0.06 |
| CO2 | | | | <0.01 | | | | | | | | | <0.01 | | <0.01 |
| Nb | 14 | 13 | 12 | 11 | 12 | 10 | 15 | 10 | 10 | 13 | <10 | 16 | 12 | 11 | 12 |
| Pb | 11 | 15 | <10 | 12 | 10 | 10 | 14 | 10 | 10 | 18 | 14 | 15 | 16 | <10 | 15 |
| Sr | 475 | 455 | 455 | 453 | 463 | 415 | 519 | 420 | 500 | 560 | 586 | 549 | 495 | 509 | 505 |
| Zr | 136 | 140 | 138 | 140 | 134 | 122 | 192 | 130 | 140 | 142 | 120 | 169 | 130 | 143 | 143 |
| Y | 24 | 25 | 23 | 24 | 25 | 20 | 26 | 20 | 18 | 22 | 22 | 30 | 27 | 21 | 22 |
| Cu | | | | 70 | | 72 | 60 | 78 | 74 | 60 | 60 | 60 | | | 60 |
| Ni | | | | 130 | | 156 | 90 | 136 | 98 | 110 | 50 | 30 | | | 130 |
| Zn | | | | 70 | | 74 | 80 | 74 | 82 | 80 | 90 | 100 | | | 70 |
| Cr | | | | 240 | | 278 | 200 | 250 | 146 | 180 | 65 | 30 | | | 295 |
| Ba | | | | | | | 285 | | | | | 416 | | | |
| Co | | | | | | | 34.8 | | | | | 31.3 | | | |
| Ni | | | | | | | 117 | | | | | 48.8 | | | |
| Cr | | | | | | | 166 | | | | | 23.6 | | | |
| Cs | | | | | | | 0.314 | | | | | 0.311 | | | |
| Hf | | | | | | | 4.07 | | | | | 3.94 | | | |
| Pb | | | | | | | 10.1 | | | | | 11.5 | | | |
| Ta | | | | | | | 0.817 | | | | | 0.807 | | | |
| Th | | | | | | | 1.13 | | | | | 0.992 | | | |
| U | | | | | | | 0.417 | | | | | 0.504 | | | |
| Zn | | | | | | | 88.1 | | | | | 123 | | | |
| Zr | | | | | | | 181 | | | | | 151 | | | |
| Sc | | | | | | | 26.3 | | | | | 22.8 | | | |
| Latitude | 43 50 40 | 43 52 51 | 43 51 38 | 43 52 35 | 43 51 52 | 43 56 05 | 43 55 04 | 44 58 00 | 44 00 33 | 43 54 28 | 43 54 54 | 43 53 18 | 43 53 45 | 43 56 25 | 43 56 05 |
| Longitude | 121 39 15 | 121 37 33 | 121 42 58 | 121 41 00 | 121 37 48 | 121 46 18 | 121 45 47 | 121 46 00 | 121 43 30 | 121 44 52 | 121 37 39 | 121 36 28 | 121 36 02 | 121 45 50 | 121 43 56 |

*Appendix C.*

| Sample No. | 8407272 | 8407293 | 8509051 | 8407224 | 8408041 | 8507196 | 8507093 | 8509053 | 8407255 | 8407251 | 8407225 | 8407292 | 8409136 | 8408172 | 8408175 |
|---|---|---|---|---|---|---|---|---|---|---|---|---|---|---|---|
| Map Unit | mb3c | mb3c | mb3c | mb3c | mb3c | mb3d | mb3d | mb3d | mb3d | mb3d | mb3d | mb3d | mb4 | mb4 | mb4 |
| SiO2 | 50.6 | 51.0 | 51.2 | 50.4 | 50.5 | 52.9 | 52.2 | 53.8 | 52.7 | 53.7 | 52.9 | 52.9 | 50.6 | 50.5 | 50.8 |
| Al2O3 | 17.3 | 17.2 | 17.0 | 17.4 | 17.3 | 17.2 | 17.2 | 17.5 | 17.4 | 17.7 | 17.2 | 17.2 | 17.0 | 16.9 | 17.2 |
| FeTO3 | 9.64 | 9.57 | 9.60 | 9.66 | 9.65 | 9.05 | 9.22 | 8.79 | 9.05 | 8.54 | 8.98 | 9.06 | 9.55 | 9.54 | 9.33 |
| MgO | 7.64 | 7.27 | 7.30 | 7.80 | 7.78 | 5.90 | 6.37 | 5.29 | 5.87 | 5.39 | 6.51 | 6.34 | 7.92 | 8.13 | 7.83 |
| CaO | 9.15 | 8.91 | 8.90 | 9.17 | 9.20 | 8.53 | 8.69 | 8.41 | 8.61 | 8.47 | 8.36 | 8.45 | 9.30 | 9.24 | 9.30 |
| Na2O | 3.27 | 3.38 | 3.40 | 3.32 | 3.32 | 3.59 | 3.47 | 3.51 | 3.49 | 3.53 | 3.46 | 3.44 | 3.32 | 3.23 | 3.26 |
| K2O | 0.58 | 0.76 | 0.75 | 0.57 | 0.55 | 0.94 | 0.90 | 1.03 | 0.93 | 1.01 | 0.89 | 0.88 | 0.59 | 0.63 | 0.63 |
| TiO2 | 1.33 | 1.43 | 1.43 | 1.33 | 1.34 | 1.34 | 1.40 | 1.20 | 1.38 | 1.20 | 1.22 | 1.27 | 1.36 | 1.29 | 1.27 |
| P2O5 | 0.28 | 0.34 | 0.34 | 0.27 | 0.26 | 0.37 | 0.38 | 0.35 | 0.37 | 0.34 | 0.34 | 0.34 | 0.29 | 0.29 | 0.28 |
| MnO | 0.15 | 0.14 | 0.15 | 0.15 | 0.15 | 0.14 | 0.15 | 0.14 | 0.14 | 0.13 | 0.14 | 0.14 | 0.15 | 0.17 | 0.15 |
| FeO | | | | | 4.27 | | 6.75 | | | | | | 7.35 | 6.35 | 5.44 |
| H2O+ | | | | | 0.26 | | 0.40 | | | | | | 0.17 | 0.26 | 0.36 |
| H2O- | | | | | 0.05 | | 0.04 | | | | | | 0.02 | 0.04 | 0.08 |
| CO2 | | | | | <0.01 | | <0.01 | | | | | | <0.01 | 0.03 | <0.01 |
| Nb | 14 | 13 | | 12 | 10 | | 16 | | 19 | 18 | 16 | 15 | 12 | 13 | <10 |
| Pb | 15 | 11 | | 15 | 12 | | 19 | | 23 | 28 | 21 | 18 | 10 | 10 | <10 |
| Sr | 507 | 508 | | 505 | 486 | | 526 | | 549 | 566 | 536 | 555 | 408 | 412 | 408 |
| Zr | 137 | 149 | | 128 | 127 | | 162 | | 172 | 163 | 149 | 156 | 130 | 132 | 126 |
| Y | 25 | 23 | | 27 | 23 | | 27 | | 28 | 28 | 26 | 26 | 20 | 20 | 20 |
| Cu | 70 | | | 60 | | 70 | 70 | 65 | | | 60 | | | 65 | |
| Ni | 140 | | | 135 | | 105 | 100 | 80 | | | 100 | | | 170 | |
| Zn | 80 | | | 80 | | 80 | 80 | 80 | | | 90 | | | 80 | |
| Cr | 250 | | | 250 | | 160 | 160 | 100 | | | 160 | | | 290 | |
| Ba | | | | | | | | | | | | 356 | | 231 | |
| Co | | | | | | | | | | | | 32.5 | | 38 | |
| Ni | | | | | | | | | | | | 101 | | 161 | |
| Cr | | | | | | | | | | | | 147 | | 259 | |
| Cs | | | | | | | | | | | | 0.5 | | 0.256 | |
| Hf | | | | | | | | | | | | 3.26 | | 2.96 | |
| Pb | | | | | | | | | | | | 16.1 | | 9.41 | |
| Ta | | | | | | | | | | | | 0.719 | | 0.542 | |
| Th | | | | | | | | | | | | 1.59 | | 1.1 | |
| U | | | | | | | | | | | | 0.579 | | 0.418 | |
| Zn | | | | | | | | | | | | 96 | | 89.8 | |
| Zr | | | | | | | | | | | | 137 | | 129 | |
| Sc | | | | | | | | | | | | 23.4 | | 27.2 | |
| Latitude | 43 55 33 | 43 54 55 | 43 53 28 | 43 54 12 | 43 54 55 | 43 56 57 | 43 56 13 | 43 54 55 | 43 56 52 | 43 56 02 | 43 54 27 | 43 55 35 | 43 58 45 | 44 00 45 | 44 00 40 |
| Longitude | 121 40 35 | 121 36 31 | 121 38 10 | 121 38 21 | 121 44 58 | 121 37 15 | 121 43 28 | 121 44 45 | 121 40 45 | 121 41 44 | 121 38 44 | 121 37 02 | 121 41 09 | 121 42 10 | 121 42 15 |

*Appendix C.*

| Sample No. | 8408174 | 8507221 | 8507015 | 8507223 | 8407303 | 8507112 | 8407294 | 8408066 | 8507192 | 8507016 | 8507194 | 8408076 | 8507191 | 8507201 | 8507193 |
|---|---|---|---|---|---|---|---|---|---|---|---|---|---|---|---|
| Map Unit | mb4 | mb4a | mb4a | mb4a | mb4a | mb4b | mb4b | mb4b | mb4b | mb4b | mb4b | mb4b | mb4b | mb4b | mb4b |
| SiO2 | 50.9 | 51.2 | 51.6 | 50.7 | 51.0 | 54.1 | 53.0 | 54.2 | 53.6 | 53.9 | 54.6 | 54.1 | 53.6 | 54.6 | 53.8 |
| Al2O3 | 17.5 | 17.2 | 17.2 | 17.1 | 17.0 | 17.4 | 17.2 | 18.0 | 17.6 | 17.6 | 17.4 | 17.2 | 17.8 | 17.4 | 17.8 |
| FeTO3 | 9.26 | 9.27 | 9.42 | 9.61 | 9.61 | 8.36 | 8.94 | 8.37 | 8.65 | 8.60 | 8.23 | 8.40 | 8.59 | 8.23 | 8.58 |
| MgO | 7.47 | 7.33 | 6.78 | 7.63 | 7.56 | 5.93 | 6.42 | 4.73 | 5.82 | 5.42 | 5.45 | 6.16 | 5.71 | 5.54 | 5.21 |
| CaO | 9.54 | 9.33 | 8.86 | 9.24 | 8.91 | 8.25 | 8.37 | 8.50 | 8.37 | 8.41 | 8.20 | 8.20 | 8.38 | 8.20 | 8.44 |
| Na2O | 3.15 | 3.28 | 3.33 | 3.32 | 3.29 | 3.50 | 3.42 | 3.50 | 3.57 | 3.41 | 3.53 | 3.46 | 3.50 | 3.51 | 3.54 |
| K2O | 0.59 | 0.67 | 0.84 | 0.66 | 0.75 | 0.94 | 0.94 | 1.05 | 0.86 | 1.02 | 1.01 | 0.91 | 0.84 | 1.01 | 1.02 |
| TiO2 | 1.22 | 1.28 | 1.43 | 1.32 | 1.43 | 1.08 | 1.30 | 1.22 | 1.13 | 1.18 | 1.08 | 1.08 | 1.12 | 1.09 | 1.21 |
| P2O5 | 0.27 | 0.28 | 0.37 | 0.29 | 0.33 | 0.30 | 0.36 | 0.34 | 0.30 | 0.33 | 0.29 | 0.31 | 0.29 | 0.29 | 0.34 |
| MnO | 0.15 | 0.15 | 0.15 | 0.15 | 0.15 | 0.13 | 0.14 | 0.13 | 0.13 | 0.14 | 0.13 | 0.13 | 0.13 | 0.13 | 0.13 |
| FeO | 6.41 | 6.31 | 6.79 | 6.78 | | 6.20 | | | 6.30 | 6.16 | 6.04 | | 6.35 | 5.86 | 6.39 |
| H2O+ | 0.48 | 0.37 | 0.39 | 0.27 | | 0.42 | | | 0.42 | 0.52 | 0.40 | | 0.44 | 0.44 | 0.49 |
| H2O- | 0.10 | 0.09 | 0.04 | 0.05 | | 0.05 | | | 0.04 | 0.03 | 0.07 | | 0.05 | 0.12 | 0.06 |
| CO2 | <0.01 | <0.01 | <0.01 | <0.01 | | <0.01 | | | <0.01 | <0.01 | <0.01 | | <0.01 | <0.01 | <0.01 |
| Nb | 10 | 10 | 17 | 12 | 17 | 12 | 15 | 13 | 12 | 14 | 14 | 15 | 14 | 13 | 14 |
| Pb | 10 | 13 | 22 | 15 | 17 | 21 | 24 | 22 | 22 | 26 | 27 | 24 | 24 | 29 | 25 |
| Sr | 402 | 446 | 528 | 482 | 518 | 526 | 544 | 552 | 573 | 549 | 537 | 536 | 581 | 558 | 552 |
| Zr | 120 | 141 | 158 | 142 | 155 | 146 | 159 | 162 | 142 | 163 | 150 | 149 | 144 | 159 | 159 |
| Y | 20 | 27 | 28 | 27 | 24 | 24 | 26 | 24 | 24 | 29 | 29 | 25 | 24 | 27 | 26 |
| Cu | | 75 | | | | | | 65 | | | 70 | 65 | 70 | 60 | |
| Ni | | 130 | | | | | | 50 | | | 80 | 85 | 115 | 75 | |
| Zn | | 80 | | | | | | 80 | | | 85 | 80 | 80 | 80 | |
| Cr | | 220 | | | | | | 80 | | | 130 | 165 | 120 | 120 | |
| Ba | | | | | | | | | | | | | | 357 | |
| Co | | | | | | | | | | | | | | 31.6 | |
| Ni | | | | | | | | | | | | | | 105 | |
| Cr | | | | | | | | | | | | | | 95.2 | |
| Cs | | | | | | | | | | | | | | 0.462 | |
| Hf | | | | | | | | | | | | | | 3.14 | |
| Pb | | | | | | | | | | | | | | 14.4 | |
| Ta | | | | | | | | | | | | | | 0.567 | |
| Th | | | | | | | | | | | | | | 1.17 | |
| U | | | | | | | | | | | | | | 0.42 | |
| Zn | | | | | | | | | | | | | | 91.5 | |
| Zr | | | | | | | | | | | | | | 119 | |
| Sc | | | | | | | | | | | | | | 22.3 | |
| Latitude | 44 00 25 | 43 58 45 | 43 57 38 | 43 59 15 | 43 56 23 | 44 00 00 | 43 54 23 | 43 56 42 | 43 58 21 | 43 57 45 | 43 58 20 | 43 58 18 | 43 58 25 | 44 00 00 | 43 57 53 |
| Longitude | 121 42 15 | 121 45 27 | 121 45 24 | 121 45 02 | 121 36 45 | 121 42 53 | 121 35 57 | 121 45 45 | 121 38 00 | 121 44 27 | 121 38 21 | 121 43 11 | 121 37 48 | 121 39 50 | 121 38 05 |

*Appendix C.*

| Sample No. | 8507115 | 8507116 | 8507195 | 8409135 | 8407254 | 8507117 | 8408071 | 8409134 | 8408072 | 8507114 | 8408071 | 8409148 | 84091310 | 8507172 | 8409139 |
|---|---|---|---|---|---|---|---|---|---|---|---|---|---|---|---|
| Map Unit | mb4b | mb4b | mb4b | mb5 | mb5 | mb5 | mb5 | mb5 | mb5 | mb5 | mb5 | mb5a | mb5a | mb5a | mb5a |
| SiO2 | 54.2 | 54.2 | 54.7 | 56.8 | 55.8 | 55.6 | 56.7 | 56.8 | 56.8 | 56.5 | 56.8 | 56.3 | 56.7 | 56.7 | 56.7 |
| Al2O3 | 17.3 | 17.3 | 17.4 | 18.1 | 17.8 | 18.3 | 18.0 | 18.2 | 17.9 | 18.0 | 17.9 | 18.2 | 18.1 | 18.0 | 18.0 |
| FeTO3 | 8.39 | 8.40 | 8.18 | 7.93 | 7.80 | 7.77 | 7.93 | 7.78 | 7.90 | 7.64 | 7.95 | 7.55 | 7.82 | 7.66 | 7.91 |
| MgO | 6.07 | 6.06 | 5.49 | 3.12 | 4.47 | 4.02 | 3.23 | 3.08 | 3.19 | 3.64 | 3.19 | 3.63 | 3.16 | 3.56 | 3.21 |
| CaO | 8.30 | 8.23 | 8.31 | 7.36 | 8.09 | 8.02 | 7.35 | 7.38 | 7.37 | 7.87 | 7.34 | 7.97 | 7.44 | 7.70 | 7.46 |
| Na2O | 3.39 | 3.40 | 3.36 | 3.97 | 3.54 | 3.69 | 3.98 | 4.06 | 4.04 | 3.71 | 4.05 | 3.78 | 3.98 | 3.81 | 3.97 |
| K2O | 0.92 | 0.94 | 1.01 | 1.26 | 1.10 | 1.15 | 1.25 | 1.26 | 1.24 | 1.23 | 1.22 | 1.19 | 1.26 | 1.24 | 1.25 |
| TiO2 | 1.08 | 1.08 | 1.07 | 1.11 | 1.04 | 1.03 | 1.10 | 1.09 | 1.10 | 1.01 | 1.11 | 1.00 | 1.09 | 1.04 | 1.10 |
| P2O5 | 0.30 | 0.30 | 0.29 | 0.29 | 0.28 | 0.27 | 0.28 | 0.28 | 0.28 | 0.25 | 0.28 | 0.26 | 0.28 | 0.26 | 0.28 |
| MnO | 0.13 | 0.14 | 0.13 | 0.12 | 0.12 | 0.12 | 0.12 | 0.12 | 0.12 | 0.12 | 0.12 | 0.12 | 0.12 | 0.12 | 0.12 |
| FeO | 6.27 | 6.20 | 5.90 | 5.71 | | 4.77 | | 5.53 | | 5.46 | | 5.42 | 5.61 | 5.32 | 5.72 |
| H2O+ | 0.32 | 0.36 | 0.38 | 0.59 | | 0.68 | | 0.28 | | 0.47 | | 0.36 | 0.44 | 0.54 | 0.47 |
| H2O- | 0.09 | 0.06 | 0.06 | 0.13 | | 0.11 | | 0.08 | | 0.03 | | 0.10 | 0.05 | 0.05 | 0.09 |
| CO2 | <0.01 | <0.01 | <0.01 | <0.01 | | <0.01 | | <0.01 | | <0.01 | | <0.01 | <0.01 | <0.01 | 0.01 |
| Nb | 15 | 14 | 14 | 12 | 17 | 13 | 13 | 14 | 15 | 13 | <10 | 14 | 12 | 14 | 10 |
| Pb | 30 | 25 | 29 | 25 | 29 | 34 | 33 | 30 | 32 | 35 | 17 | 28 | 27 | 37 | 28 |
| Sr | 548 | 550 | 554 | 520 | 592 | 573 | 560 | 530 | 550 | 555 | 515 | 525 | 520 | 573 | 520 |
| Zr | 149 | 153 | 151 | 150 | 161 | 157 | 163 | 157 | 165 | 147 | 162 | 144 | 152 | 157 | 150 |
| Y | 26 | 28 | 26 | 25 | 23 | 27 | 25 | 26 | 28 | 24 | 23 | 25 | 20 | 27 | 20 |
| Cu | 70 | | | | 60 | | | | 50 | 70 | | | 50 | | |
| Ni | 90 | | | | 50 | | | | -20 | 28 | | | <20 | | |
| Zn | 80 | | | | 80 | | | | 85 | 80 | | | 80 | | |
| Cr | 160 | | | | 85 | | | | -20 | 35 | | | <20 | | |
| Ba | | | | | | | | | | | | | 461 | | |
| Co | | | | | | | | | | | | | 21.1 | | |
| Ni | | | | | | | | | | | | | 20.7 | | |
| Cr | | | | | | | | | | | | | 10.7 | | |
| Cs | | | | | | | | | | | | | 0.954 | | |
| Hf | | | | | | | | | | | | | 3.63 | | |
| Pb | | | | | | | | | | | | | 28.1 | | |
| Ta | | | | | | | | | | | | | 0.632 | | |
| Th | | | | | | | | | | | | | 2.68 | | |
| U | | | | | | | | | | | | | 0.781 | | |
| Zn | | | | | | | | | | | | | 94.6 | | |
| Zr | | | | | | | | | | | | | 157 | | |
| Sc | | | | | | | | | | | | | 19.5 | | |
| Latitude | 43 58 53 | 43 58 37 | 43 57 55 | 43 58 45 | 43 57 00 | 43 57 37 | 43 58 43 | 43 58 47 | 43 58 38 | 43 59 19 | 43 58 43 | 43 59 22 | 43 58 40 | 43 59 00 | 43 58 38 |
| Longitude | 121 43 09 | 121 43 25 | 121 37 04 | 121 41 13 | 121 41 13 | 121 43 24 | 121 41 22 | 121 41 18 | 121 41 40 | 121 42 50 | 121 41 22 | 121 39 55 | 121 41 05 | 121 38 52 | 121 41 10 |

*Appendix C.*

| Sample No. | 84091311 | 8409137 | 8409147 | 8409132 | 84091312 | 8409133 | 8409131 | 8507222 | 8507111 | 84-22 | 8608223 | 85-9 | 8608222 | 8608221 | 8507216 |
|---|---|---|---|---|---|---|---|---|---|---|---|---|---|---|---|
| Map Unit | mb5a | mb5a | mb5b | mb5b | mb5b | mb5b | mb5b | mb6 | mb6 | mb6 | mb6 | mb6 | mb6 | mb6 | mb6 |
| SiO2 | 56.8 | 56.6 | 56.4 | 56.9 | 56.2 | 56.5 | 56.4 | 53.8 | 53.6 | 51.2 | 51.2 | 51.1 | 50.7 | 51.2 | 51.3 |
| Al2O3 | 18.0 | 18.1 | 18.2 | 18.1 | 18.4 | 18.0 | 18.2 | 17.7 | 17.8 | 17.2 | 17.2 | 17.2 | 17.2 | 17.2 | 17.1 |
| FeTO3 | 7.88 | 7.87 | 7.63 | 7.81 | 7.62 | 7.85 | 7.58 | 8.54 | 8.58 | 11.26 | 11.10 | 11.19 | 11.40 | 11.10 | 11.20 |
| MgO | 3.21 | 3.23 | 3.54 | 3.07 | 3.50 | 3.29 | 3.65 | 5.74 | 5.78 | 5.37 | 5.42 | 5.40 | 5.56 | 5.31 | 5.24 |
| CaO | 7.35 | 7.49 | 7.82 | 7.38 | 7.81 | 7.61 | 7.87 | 8.37 | 8.40 | 8.32 | 8.43 | 8.39 | 8.47 | 8.40 | 8.27 |
| Na2O | 3.99 | 3.97 | 3.79 | 3.99 | 3.89 | 3.99 | 3.72 | 3.47 | 3.50 | 3.51 | 3.63 | 3.68 | 3.62 | 3.55 | 3.61 |
| K2O | 1.26 | 1.24 | 1.21 | 1.25 | 1.20 | 1.23 | 1.21 | 0.84 | 0.80 | 0.66 | 0.64 | 0.65 | 0.61 | 0.67 | 0.69 |
| TiO2 | 1.10 | 1.10 | 1.03 | 1.10 | 1.03 | 1.09 | 1.02 | 1.10 | 1.12 | 1.71 | 1.71 | 1.72 | 1.77 | 1.73 | 1.75 |
| P2O5 | 0.28 | 0.28 | 0.26 | 0.28 | 0.26 | 0.28 | 0.26 | 0.29 | 0.29 | 0.54 | 0.55 | 0.53 | 0.59 | 0.56 | 0.56 |
| MnO | 0.12 | 0.12 | 0.11 | 0.12 | 0.12 | 0.12 | 0.12 | 0.13 | 0.13 | 0.15 | 0.17 | 0.18 | 0.18 | 0.17 | 0.18 |
| FeO | 5.70 | 5.72 | 5.53 | 5.54 | 5.55 | 5.69 | 5.44 | 6.20 | 6.39 | 8.70 | | 8.51 | | | 8.18 |
| H2O+ | 0.30 | 0.37 | 0.36 | 0.43 | 0.39 | 0.35 | 0.45 | 0.38 | 0.48 | 0.03 | | 0.13 | | | 0.33 |
| H2O- | 0.06 | 0.10 | 0.10 | 0.12 | 0.01 | 0.10 | 0.11 | 0.04 | 0.05 | 0.32 | | 0.32 | | | 0.07 |
| CO2 | <0.01 | <0.01 | <0.01 | <0.01 | <0.01 | <0.01 | <0.01 | <0.01 | <0.01 | <0.01 | | <0.01 | | | <0.01 |
| Nb | 17 | 14 | 14 | 13 | 12 | 13 | 12 | <10 | <10 | 13 | | 11 | | | <10 |
| Rb | 33 | 30 | 26 | 28 | 26 | 28 | 28 | 21 | 17 | <10 | | <10 | | | 13 |
| Sr | 515 | 520 | 520 | 515 | 520 | 525 | 525 | 579 | 566 | 490 | | 490 | | | 509 |
| Zr | 153 | 155 | 146 | 153 | 147 | 145 | 140 | 133 | 127 | 150 | | 150 | | | 155 |
| Y | 25 | 25 | 24 | 24 | 22 | 20 | 20 | 22 | 20 | 30 | | 28 | | | 37 |
| Cu | | | 60 | 50 | | | 50 | 75 | 70 | 40 | | 50 | | | 45 |
| Ni | | | -20 | -20 | | | -20 | 60 | 115 | 50 | | 60 | | | 50 |
| Zn | | | 80 | 70 | | | 70 | 80 | 80 | 90 | | 100 | | | 100 |
| Cr | | | 25 | -20 | | | 20 | 125 | 130 | 50 | | 65 | | | 60 |
| Ba | | | | | | | | 382 | | | | | | | 389 |
| Co | | | | | | | | 31.5 | | | | | | | 34.7 |
| Ni | | | | | | | | 112 | | | | | | | 61.2 |
| Cr | | | | | | | | 98.2 | | | | | | | 58.7 |
| Cs | | | | | | | | 0.38 | | | | | | | 0.33 |
| Hf | | | | | | | | 3.03 | | | | | | | 3.58 |
| Rb | | | | | | | | 11.5 | | | | | | | 16.3 |
| Ta | | | | | | | | 0.529 | | | | | | | 0.565 |
| Th | | | | | | | | 1.19 | | | | | | | 0.895 |
| U | | | | | | | | 0.487 | | | | | | | 0.407 |
| Zn | | | | | | | | 91.2 | | | | | | | 118 |
| Zr | | | | | | | | 133 | | | | | | | 171 |
| Sc | | | | | | | | 22.1 | | | | | | | 25.8 |
| Latitude | 43 58 35 | 43 58 45 | 43 59 09 | 43 59 08 | 43 59 27 | 43 58 50 | 43 59 24 | 43 59 39 | 44 00 25 | 44 00 50 | 44 00 03 | 44 00 30 | 44 00 15 | 44 00 25 | 44 00 35 |
| Longitude | 121 41 03 | 121 41 09 | 121 40 22 | 121 41 11 | 121 40 44 | 121 41 15 | 121 41 07 | 121 44 12 | 121 43 40 | 121 41 00 | 121 41 10 | 121 41 15 | 121 41 10 | 121 41 25 | 121 41 30 |

*Appendix C.*

| Sample No. | G86-3 | G86-5 | 85-24 | 8507011 | 8408068 | 8408064 | 8408067 | 8408062 | 8507012 | 8409124 | 8409123 | 8409142 | 8409141 | 8409121 | 840912 |
|---|---|---|---|---|---|---|---|---|---|---|---|---|---|---|---|
| Map Unit | mb6 | mb6 | mr? | mr | mr | mr | mr | mr | mr? | mk | mk | mw | mw | mc | ml |
| SiO2 | 52.9 | 53.5 | 49.2 | 49.7 | 49.3 | 49.3 | 49.4 | 49.5 | 51.0 | 51.2 | 51.0 | 51.4 | 50.7 | 51.4 | 54.0 |
| Al2O3 | 17.8 | 17.9 | 16.2 | 16.6 | 16.7 | 16.6 | 16.5 | 16.6 | 17.2 | 16.8 | 16.8 | 17.0 | 17.0 | 16.6 | 16.4 |
| FeTO3 | 9.92 | 9.72 | 11.69 | 11.67 | 11.60 | 11.68 | 11.89 | 11.91 | 10.53 | 9.66 | 9.71 | 9.75 | 10.12 | 9.31 | 8.87 |
| MgO | 4.99 | 4.73 | 7.03 | 6.85 | 7.20 | 7.14 | 6.95 | 6.71 | 6.43 | 7.31 | 7.56 | 7.04 | 7.31 | 8.37 | 6.54 |
| CaO | 8.15 | 8.03 | 8.62 | 8.71 | 8.70 | 8.69 | 8.69 | 8.63 | 8.73 | 9.22 | 9.23 | 8.72 | 8.90 | 9.20 | 7.64 |
| Na2O | 3.60 | 3.61 | 3.25 | 3.30 | 3.46 | 3.44 | 3.26 | 3.43 | 3.35 | 3.35 | 3.23 | 3.45 | 3.31 | 3.09 | 3.64 |
| K2O | 0.69 | 0.72 | 0.54 | 0.60 | 0.58 | 0.61 | 0.63 | 0.63 | 0.64 | 0.64 | 0.64 | 0.77 | 0.65 | 0.64 | 1.14 |
| TiO2 | 1.41 | 1.32 | 1.87 | 1.85 | 1.82 | 1.85 | 1.95 | 1.90 | 1.57 | 1.39 | 1.35 | 1.40 | 1.44 | 1.06 | 1.33 |
| P2O5 | 0.39 | 0.33 | 0.52 | 0.47 | 0.51 | 0.53 | 0.55 | 0.53 | 0.42 | 0.33 | 0.32 | 0.40 | 0.39 | 0.22 | 0.34 |
| MnO | 0.15 | 0.15 | 0.18 | 0.18 | 0.18 | 0.18 | 0.18 | 0.18 | 0.16 | 0.15 | 0.15 | 0.15 | 0.16 | 0.15 | 0.14 |
| FeO | | | 7.39 | 7.44 | | | | | 6.23 | 6.89 | 5.94 | 6.69 | 6.54 | 6.20 | |
| H2O+ | | | 0.47 | 0.17 | | | | | 0.21 | 0.17 | 0.24 | 0.39 | 0.39 | 0.26 | |
| H2O- | | | 0.52 | <0.01 | | | | | 0.03 | 0.06 | 0.07 | 0.07 | 0.09 | 0.11 | |
| CO2 | | | 0.02 | <0.01 | | | | | <0.01 | <0.01 | <0.01 | <0.01 | <0.01 | <0.01 | |
| Nb | 12 | 10 | 15 | 17 | 13 | 15 | 17 | 14 | 13 | 10 | 13 | 14 | 12 | 12 | 16 |
| Pb | 10 | 10 | <10 | 19 | 6 | <10 | <10 | 6 | 16 | 10 | 10 | 10 | <10 | 14 | 24 |
| Sr | 520 | 520 | 450 | 505 | 485 | 485 | 500 | 492 | 527 | 452 | 454 | 464 | 454 | 428 | 434 |
| Zr | 132 | 130 | 185 | 186 | 190 | 192 | 207 | 192 | 161 | 123 | 126 | 162 | 164 | 100 | 160 |
| Y | 24 | 18 | 30 | 36 | 34 | 33 | 39 | 33 | 28 | 20 | 20 | 20 | 24 | <20 | 25 |
| Cu | 58 | 54 | 65 | 70 | | | 60 | 65 | 50 | | 55 | | 60 | | |
| Ni | 54 | 48 | 120 | 100 | | | 115 | 110 | 90 | | 100 | | 125 | | |
| Zn | 92 | 94 | 90 | 85 | | | 100 | 100 | 90 | | 70 | | 85 | | |
| Cr | 42 | 42 | 180 | 215 | | | 210 | 180 | 160 | | 295 | | 250 | | |
| Ba | | | | 310 | | | | 291 | | | 278 | | | 173 | |
| Co | | | | 40.5 | | | | 39.7 | | | 36.4 | | | 39.7 | |
| Ni | | | | 118 | | | | 131 | | | 120 | | | 148 | |
| Cr | | | | 184 | | | | 172 | | | 253 | | | 451 | |
| Cs | | | | 0.25 | | | | 0.228 | | | 0.26 | | | 0.6 | |
| Hf | | | | 3.94 | | | | 4.17 | | | 2.89 | | | 2.3 | |
| Pb | | | | 7.31 | | | | 10.1 | | | 11.3 | | | 11 | |
| Ta | | | | 0.691 | | | | 0.792 | | | 0.544 | | | 0.48 | |
| Th | | | | 0.606 | | | | 0.625 | | | 0.887 | | | 1.2 | |
| U | | | | 0.231 | | | | 0.341 | | | 0.354 | | | 0.5 | |
| Zn | | | | 124 | | | | 122 | | | 93 | | | 54 | |
| Zr | | | | 166 | | | | 169 | | | 132 | | | 105 | |
| Sc | | | | 27.4 | | | | 26.1 | | | 26.5 | | | 27.7 | |
| Latitude | 44 01 00 | 44 01 30 | 43 56 36 | 43 57 00 | 43 56 43 | 43 56 22 | 43 57 10 | 43 55 58 | 43 57 10 | 44 00 55 | 44 00 55 | 43 45 05 | 43 47 10 | 44 03 30 | 44 01 30 |
| Longitude | 121 43 10 | 121 43 25 | 121 46 30 | 121 47 45 | 121 46 25 | 121 46 05 | 121 46 51 | 121 43 25 | 121 46 20 | 121 45 45 | 121 45 45 | 121 46 17 | 121 46 17 | 121 42 35 | 121 46 20 |

Appendix D. Analytical limits of detection and accuracy for major and trace elements. Major elements WDXRF (Taggart and others, 1987).

| (1) Sample Composition | | (2) Contribution of error by counting statistics | (3) Precision, one sample counted 50x in one day (Std. Deviation) | (4) 49 separately prepared discs counted once each, same day (Standard Deviation) | (5) 1 disc counted 62x from 7/81 to 12/81 (Std. Deviation) | (6) 1 disc counted 62x from 1/85 to 5/85 (Std. Deviation) |
|---|---|---|---|---|---|---|
| $SiO_2$ | 52.8% | ± 0.04 | 0.04 | 0.13 | 0.19 | 0.09 |
| $Al_2O_3$ | 16.7% | ± 0.03 | 0.02 | 0.07 | 0.05 | 0.05 |
| $Fe_2O_3$[1] | 9.35% | ± 0.01 | 0.01 | 0.03 | 0.02 | 0.01 |
| MgO | 3.54% | ± 0.02 | 0.02 | 0.02 | 0.06 | 0.04 |
| CaO | 6.60% | ± 0.01 | 0.01 | 0.02 | 0.02 | 0.02 |
| $Na_2O$ | 3.20% | ± 0.03 | 0.03 | 0.09 | 0.07 | 0.04 |
| $K_2O$ | 4.38% | ± 0.01 | 0.01 | 0.01 | 0.03 | 0.01 |
| $TiO_2$ | 0.88% | ± 0.01 | 0.01 | 0.01 | 0.01 | 0.01 |
| $P_2O_5$ | 0.60% | ± 0.01 | 0.01 | 0.01 | 0.01 | 0.01 |
| MnO | 0.18% | ± 0.01 | 0.01 | 0.01 | 0.01 | <0.01 |

[1]Total Fe as $Fe_2O_3$

Appendix D. (continued). Trace elements (Johnson and King, 1987).

SENSITIVITY, PRECISION AND ACCURACY

The precision of EDXRF measurements depends primarily on instrument stability, although it can also be influenced by variations in specimen preparation, or differences in sample geometry within the spectrometer. The particular spectrometers being used for EDXRF analysis at the USGS are very stable, and single intensity measurements are commonly reproducible to within a ± 1% relative error, limited mainly by counting statistics. Accuracy, that is the ability to reduce or eliminate systematic errors, depends on many factors. Non-uniform sample preparation, errors in standard reference material values, atomic number of analyte elements (lighter elements being affected by the matrix to a greater extent), the presence of interfering lines, and the ability of the correction algorithm to model the actual inter element effects all contribute to the accuracy of a determination. Experience has shown that with some diligence on the part of the analyst, a relative error of ± 5% is common for most of the concentration ranges, although it decreases to as much as 50% near the lower limit of detection (about 2 to 10 ppm for most elements).

| Element | Lower Limit | Upper Limit |
|---|---|---|
| Cr | 20 ppm | 4000 ppm |
| Ni | 2 | 3000 |
| Cu | 2 | 1000 |
| Zn | 2 | 1000 |
| Rb | 2 | 2000 |
| Sr | 2 | 2000 |
| Y | 2 | 500 |
| Zr | 5 | 2000 |
| Nb | 10 | 500 |
| Ba | 5 | 4000 |
| La | 5 | 500 |
| Ce | 5 | 500 |

Appendix E. INAA data.

| SAMPLE # | DESCRIPTION | SIO2 | Fe | Na | Ba | Co | Ni | Cr | Cs | Hf | Rb | Sb | Ta | Th |
|---|---|---|---|---|---|---|---|---|---|---|---|---|---|---|
| 8408062 | RED CRATER FLOW | 49.5 | 8.6 | 2.56 | 8.49 | 39.7 | 131 | 172 | 0.228 | 4.17 | 10.10 | n.d. | 0.792 | 0.625 |
| 8507011 | HWY 46 RED CRATER | 49.7 | 8.6 | 2.69 | 310 | 40.5 | 118 | 184 | 0.250 | 3.94 | 7.31 | 0.087 | 0.691 | 0.606 |
| 8408021 | SIAH TRANS OPG | 50.2 | 6.9 | 2.45 | 214 | 40.0 | 153 | 241 | 0.244 | 2.86 | 4.86 | 0.036 | 0.471 | 0.630 |
| 8408172 | TODD - N | 50.5 | 6.7 | 2.45 | 231 | 38.0 | 161 | 259 | 0.268 | 2.96 | 9.41 | 0.124 | 0.542 | 1.100 |
| 8407053 | SIAH POG | 50.6 | 7.0 | 2.67 | 218 | 39.1 | 136 | 211 | 0.299 | 3.02 | 10.40 | 0.099 | 0.615 | 0.841 |
| 8409123 | KATSUK | 51.0 | 6.7 | 2.44 | 278 | 36.4 | 120 | 253 | 0.260 | 2.89 | 11.30 | 0.214 | 0.544 | 0.887 |
| 8507216 | EGAN | 51.3 | 8.3 | 2.89 | 389 | 34.7 | 61 | 58 | 0.330 | 3.58 | 16.30 | 0.120 | 0.565 | 0.895 |
| 8408061 | FP AROUND LAVA L | 51.4 | 6.8 | 2.67 | 285 | 34.8 | 117 | 166 | 0.314 | 4.07 | 10.10 | n.d. | 0.817 | 1.130 |
| 8407071 | W SIAH OLDER OL | 52.1 | 7.2 | 2.76 | 352 | 34.6 | 116 | 164 | 0.461 | 4.02 | 15.60 | 0.095 | 0.640 | 1.110 |
| 8407214 | SHER BIG PLAG | 52.3 | 6.5 | 2.72 | 252 | 33.9 | 92 | 64 | 0.340 | 2.27 | 11.20 | 0.099 | 0.284 | 0.710 |
| 8407064 | APHANITIC 6268' | 52.6 | 6.3 | 2.74 | 321 | 31.7 | 86 | 89 | 0.338 | 2.44 | 13.90 | 0.051 | 0.341 | 0.793 |
| 8407244 | BACH BIG PLAG | 52.7 | 7.8 | 2.99 | 416 | 31.3 | 49 | 24 | 0.311 | 3.94 | 11.50 | 0.102 | 0.807 | 0.992 |
| 8407292 | LATE KWOHL | 52.9 | 6.4 | 2.67 | 356 | 32.5 | 101 | 157 | 0.500 | 3.26 | 16.10 | 0.160 | 0.719 | 1.590 |
| 8507191 | BACH - E, FP | 53.6 | 6.2 | 2.81 | 357 | 31.6 | 105 | 95 | 0.462 | 3.14 | 14.40 | 0.109 | 0.567 | 1.170 |
| 8507222 | BACH INT W SIDE | 53.8 | 6.2 | 2.86 | 382 | 31.5 | 112 | 98 | 0.380 | 3.03 | 11.50 | 0.087 | 0.529 | 1.190 |
| 8507271 | SHERIDAN FP | 53.8 | 6.1 | 2.80 | 362 | 28.3 | 39 | 94 | 0.548 | 3.43 | 16.20 | 0.072 | 0.764 | 1.620 |
| 8407011 | W FLANK SHER POG | 54.1 | 6.0 | 2.65 | 391 | 26.9 | 49 | 96 | 0.553 | 3.61 | 20.10 | 0.033 | 0.766 | 1.730 |
| 84091310 | SUMMIT | 56.7 | 5.5 | 2.96 | 461 | 21.1 | 21 | 11 | 0.954 | 3.63 | 28.10 | 0.211 | 0.632 | 2.680 |

Appendix E. (continued).

| SAMPLE # | DESCRIPTION | U | Zn | Zr | Sc | La | Ce | Nd | Sm | Eu | Gd | Tb | Tm | Yb | Lu |
|---|---|---|---|---|---|---|---|---|---|---|---|---|---|---|---|
| 8408062 | RED CRATER FLOW | 0.341 | 122.0 | 169 | 26.1 | 14.9 | 40.1 | 23.2 | 5.86 | 1.98 | 6.74 | 1.070 | 0.522 | 3.15 | 0.459 |
| 8507011 | HWY 46 RED CRATER | 0.231 | 124.0 | 166 | 27.4 | 14.8 | 37.6 | 22.5 | 5.77 | 1.98 | 6.38 | 0.956 | 0.505 | 3.07 | 0.456 |
| 8408021 | SIAH TRANS OPG | 0.353 | 92.6 | 131 | 26.6 | 10.1 | 25.9 | 14.7 | 3.89 | 1.41 | 4.60 | 0.716 | n.d | 2.33 | 0.355 |
| 8408172 | TODD - N | 0.418 | 89.8 | 129 | 27.2 | 10.7 | 27.7 | 16.1 | 4.27 | 1.34 | 4.68 | 0.718 | 0.413 | 2.46 | 0.363 |
| 8407053 | SIAH POG | 0.425 | 85.9 | 139 | 28.3 | 11.8 | 28.8 | 15.2 | 4.15 | 1.49 | 4.77 | 0.734 | 0.395 | 2.43 | 0.363 |
| 8409123 | KATSUK | 0.345 | 93.0 | 132 | 26.5 | 11.5 | 27.2 | 16.3 | 4.23 | 1.51 | 4.57 | 0.729 | 0.366 | 2.27 | 0.333 |
| 8507216 | EGAN | 0.407 | 118.0 | 171 | 25.8 | 15.4 | 38.6 | 22.7 | 6.20 | 2.13 | 6.89 | 1.050 | 0.550 | 3.40 | 0.501 |
| 8408061 | FP AROUND LAVA L | 0.417 | 88.1 | 181 | 26.3 | 15.3 | 42.1 | 20.5 | 5.18 | 1.72 | 5.60 | 0.837 | 0.431 | 2.66 | 0.391 |
| 8407071 | W SIAH OLDER OL | 0.562 | 105.0 | 173 | 23.6 | 16.4 | 43.5 | 21.6 | 5.84 | 1.83 | 5.95 | 0.885 | 0.454 | 2.77 | 0.412 |
| 8407214 | SHER BIG PLAG | 0.307 | 91.6 | 69 | 22.9 | 9.0 | 21.1 | 12.9 | 3.33 | 1.18 | 3.45 | 0.509 | 0.273 | 1.66 | 0.242 |
| 8407064 | APHANITIC 6268' | 0.336 | 93.3 | 105 | 22.0 | 10.4 | 25.5 | 14.0 | 3.67 | 1.26 | 3.71 | 0.536 | 0.285 | 1.75 | 0.263 |
| 8407244 | BACH BIG PLAG | 0.504 | 123.0 | 151 | 22.8 | 16.2 | 41.2 | 23.8 | 5.95 | 1.95 | 6.11 | 0.933 | 0.458 | 2.83 | 0.418 |
| 8407292 | LATE KWOHL | 0.576 | 96.0 | 137 | 23.4 | 15.8 | 37.3 | 18.7 | 4.32 | 1.47 | 4.70 | 0.749 | 0.394 | 2.41 | 0.345 |
| 8507191 | BACH - E, FP | 0.420 | 91.5 | 119 | 22.3 | 14.9 | 33.4 | 16.3 | 4.15 | 1.40 | 4.42 | 0.666 | 0.364 | 2.12 | 0.311 |
| 8507222 | BACH INT W SIDE | 0.487 | 91.2 | 133 | 22.1 | 14.5 | 33.3 | 16.0 | 3.91 | 1.35 | 4.39 | 0.650 | 0.345 | 2.09 | 0.293 |
| 8507271 | SHERIDAN FP | 0.625 | 91.3 | 157 | 26.1 | 16.9 | 39.5 | 20.3 | 4.50 | 1.47 | 4.66 | 0.761 | 0.395 | 2.40 | 0.354 |
| 8407011 | W FLANK SHER POG | 0.853 | 91.7 | 147 | 24.9 | 17.8 | 42.6 | 20.2 | 4.86 | 1.54 | 5.24 | 0.806 | 0.430 | 2.65 | 0.397 |
| 84091310 | SUMMIT | 0.781 | 94.6 | 157 | 19.5 | 18.3 | 40.4 | 18.5 | 4.62 | 1.42 | 4.91 | 0.757 | 0.411 | 2.55 | 0.373 |

Appendix F. Distribution coefficents used for trace-element modeling. First are the compilations that were taken from Clark, 1983; Hughes, 1983; and Reagan and others, 1987. The final list is the minimum and maximum distribution coefficents that I used in my calculation.

From Clark, 1983

| | Olivine | Clinopyroxene | Plagioclase | Magnetite |
|---|---|---|---|---|
| Rb | .01-.02 | .01-.14 | .02-.20 | .02-.20 |
| Sr | .01-.10 | .05-.15 | 1.0-3.5 | 1.0-3.5 |
| Zr | .01-.02 | .20-.50 | .01-.08 | .01-.08 |
| Ba | .01-.02 | .01-.10 | .10-.50 | .10-.50 |
| Ni | 5.0-25.0 | 4.0-9.0 | .02-.40 | 5.0-20.0 |
| Cr | .20-50.0 | 10.0-100.0 | .01-.20 | 10.0-100.0 |

From Hughes, 1983

| | Olivine | Clinopyroxene | Plagioclase | Magnetite |
|---|---|---|---|---|
| K | 0.004 | 0.03 | 0.06 | 0.01 |
| Ba | 0.004 | 0.12 | 0.06 | 0.01 |
| Sr | 0.004 | 0.12 | 1.78 | 0.01 |
| Ce | 0.008 | 0.11 | 0.73 | 0.03 |
| Nd | 0.009 | 0.21 | 0.04 | 0.059 |
| Sc | 0.25 | 0.61 | 0.025 | 0.05 |
| Co | 2.5 | 0.8 | 0.05 | 2.5 |

From Reagan and others, 1987

| | Olivine | Clinopyroxene | Plagioclase | Magnetite |
|---|---|---|---|---|
| Ni | 10.00 | 6.00 | 0.01 | 10.00 |
| Cr | 4.00 | 15.00 | 0.01 | 32.00 |
| Sc | 0.30 | 3.00 | 0.01 | 2.00 |
| V | 0.08 | 1.10 | 0.01 | 10.00 |
| Ba | 0.01 | 0.02 | 0.16 | 0.01 |
| Ce | 0.01 | 0.25 | 0.20 | 0.20 |
| Nd | 0.01 | 0.50 | 0.15 | 0.25 |
| K | 0.01 | 0.02 | 0.11 | 0.01 |
| Ti | 0.03 | 0.40 | 0.05 | 10.00 |
| Zr | 0.01 | 0.25 | 0.01 | 0.40 |
| Y | 0.01 | 0.90 | 0.06 | 0.50 |
| Sr | 0.01 | 0.08 | 2.00 | 0.01 |
| Rb | 0.01 | 0.02 | 0.07 | 0.01 |

Appendix F. (continued).

Range of Distribution Coeffients used in this study compiled from Hughes (1983), Clark (1983), and Reagan and others (1987)

| | Olivine | Clinopyroxene | Plagioclase | Magnetite |
|---|---|---|---|---|
| Ni | 5.0-25.0 | 4.0-9.0 | 0.01-0.40 | 5.0-20.0 |
| Cr | 0.20-50.0 | 10-100 | 0.01-0.20 | 10-100 |
| Sc | 0.25-0.30 | 2.5-3.0 | 0.025-0.01 | 2 |
| V | 0 | 0 | 0 | 0 |
| Ba | 0.004-0.02 | 0.01-0.10 | 0.06-0.50 | 0.01-0.30 |
| Ce | 0.008-0.01 | 0.11-0.25 | 0.07-0.20 | 0.03-0.2 |
| Nd | 0.009-0.01 | 0.21-0.50 | 0.06-0.15 | 0.04-0.25 |
| K | 0.004-0.01 | 0.02-0 .03 | 0.06-0.11 | 0.01 |
| Ti | 0.03 | 0.4 | 0.05 | 10 |
| Zr | 0.01-0.02 | 0.2-0.5 | 0.01-0.08 | 0.40-2.0 |
| Y | 0.01 | 0.9 | 0.06 | 0.5 |
| Sr | 0.004-0.10 | 0.05-0.15 | 1.0-3.5 | 0.01-0.30 |
| Rb | 0.01-0.02 | 0.01-0.14 | 0.02-0.20 | 0.01-0.30 |